UNIVERSIDADE FEDERAL DE MINAS GERAIS

Instituto de Ciências Biológicas

Programa de Pós-Graduação em Ciências Biológicas: Fisiologia e Farmacologia

Sabrina Mendes Silva Araujo

NANOFORMULAÇÕES DA ANGIOTENSINA-(1-7) E DO REMDESIVIR COM LIPOSSOMAS: eficácia terapêutica por via intranasal em camundongos K18-hACE2 infectados por SARS-CoV-2

Belo Horizonte

2025

Sabrina Mendes Silva Araujo

NANOFORMULAÇÕES DA ANGIOTENSINA-(1-7) E DO REMDESIVIR COM LIPOSSOMAS: eficácia terapêutica por via intranasal em camundongos K18-hACE2 infectados por SARS-CoV-2

Tese apresentada ao Programa de Pós-Graduação em Ciências Biológicas: Fisiologia e Farmacologia da Universidade Federal de Minas Gerais, como requisito parcial à obtenção do título de Doutor em Fisiologia.

Orientador: Prof. Dr. Frédéric Jean Georges Frézard
Coorientador: Prof. Dr. Pedro Pires Goulart Guimarães

Belo Horizonte
2025

043 Araujo, Sabrina Mendes Silva.
Nanoformulações da angiotensina-(1-7) e do remdesivir com lipossomas: eficácia terapêutica por via intranasal em camundongos K18-hACE2 infectados por SARS-CoV-2 [manuscrito] / Sabrina Mendes Silva Araujo. – 2025.
79 f. : il. ; 29,5 cm.

Orientador: Prof. Dr. Frédéric Jean Georges Frézard. Coorientador: Prof. Dr. Pedro Pires Goulart Guimarães.
Tese (doutorado) – Universidade Federal de Minas Gerais, Instituto de Ciências Biológicas. Programa de Pós-Graduação em Fisiologia e Farmacologia.

1. Fisiologia. 2. COVID-19. 3. Angiotensinas. 4. Lipossomos. 5. Absorção Nasal. I. Frézard, Frédéric Jean Georges. II. Guimarães, Pedro Pires Goulart. III. Universidade Federal de Minas Gerais. Instituto de Ciências Biológicas. IV. Título.

CDU: 612

Ficha catalográfica elaborada pela Bibliotecária Fabiane C M Reis, CRB 6 - 2680

UNIVERSIDADE FEDERAL DE MINAS GERAIS
ICB - COLEGIADO DE PÓS-GRADUAÇÃO EM FISIOLOGIA E FARMACOLOGIA - SECRETARIA

ATA DA DEFESA DA TESE DE DOUTORADO N° 393 DE SABRINA MENDES SILVA ARAÚJO

Às 14:00 horas do dia 10 do mês de março de 2025, na Sala Hugo Godinho - J3, realizou-se a sessão pública para a defesa da Tese de **Sabrina Mendes Silva Araújo.** A presidência da sessão coube ao **Prof. Dr. Frédéric Jean Georges Frézard,** orientador. Inicialmente, o presidente fez a apresentação da Comissão Examinadora assim constituída: **Prof. Dr. Frédéric Jean Georges Frézard,** ICB/Universidade Federal de Minas Gerais, **Profa. Dra. Eliana Martins Lima,** Universidade Federal de Goiás, **Profa. Dra. Daisy Motta Santos,** Universidade do Estado de Minas Gerais, **Prof. Dr. André Luís Branco de Barros,** FaFar/Universidade Federal de Minas Gerais e a **Profa. Dra. Luciene Bruno Vieira,** ICB/Universidade Federal de Minas Gerais. Em seguida, a candidata fez a apresentação do trabalho que constitui sua **Tese de Doutorado**, intitulada: **"Nanoformulações da Angiotensina-(1-7) e do Remdesivir Com Lipossomas: Eficácia Terapêutica por Via Intranasal em Camundongos K18-hACE2 Infectados por Sars-CoV-2".** Seguiu-se a arguição pelos examinadores e logo após, a Comissão reuniu-se, sem a presença da candidata e do público e decidiu considerar **APROVADA** a Tese de Doutorado. O resultado final foi comunicado publicamente a candidata pelo presidente da Comissão. Nada mais havendo a tratar, o presidente encerrou a sessão e lavrou a presente ata que, depois de lida, será assinada pela Comissão Examinadora.

Belo Horizonte, 10 de março de 2025.

Assinatura dos membros da banca examinadora:

Documento assinado eletronicamente por **Frederic Jean Georges Frezard**, **Professor do Magistério Superior**, em 14/03/2025, às 15:54, conforme horário oficial de Brasília, com fundamento no art. 5º do Decreto nº 10.543, de 13 de novembro de 2020.

Documento assinado eletronicamente por **Daisy Motta Santos**, **Usuário Externo**, em 14/03/2025, às 16:46, conforme horário oficial de Brasília, com fundamento no art. 5º do Decreto nº 10.543, de 13 de novembro de 2020.

Documento assinado eletronicamente por **Luciene Bruno Vieira**, **Professor(a)**, em 18/03/2025, às 15:01, conforme horário oficial de Brasília, com fundamento no art. 5º do Decreto nº 10.543, de 13 de novembro de 2020.

Documento assinado eletronicamente por **Andre Luis Branco de Barros**, **Professor do Magistério Superior**, em 18/03/2025, às 17:26, conforme horário oficial de Brasília, com fundamento no art. 5º do Decreto nº 10.543, de 13 de novembro de 2020.

Documento assinado eletronicamente por **Eliana Martins Lima**, **Usuária Externa**, em 26/03/2025, às 06:34, conforme horário oficial de Brasília, com fundamento no art. 5º do Decreto nº 10.543, de 13 de novembro de 2020.

AGRADECIMENTOS

Gostaria de agradecer, primeiramente, à minha família, que sempre me deu todo apoio e esteve comigo. Em especial, agradeço à minha mãe, Elisangela, aos meus irmãos, Neto e Lissa, e à minha avó materna, Ieda. Vocês são minha base.

Expresso minha mais sincera gratidão ao meu orientador, Professor Frédéric Frézard, por me conceder esta oportunidade e por acreditar no meu potencial. Sou imensamente grata por todo o conhecimento compartilhado ao longo desses anos, que contribuiu não apenas para o meu crescimento profissional, mas também para o meu desenvolvimento pessoal. Além de um mentor excepcional, o Professor Frézard é um exemplo de integridade, uma qualidade que admiro e que seguirá me inspirando ao longo da vida.

Agradeço à Clara, que está ao meu lado e me apoia desde o primeiro dia que a conheci. Obrigada por todo o amor e dedicação ao longo desses anos. Você me tirou de lugares difíceis e sempre acreditou em mim. Você foi a peça-chave para que eu chegasse até aqui hoje, e eu serei sempre grata por todo o tempo que dedicou a mim.

Preciso agradecer aos meus amigos mais próximos, que me deram todo o suporte e apoio, especialmente à Lays, que me ajudou nos momentos difíceis, nos meus experimentos e sempre foi uma ótima conselheira. Obrigada não só pela colaboração nos artigos, mas por todos os bares que me levou, pelas sextas-feiras depois do laboratório e pelos almoços de domingo, onde eu me sentia em família. Você foi minha família aqui em BH. Quero agradecer a Pâmela, Léo, Vivian, Raquel e Audrey, grandes amigos que fiz em BH, e levarei comigo a vida inteira. Agradeço aos meus amigos de laboratório, Thais, Natália, Ana Castro, Cristiano, Gabriel e Carol. Vocês deixaram meus dias no laboratório mais leves e felizes.

Também agradeço aos professores do Departamento de Fisiologia e Biofísica por todo o auxílio e suporte científico. Agradeço ao professor Pedro Guimarães, meu coorientador e ao professor Robson Santos. Agradeço à professora Vivian, do Departamento de Morfologia, e ao professor Mauro, do Departamento de Bioquímica e Imunologia, por nos concederem acesso ao modelo animal K18-hACE2.

Agradeço às agências de fomento CAPES, CNPq e FAPEMIG que tornaram possível a realização deste projeto e que desempenham um papel fundamental em manter a ciência ativa e em constante evolução.

"Nada é mais poderoso do que uma ideia cujo tempo chegou" (Victor Hugo, 1877).

RESUMO

A pandemia de COVID-19 destacou a necessidade urgente de estratégias terapêuticas eficazes para reduzir o impacto da doença e proteger os indivíduos da síndrome respiratória aguda grave. Foram exploradas estratégias como a busca por moléculas inéditas com potencial terapêutico, o reposicionamento de fármacos anti-inflamatórios e antivirais e o desenvolvimento de novas formulações para administração pulmonar de fármacos. O peptídeo endógeno angiotensina-(1-7) [Ang-(1-7)] emergiu como um agente anti-inflamatório promissor, enquanto o remdesivir (RDV) tem sido amplamente utilizado devido às suas propriedades antivirais, apesar das limitações associadas à sua formulação farmacêutica Veklury®, como eficácia moderada, alta toxicidade e necessidade de administração parenteral. Diante desse contexto, os trabalhos que deram origem a esta tese tiveram como objetivo central desenvolver formulações lipossomais para administração intranasal de Ang-(1-7) [LAng (1-7)] e RDV [LRDV] e avaliar sua eficácia em modelos de infecção por SARS-CoV-2, incluindo camundongos transgênicos K18-hACE2. As formulações LAng (1-7) e LRDV foram obtidas pelo método de injeção de solução etanólica, apresentando vesículas com diâmetros médios de 100 nm e 120 nm, respectivamente, e índices de polidispersão inferiores a 0,1. As taxas de encapsulação da Ang-(1-7) e do RDV foram de 13% e 65% e as meia-vidas de liberação a 37ºC de 9,3 h e 5,3 h, respectivamente. Ensaios *in vitro* de citotoxicidade e atividade antiviral de LRDV mostraram um índice de seletividade 3,5 vezes maior em comparação ao fármaco livre. O estudo farmacocinético do LRDV por via intranasal evidenciou a entrega efetiva do fármaco aos pulmões. Camundongos K18-hACE2 infectados com SARS-CoV-2 foram tratados a cada 12 horas por 5 dias com LAng (1-7) intranasal, LRDV intranasal ou a formulação comercial do RDV (Veklury®) intraperitoneal, com grupos controle recebendo lipossomas vazios, Ang-(1-7) livre ou PBS. O tratamento com LAng (1-7) resultou em maior sobrevivência dos animais em comparação aos grupos controle, além de reduzir significativamente a carga viral e os níveis de IL-6 e TNF nos pulmões. No tratamento com LRDV intranasal, os camundongos permaneceram vivos até 15 dias após a infecção (dpi), enquanto os grupos controle apresentaram 100% de mortalidade em 6 dpi, e o grupo tratado com Veklury® intraperitoneal apresentou 62,5% de mortalidade em 8 dpi. Além disso, LRDV reduziu significativamente as cargas virais nos pulmões e cérebro, prevenindo a resposta inflamatória induzida pelo SARS-CoV-2 nos pulmões, o que não foi observado com Veklury®. Em conclusão, essa tese apresenta prova de conceito para estratégias terapêuticas inovadoras da COVID-19 baseadas em nanoformulações lipossomais de Ang-(1-7) e RDV administradas por via intranasal. LAng (1-7) demonstrou potencial anti-inflamatório e antiviral, enquanto LRDV mostrou-se superior ao tratamento convencional, reduzindo a carga viral tanto nos pulmões quanto no cérebro e prevenindo a inflamação pulmonar, podendo ser uma alternativa promissora também para a condição pós-COVID-19. De forma mais ampla, essas descobertas destacam o potencial das nanoformulações lipossomais intranasais no tratamento da COVID-19.

Palavras chave: COVID-19, angiotensina-(1-7), remdesivir, lipossomas, intranasal, K18-hACE2.

ABSTRACT

The COVID-19 pandemic highlighted the urgent need for effective therapeutic strategies to reduce the impact of the disease and protect individuals from severe acute respiratory syndrome. Several approaches have been explored, including the search for new molecules with therapeutic potential, the repurposing of existing anti-inflammatory and antiviral drugs and the development of novel formulations for pulmonary deliveryThe endogenous peptide angiotensin-(1-7) [Ang-(1-7)] emerged as a promising anti-inflammatory agent, while remdesivir (RDV) has been widely used due to its antiviral properties, despite the limitations of its pharmaceutical formulation Veklury®, such as moderate efficacy, high toxicity, and the requirement for parenteral administration. In this context, the studies that led to this thesis were primarily aimed at developing liposomal formulations for intranasal administration of Ang-(1-7) [LAng (1-7)] and RDV [LRDV], and evaluating their efficacy in SARS-CoV-2 infection models, including K18-hACE2 transgenic mice. The LAng (1-7) and LRDV formulations were prepared by the ethanol injection method, yielding vesicles with mean diameters of 100 nm and 120 nm, respectively, and polydispersity indices below 0.1. The encapsulation efficiencies of Ang-(1-7) and RDV were 13% and 65%, respectively, with release half-lives at 37 °C of 9.3 h and 5.3 h. In vitro cytotoxicity and antiviral assays of LRDV demonstrated a 3.5-fold higher selectivity index compared to the free drug. Pharmacokinetic studies of intranasally administered LRDV confirmed efficient drug delivery to the lungs. K18-hACE2 mice infected with SARS-CoV-2 were treated every 12 hours for 5 days with intranasal LAng (1-7), intranasal LRDV, or intraperitoneal Veklury®, with control groups receiving empty liposomes, free Ang-(1-7), or PBS. Treatment with LAng (1-7) increased survival compared with control groups, while also significantly reducing viral load and levels of IL-6 and TNF in the lungs. In the case of intranasal LRDV, all mice remained alive up to 15 days post-infection (dpi), whereas control groups showed 100% mortality by 6 dpi, and the group treated with intraperitoneal Veklury® exhibited 62.5% mortality by 8 dpi. Moreover, LRDV significantly reduced viral loads in both lungs and brain, preventing SARS-CoV-2-induced inflammatory responses in the lungs, which was not observed with Veklury®. In conclusion, this thesis provides proof-of-concept for innovative COVID-19 therapeutic strategies based on intranasal liposomal nanoformulations of Ang-(1-7) and RDV. LAng (1-7) demonstrated both anti-inflammatory and antiviral potential, while LRDV outperformed conventional treatment, reducing viral burden in lungs and brain and preventing pulmonary inflammation, making it a promising alternative also for post-COVID-19 conditions. More broadly, these findings underscore the therapeutic potential of intranasal liposomal nanoformulations in the treatment of COVID-19.

Keywords: COVID-19, angiotensin-(1-7), remdesivir, liposomes, intranasal, K18-hACE2.

SUMÁRIO

1 INTRODUÇÃO

A pandemia de COVID-19, causada pelo SARS-CoV-2, continua a representar um desafio significativo para a saúde pública global (Filip et al., 2022). Esse vírus se espalhou rapidamente pelo mundo e, em março de 2020, a Organização Mundial da Saúde (OMS) declarou a COVID-19 uma pandemia. Desde então, o vírus já infectou mais de 777 milhões de pessoas e causou mais de 7 milhões de mortes globalmente até fevereiro de 2025 ("COVID-19 deaths | WHO COVID-19 dashboard", 2025). O SARS-CoV-2 é um vírus de RNA de fita simples positiva, pertencente à família *Coronaviridae*, que também inclui os altamente patogênicos coronavírus da síndrome respiratória aguda grave (SARS-CoV) e da síndrome respiratória do Oriente Médio (MERS-CoV), responsáveis por surtos significativos nas últimas duas décadas (Katiyar et al., 2024). Desde o seu surgimento em 2019 (Zhu et al., 2020), o vírus tem evoluído, resultando em diversas variantes que afetam a epidemiologia e a transmissibilidade da doença (Harvey et al., 2021).

Até o momento, a OMS e agências nacionais de saúde públicas classificaram cinco variantes do SARS-CoV-2 como Variantes de Preocupação (VOCs, do inglês *Variants of Concern*), devido a alterações significativas na transmissibilidade ou capacidade de escape imunológico, exigindo monitoramento rigoroso ("Tracking SARS-CoV-2 variants", 2025). Cada VOC demonstrou uma vantagem competitiva em relação às variantes anteriores, tornando-se dominante em diferentes regiões (Harvey et al., 2021). As variantes Alpha (linhagem PANGO B.1.1.7) ("COVID-19 variants | WHO COVID-19 dashboard", 2025; O'Toole et al., 2022), Beta (B.1.351) e Gamma (P.1) predominaram, respectivamente, na Europa, no sul da África e na América do Sul. Já as variantes Delta (sublinhagens B.1.617.2/AY) e Ômicron (B.1.1.529 e suas sublinhagens, como BA.1, BA.2 e BA.5) apresentaram ampla disseminação global, consolidando-se como as linhagens predominantes em sucessivos períodos da pandemia (Carabelli et al., 2023).

Os casos de COVID-19 apresentam uma ampla variedade de manifestações clínicas, que podem variar desde sintomas leves, como tosse seca, febre e dor de garganta, até condições graves, incluindo síndrome do desconforto respiratório agudo, falência múltipla de órgãos e, em alguns casos, óbito (Hu et al., 2021). A condição pós-COVID-

19 também emergiu como uma síndrome pós-infecção aguda em vários pacientes relatando manifestações persistentes, como hiposmia, hipogeusia, distúrbios do sono e comprometimento cognitivo substancial, este último afetando aproximadamente um em cada quatro casos de COVID-19 (Li et al., 2024).

A gravidade da COVID-19 está associada à resposta imune do hospedeiro ao SARS-CoV-2 (Tay et al., 2020). Uma resposta imune eficaz é crucial para a eliminação viral, enquanto uma resposta disfuncional leva à persistência viral e à produção excessiva de fatores inflamatórios, resultando em tempestade de citocinas e progressão da doença (Li et al., 2024). O SARS-CoV-2 infecta células ligando-se ao receptor da enzima conversora de angiotensina II (ECA2). A glicoproteína Spike (S) do SARS-CoV-2 é preparada para iniciar a fusão vírus-célula por meio de um evento de clivagem proteolítica, que pode ser mediado pela serina protease transmembrana 2 (TMPRSS2) na superfície celular (Trougakos et al., 2021). Existe também o envolvimento da protease furina no processo de infecção pelo SARS-CoV-2, uma vez que esse vírus apresenta um local de clivagem incomum para coronavírus na proteína S (Hoffmann; Kleine-Weber; Pöhlmann, 2020). Após se ligar ao receptor ECA2 e entrar na célula, o SARS-CoV-2 libera seu RNA, que é traduzido pela maquinaria celular para produzir proteínas virais e replicar o genoma, permitindo a montagem de novos vírions que são liberados por exocitose para infectar outras células (V'kovski et al., 2021).

Após a interação com o receptor, a subunidade S1 do domínio de ligação ao receptor (RBD) reduz a expressão dos receptores ECA2, ao mesmo tempo em que aumenta a produção de angiotensina II, uma molécula reconhecida pelas suas ações vasodilatadoras e inflamatórias (Kuba et al., 2005). Com o aumento da angiotensina II, ocorre um agravamento da lesão tecidual devido ao aumento da permeabilidade vascular nos pulmões (Imai et al., 2005). Além disso, o SARS-CoV-2 é capaz de interagir com células apresentadoras de antígenos (APCs), facilitando a adesão às células dendríticas do hospedeiro (Attiq et al., 2024). Essa interação estimula a ativação de macrófagos e outras células do sistema imune, intensificando a produção e liberação de citocinas pró-inflamatórias (18). O acúmulo excessivo dessas moléculas, como TNF, IL-1α, IL-6, IL-7, IL-8, IL-9, IL-10, G-CSF, GM-CSF, IFN-γ, IP-10, MCP-1, MIP-1β, PDGF e VEGF, compromete a função celular, provoca danos nos tecidos viscerais e contribui para um

estado de inflamação sistêmica, característico da chamada "tempestade de citocinas", uma condição potencialmente fatal (Attiq et al., 2021, 2024; Lanza et al., 2020).

O Sistema Renina Angiotensina (SRA) é um regulador crítico do volume sanguíneo, equilíbrio eletrolítico e resistência vascular sistêmica (Fountain; Kaur; Lappin, 2025). Conforme ilustrado na Figura 1, a renina liberada pelo rim cliva o pré-pró-hormônio angiotensinogênio para formar angiotensina I (Ang-(1–10)). A angiotensina I é subsequentemente clivada pela atividade da enzima conversora da angiotensina (ECA) para a angiotensina II ativa (Ang-(1–8)), atuando nos receptores AT1 e AT2 (Ksiazek et al., 2024). Alternativamente, a angiotensina I é clivada diretamente através da neprilisina (NEP) para angiotensina-(1–7) (Ang-(1–7)), e através da ECA2 para Ang-(1–9), que é subsequentemente convertida para Ang-(1–7). Outra via importante é a conversão da angiotensina II para Ang-(1–7) pela ECA2. Ang-(1–7) medeia seus efeitos ligando-se ao receptor Mas. Posteriormente, pode ser clivada pela ECA para Ang-(1–5), e por descarboxilação para alamandina, um substrato de MrgDR. A clivagem subsequente resulta na formação de Ang-(1–7), Ang A e alamandina. A angiotensina II também é convertida para Ang III. Ang III, que é fonte para Ang IV, a qual pode se ligar ao receptos AT4 (Triebel; Castrop, 2024).

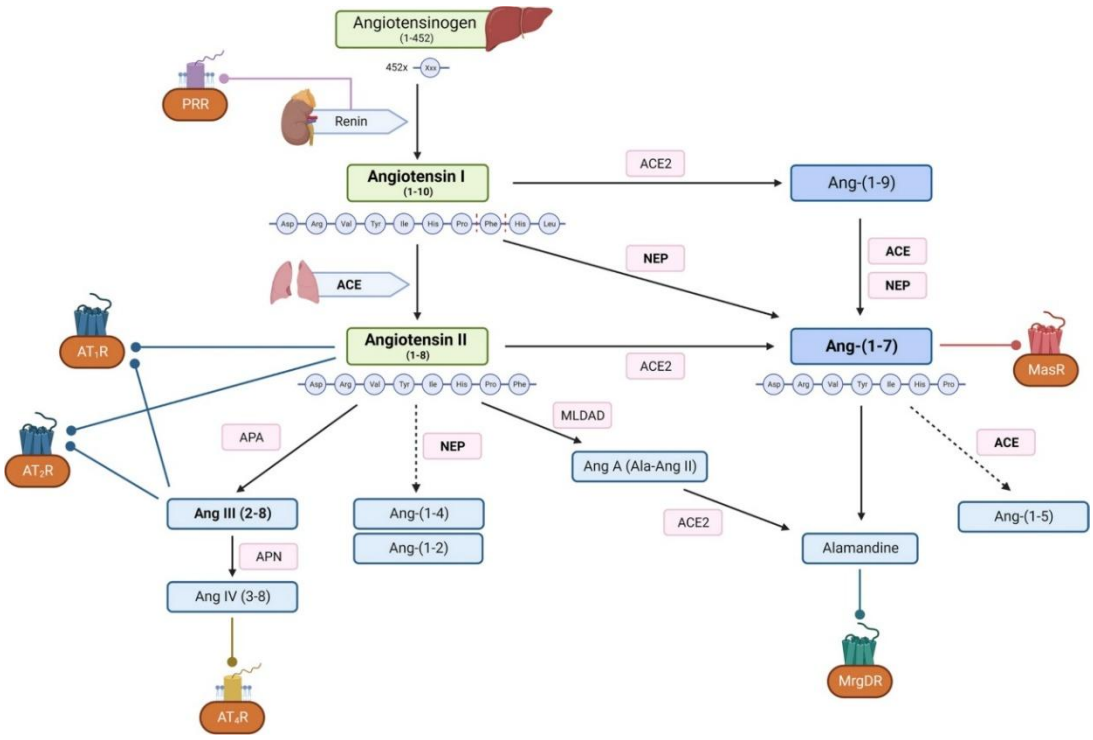

Figura 1. A cascata proteolítica do Sistema Renina Angiotensina: ACE, enzima conversora de angiotensina; ECA2, enzima conversora de angiotensina tipo 2; NEP, neprilisina; Ang, angiotensina; APA, aminopeptidase A; APN, aminopeptidase N; MLDAD, aspartato descarboxilase derivada de leucócitos mononucleares; PRR, receptor de prorenina; AT_1R, receptor de angiotensina II tipo 1; AT_2R, receptor de

angiotensina II tipo 2; AT_4R, receptor de angiotensina II tipo 4; MrgDR, membro D do receptor acoplado à proteína G relacionada ao Mas; MasR, receptor Mas. Fonte: Triebel H & Castrop H (2024) (Triebel; Castrop, 2024).

A enzima ECA 2 diminui os níveis de angiotensina II ao clivá-la no peptídeo classificador Ang-(1–7), que por sua vez, pode ativar o receptor Mas (MASR), promovendo vasodilatação e ação anti-inflamatória (Li; Zhang; Zhuo, 2017). A redução na expressão da ECA2 durante a infecção viral provoca um desequilíbrio no SRA, intensificando fatores pró-inflamatórios, principalmente nos pulmões (Issa et al., 2021). Em pacientes com COVID-19, os níveis elevados de angiotensina II apresentam uma correlação linear com a gravidade da lesão pulmonar e a carga viral, devido à redução de sua molécula contrarreguladora, Ang-(1–7) (Miesbach, 2020).

Anti-inflamatórios e antivirais representam os principais recursos terapêuticos contra a COVID-19 (“Therapeutics and COVID-19: living guideline”, 2025). Entre os anti-inflamatórios, os corticosteroides, como a dexametasona, são recomendados para pacientes com quadros graves ou críticos da doença (“Coronavirus disease (COVID-19)”, 2025; “Therapeutics and COVID-19: living guideline”, 2025). Seu mecanismo de ação envolve a ligação a receptores intracelulares de glicocorticoides, modulando a expressão gênica e inibindo a produção de citocinas pró-inflamatórias, como IL-6 e TNF (Johnson; Lopez; Kelley, 2025; Sharma, 2021). Vale mencionar ainda o Baricitinibe, inibidor seletivo das Janus quinases (JAK1 e JAK2), enzimas envolvidas na sinalização de citocinas pró-inflamatórias (Ahmad; Zaheer; Balis, 2025), e o tocilizumabe, anticorpo monoclonal que bloqueia o receptor de IL-6 (Preuss; Anjum, 2025). Ambos foram administrados em pacientes com COVID-19 como objetivo modular a resposta inflamatória exacerbada. Recentemente, Ang-(1-7) se destacou também pelos seus efeitos terapêuticos promissores em modelo pré-clínico de COVID-19, i.e. camundongos transgênicos superexpressando a ECA2 humana (K18-hACE2) infectados com SARS-CoV-2. O tratamento com Ang-(1–7) por via intraperitoneal atenuou a inflamação pulmonar e reduziu a carga viral, melhorando a sobrevivência dos camundongos (Lima et al., 2024). Um estudo clínico piloto randomizado de Ang-(1–7) administrado por via intravenosa em pacientes com COVID-19 grave foi sugestivo de uma resposta terapêutica benéfica, além de não evidenciar quaisquer eventos adversos (Wagener et al., 2022). Contudo, o uso terapêutico da Ang-(1–7) no tratamento de doenças pulmonares é limitado

pelo rápido metabolismo do peptídeo e necessidade de infusão contínua por longos períodos (Aleem et al., 2021; Furbish et al., 2024).

De acordo com a diretriz *Therapeutics and COVID-19: Living Guideline 2023*, que apresenta as recomendações mais atualizadas das estratégias terapêuticas para a COVID-19 e foi revisada em 29 de setembro de 2025 ("Therapeutics and COVID-19: living guideline", 2025), Lagevrio® (molnupiravir), Veklury® (remdesivir) e Paxlovid® (nirmatrelvir e ritonavir) são medicamentos antivirais efetivos no tratamento de pacientes com COVID-19 (Huang et al., 2022; "Medicamentos aprovados", 2021). O remdesivir (RDV) foi o primeiro medicamento antiviral aprovado pela *Food and Drug Administration* para o tratamento de pacientes com COVID-19 grave. A aprovação ocorreu em 22 de outubro de 2020, após análises de estudos clínicos que demonstraram sua eficácia na redução do tempo de recuperação de pacientes hospitalizados com COVID-19 (Pan et al., 2023).

O RDV (GS-5734) é um pró-fármaco fosforamidita de um análogo de nucleosídeo (GS-441524) cujo metabolito final atua como um inibidor da RNA polimerase dependente de RNA (RdRp), bloqueando assim o processo de replicação do genoma viral (Aleem; Kothadia, 2025; Pan et al., 2023). Devido à baixa solubilidade em água, o RDV (Veklury®) é produzido na forma de um complexo com a sulfobutiléter β-ciclodextrina para administração intravenosa (Gilead, 2020). Como ilustrado na Figura 2, após entrar na célula, o RDV sofre transformações metabólicas sucessivas: primeiramente, forma-se o metabólito de alanina (GS 704277), pela ação de enzimas do tipo fosforamidase, seguida da formação do nucleosídeo monofosfato e, finalmente, o nucleosídeo trifosfato, derivado do RDV. O metabólito ativo do RDV inibe o processo de replicação viral, pois é reconhecido e utilizado pela RdRp viral como um análogo da adenosina trifosfato, levando à interrupção prematura da síntese de RNA. Essa ação específica confere ao RDV uma eficácia direcionada contra vírus de RNA, tornando-o uma ferramenta importante no tratamento de infecções virais sistêmicas, especialmente em contextos clínicos graves, onde a rápida inibição da replicação viral é crucial para a redução da carga viral e prevenção da progressão da doença (Aleem; Kothadia, 2025; Chatterjee; Thakur, 2022; Gordon et al., 2020).

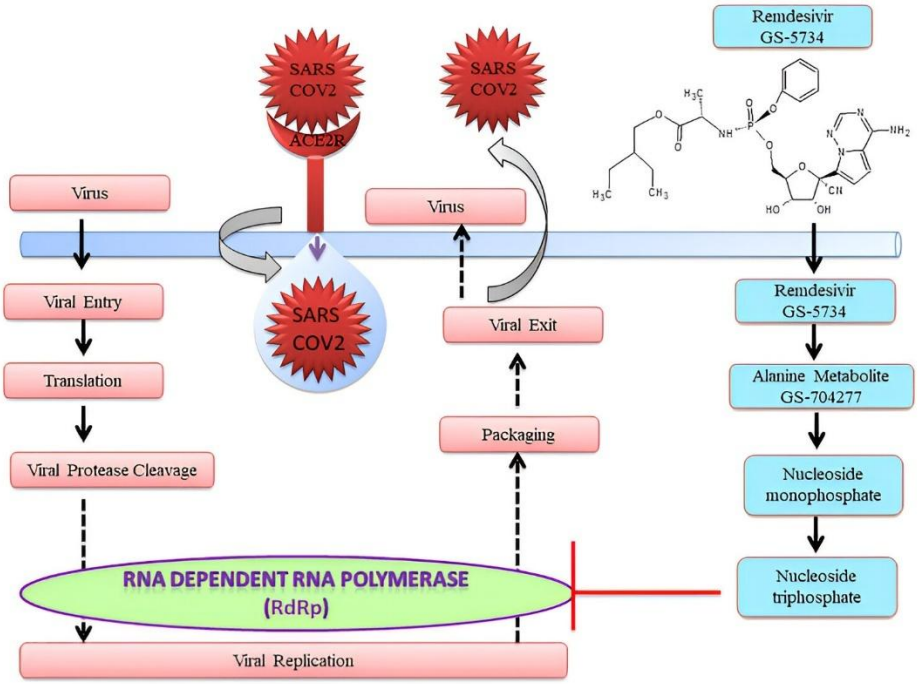

Figura 2. Representação esquemática do mecanismo de ação do remdesivir (GS 5734) na replicação do SARS-CoV-2, demonstrando sua ativação intracelular em metabólitos intermediários (alanina metabólito GS-704277, nucleosídeo monofosfato e nucleosídeo trifosfato). Fonte: Chatterjee B e Thakur SS (2022) (Chatterjee; Thakur, 2022).

A curta meia-vida plasmática e a instabilidade tecidual do RDV resultam em baixa distribuição e penetração nos tecidos, especialmente no pulmão e no cérebro (Chatterjee; Thakur, 2022; Richardson et al., 2020). O uso terapêutico do RDV na COVID-19 é limitado também pela sua elevada toxicidade, principalmente a nível hepático e renal (Aleem et al., 2021; Richardson et al., 2020).

Dadas as limitações do perfil farmacológico de Ang-(1–7) e RDV, diversas estratégias têm sido investigadas para viabilizar sua administração por vias não invasivas e otimizar o direcionamento para os tecidos-alvo. Assim, novas formulações e vias de administração foram propostas. Nesse contexto, a nanotecnologia aplicada à entrega de fármacos tem sido amplamente investigada, destacando-se pelas suas vantagens significativas em relação às abordagens convencionais. O uso de nanossistemas carreadores permite superar barreiras biológicas, prolongar a ação dos fármacos e melhorar o seu índice terapêutico, além de possibilitar novas abordagens terapêuticas, ampliando o alcance da medicina personalizada e minimamente invasiva (Salie; Saidi, 2024). Em relação a Ang-(1–7), vale mencionar uma formulação a base de ciclodextrina, que permite o peptídeo ser administrado por via oral (Marques et al., 2011). Para o RDV, formulações baseadas em lipossomas foram propostas visando uma administração inalatória (Li et al., 2021;

Vartak et al., 2021). No entanto, nenhuma dessas formulações chegou a ser avaliada pela sua eficácia em modelo pré-clínico da COVID-19.

Os lipossomas são vesículas esféricas, constituídas de uma ou mais bicamadas concêntricas de lipídeos, que formam compartimentos aquosos internos isolados do meio externo (Frézard et al., 2005). Como ilustrado na Figura 3, essas vesículas podem encapsular ativos hidrofílicos e hidrofóbicos (Luo et al., 2023), além de ser uma opção emergente para administração pulmonar de medicamentos devido à sua excelente biocompatibilidade com surfactantes alveolares (Trapnell et al., 2019). A fluidez da membrana e a eficiência de encapsulação do ativo são geralmente influenciadas pela composição lipídica da membrana (Li et al., 2021). Os lipossomas são veículos excepcionais para a administração de fármacos, pois oferecem proteção contra a degradação biológica (Antimisiaris et al., 2021; Liu; Chen; Zhang, 2022), prolongam a meia-vida dos ativos encapsulados e permitem o controle da liberação do fármaco, além de apresentarem excelente perfil de segurança (Chakravarty; Vora, 2021). A incorporação de lipídeo acoplado a polímero de etilenoglicol (PEG) na membrana lipossomal tende a aumentar a estabilidade coloidal da suspensão lipossomal. Tanto a PEGuilação, quanto o tamanho da vesícula influenciam a eficiência de captura celular (Figura 3). Além disso, sua capacidade de entrega seletiva ao local-alvo, por meio de mecanismos de direcionamento passivo e/ou ativo, reduz os efeitos colaterais sistêmicos, aumenta a dose máxima tolerada e potencializa a eficácia terapêutica (Liu; Chen; Zhang, 2022).

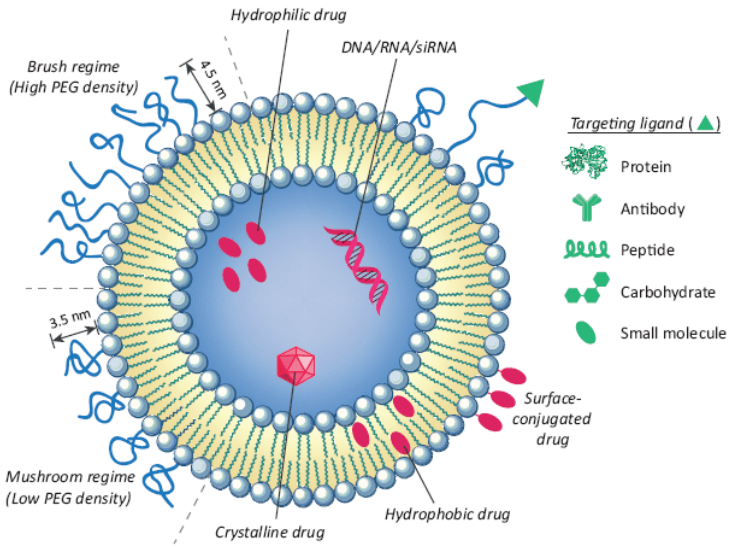

Figura 3. Representação esquemática de um lipossoma como nanossistema carreador de fármacos. Fonte: Kumar *et al,* (2021) ("(PDF) LIPOSOMES", 2024).

A via de administração intranasal surge como uma alternativa promissora, pois permite acesso direto aos pulmões (Salie; Saidi, 2024). Estima-se que cerca de 80% das partículas menores que 3 μm têm chance de entrar nas vias aéreas inferiores, e 50–60% delas acabam nos alvéolos (Elsayed; How; Foo, 2025). Além disso, a via intranasal tem se consolidado como uma rota estratégica para a administração de fármacos devido à sua extensa vascularização, elevada permeabilidade da mucosa e acesso direto ao sistema nervoso central pelas rotas olfatória e trigeminal (Chaturvedi; Kumar; Pathak, 2011; Hong et al., 2019). Essa via possibilita não apenas a obtenção de efeitos locais e sistêmicos rápidos, mas também o transporte direto para o cérebro (*nose-to-brain*), contornando a barreira hematoencefálica, o que a torna particularmente atraente para o tratamento de doenças respiratórias e neurológicas (Hong et al., 2019). No entanto, a mucosa nasal apresenta barreiras fisiológicas importantes, como a ação do clareamento mucociliar e a presença de enzimas degradativas, que limitam a biodisponibilidade de muitos fármacos (Chaturvedi; Kumar; Pathak, 2011).

Nesse contexto, os avanços na nanotecnologia possibilitaram o desenvolvimento de nanopartículas como sistemas inovadores para a entrega eficiente de ativo no cérebro (Chaturvedi; Kumar; Pathak, 2011; Elsayed; How; Foo, 2025; Hong et al., 2019; Jeong; Jang; Lee, 2023). Assim, o encapsulamento em nanopartículas, como lipossomas, potencializa a entrega de princípios ativos ao cérebro após administração intranasal, um efeito que parece estar diretamente relacionado ao aumento da estabilidade, da absorção e do tempo de permanência dos fármacos na cavidade nasal e no epitélio (Formica et al., 2022; Hong et al., 2019). Os lipossomas quando administrados por via intranasal, apresentam vantagens adicionais, como maior estabilidade, aumento do tempo de permanência na mucosa e melhoria na permeação trans-epitelial (Hong et al., 2019). Modificações de superfície, como o recobrimento com polímeros mucoadesivos (ex.: quitosana) ou a PEGuilação, podem otimizar o perfil farmacocinético e farmacodinâmico, modulando a mucoadesão, a biodistribuição e a segurança da formulação (Duong; Nguyen; Maeng, 2023). A escolha criteriosa do tamanho das vesículas (tipicamente entre 50–200 nm), do índice de polidispersão (idealmente <0,2) e da carga superficial é essencial para assegurar eficiência de entrega de fármacos e desempenho terapêutico (Li et al., 2021). Estudos pré-clínicos reforçam o potencial dos lipossomas intranasais na entrega de antivirais, anti-inflamatórios e até vacinas mucosas (Duong; Nguyen; Maeng,

2023; Li et al., 2021). Mais amplamente, as evidências apontam que os lipossomas intranasais constituem uma plataforma versátil e promissora para o desenvolvimento de terapias baseadas em nanoformulações direcionadas à mucosa respiratória e ao sistema nervoso central (Formica et al., 2022; Khan et al., 2017; Wu et al., 2023).

O objetivo geral desta tese foi desenvolver formulações lipossomais de Ang-(1-7) e RDV e avaliar sua eficácia terapêutica por via intranasal contra a infecção letal causada por SARS-CoV-2 em camundongos transgênicos K18-hACE2. Mais especificamente, procuramos desenvolver um método para encapsulação dos ativos em lipossomas e caracterizar as nanoformulações obtidas quanto à distribuição de tamanho de partículas, eficiência de encapsulação e cinética de liberação do ativo. Avaliamos a formulação do RDV pela sua citotoxicidade e atividade antiviral *in vitro* em comparação ao Veklury®. Realizamos estudos farmacocinéticos do RDV no plasma e no fluido de lavagem broncoalveolar após administração intranasal em camundongos. Ambas as formulações foram testadas por via intranasal em modelo murino de COVID-19, pelos seus efeitos na sobrevida dos animais, na carga viral no pulmão e cérebro, na resposta inflamatória no pulmão e possíveis efeitos indesejáveis. A eficácia do tratamento foi comparada àquela alcançada com o Veklury® por via parenteral. Este trabalho se justifica pela eficácia insuficiente e os efeitos indesejáveis dos tratamentos disponíveis para a COVID-19, o que aponta para a necessidade de desenvolver novas abordagens terapêuticas.

Apresento esta tese em dois capítulos, sendo cada um composto por um artigo, nos quais sou a primeira autora. Além disso, a tese resultou em dois pedidos de patente, cujos comprovantes de depósito estão anexados.

2 CAPÍTULO 1

INTRANASAL LIPOSOMAL ANGIOTENSIN-(1-7) ADMINISTRATION REDUCES INFLAMMATION AND VIRAL LOAD IN THE LUNGS DURING SARS-CoV-2 INFECTION IN K18-hACE2 TRANSGENIC MICE

AMERICAN SOCIETY FOR MICROBIOLOGY | Antimicrobial Agents and Chemotherapy

Antimicrobial Chemotherapy | Full-Length Text

Intranasal liposomal angiotensin-(1-7) administration reduces inflammation and viral load in the lungs during SARS-CoV-2 infection in K18-hACE2 transgenic mice

Sabrina Mendes,[1] Lays Cordeiro Guimarães,[1] Pedro Augusto Carvalho Costa,[1] Clara Couto Fernandez,[2] Maria Marta Figueiredo,[3] Mauro Martins Teixeira,[2] Robson Augusto Souza dos Santos,[1] Pedro Pires Goulart Guimarães,[1] Frédéric Frézard[1]

AUTHOR AFFILIATIONS See affiliation list on p. 13.

ABSTRACT To effectively reduce the health impact of coronavirus disease (COVID-19), it is essential to adopt comprehensive strategies to protect individuals from severe acute respiratory syndrome. In that sense, much effort has been devoted to the discovery and repurposing of effective antiviral and anti-inflammatory molecules. The endogenous peptide angiotensin-(1-7) [Ang-(1-7)] has been recently proposed as a promising anti-inflammatory agent to control respiratory infections. Liposomes also emerged as a safe and effective drug carrier system for local drug delivery to the lungs. In this context, the aim of this study was to develop a liposomal formulation of Ang-(1-7) [LAng (1-7)] and investigate its impact on animal survival as well as its antiviral and anti-inflammatory efficacies after intranasal administration in transgenic K18-hACE2 mice infected with SARS-CoV-2. The liposomal formulation was prepared by the ethanol injection method, exhibiting a mean diameter of 100 nm and a polydispersity index of 0.1. Following treatment of infected mice every 12 hours for 5 days, LAng (1-7) extended animal survival compared to the control groups that received either empty liposomes, free Ang-(1-7), or phosphate-buffered saline. Furthermore, the treatment with LAng (1-7) significantly decreased the viral load, as well as IL-6 and tumor necrosis factor levels in the lungs. Conventional treatment with remdesivir by parenteral route used as a positive control promoted similar effects, leading to improved survival rates and reduced viral load in the lungs without significant effects on IL-6 level. In conclusion, liposomal Ang-(1-7) emerges as a promising formulation to improve the treatment and decrease the severity of respiratory infections, such as COVID-19.

KEYWORDS angiotensin-(1-7), COVID-19, intranasal route, liposomes, K18-hACE2 mice, remdesivir, SARS-CoV-2

Viral epidemics or pandemics of acute respiratory infections represent a global threat. Examples are influenza caused by the H1N1 virus in 2009, severe acute respiratory syndrome (SARS) in 2003 and coronavirus disease (COVID-19) caused by SARS-CoV-2 in 2019 (1). SARS-CoV-2 has caused more than 7 million deaths worldwide, making it one of the deadliest viruses in human history (2), as reported by the World Health Organization (https://covid19.who.int/). Human coronaviruses are enveloped viruses that have a positive-sense, single-stranded RNA genome and have the spike protein (S) that is responsible for binding to the host cell through the angiotensin II-converting enzyme (ACE2) receptor, which is widely distributed in the respiratory tract cells (2). When the virus establishes invasion and replication in the lower respiratory tract, it can lead to SARS, characterized by inflammatory-mediated injuries due to exaggerated levels of pro-inflammatory cytokines and chemokines released into the air space and increased permeability of liquids and proteins through the lung endothelium (3).

Editor Miguel Angel Martinez, IrsiCaixa Institut de Recerca de la Sida, Barcelona, Spain

Address correspondence to Frédéric Frézard, frezard@icb.ufmg.br.

The authors declare no conflict of interest.

See the funding table on p. 14.

Received 5 June 2024
Accepted 20 September 2024
Published 29 October 2024

A huge challenge after the emergence of COVID-19 has been the discovery of effective therapies (4). Besides the discovery or repurposing of antivirals, such as remdesivir (5–7), progress toward effective anti-inflammatory and immunomodulatory substances was also achieved (4, 8). The endogenous peptide angiotensin-(1-7) [Ang-(1-7)] and agonists of its receptor, the Mas receptor, have been suggested as candidates to control the inflammatory response triggered by SARS-CoV-2 (9–12). The level of Ang-(1-7) in the lung is critical during SARS-CoV-2 infection, because ACE2, which converts angiotensin II into Ang-(1-7), is downregulated upon virus internalization (13). Thus, in COVID-19 patients, elevated levels of inflammatory angiotensin II and reduced levels of its counterregulatory molecule Ang-(1-7) were associated with severe lung injury and high viral loads (14). Previous studies on the therapeutic efficacy of Ang-(1-7) or Mas receptor activator in COVID-19 led to conflicting results. A randomized clinical trial with Ang- (1-7) intravenous infusion at 0.5 mg/kg of body weight/day did not show improvement in clinically relevant endpoints in severe COVID-19 (15), consistent with earlier findings in a small series of patients (16). On the other hand, a recent phase 1/2 clinical trial using Ang-(1-7) at a much lower dose (10 µg/kg of body weight/day) has suggested a potential beneficial effect in COVID-19 patients, with an increase in the number of oxygen-free days (17). A placebo-controlled phase 2/3 trial of a non-peptidic Mas receptor activator also showed promising results, with a reduced risk of a composite outcome, including death or respiratory failure (12). Furthermore, a recent report indicated that treatment of SARS-CoV-2-infected K18hACE2 mice with intraperitoneal (IP) Ang-(1-7) promoted a small reduction of virus load in the lungs of animals (18). A considerable number of studies in several animal models also demonstrated the anti-inflammatory and antimicrobial effects of the ACE2/Ang-(1-7)/Mas axis in acute lung injuries, including respiratory infections caused by *Mycoplasma pneumoniae* and influenza virus (19–21).

The encapsulation of Ang-(1-7) in liposomes was previously shown to markedly prolong its pressor effect following site-specific microinjection into the brain of rats (22). This long-lasting action was attributed to the protection of the heptapeptide from rapid enzymatic metabolism and the sustained drug-release properties of liposomes. Liposomes also represent safe and effective drug carrier systems for pulmonary administration due to excellent biocompatibility with alveolar surfactants, as well as the ability to encapsulate both hydrophilic and lipophilic active agents (23–25). This makes them an attractive choice for delivering drugs at effective concentrations to less accessible locations, including the alveoli of the lungs. Some of the nebulizable antimicrobial liposomal formulations include Arikace (amikacin) and Pulmaquin (ciprofloxacin) (25).

The aim of this study was to develop a liposomal formulation of Ang-(1-7) and investigate its impact on animal survival as well as its antiviral and anti-inflammatory activities after intranasal (IN) administration in K18-hACE2 transgenic mice infected with a lethal variant of SARS-CoV-2. Our results show that IN treatment with liposomal Ang-(1-7) formulation significantly improved animal survival and reduced the virus load in the lungs of infected mice in comparison to the negative control. The antiviral activity was associated with anti-inflammatory effects, as evidenced by the reduced levels of IL-6 and tumor necrosis factor (TNF) and the inhibition of leukocyte infiltration into the lungs. The efficacy of intranasal liposomal Ang-(1-7) was comparable to the commercial remdesivir formulation given parenterally.

MATERIALS AND METHODS

Reagents

Angiotensin-(1-7) was obtained from Bachem (CA, USA). Soybean phosphatidylcholine (SPC, Phospholipon90G) was obtained from Lipoid (Ludwigshafen, Germany). Veklury (RDV-SBE) was purchased from Gilead Sciences Farmacêutica do Brasil Ltda.

Preparation of the liposomal formulations

The liposome formulation of Ang-(1-7) [LAng (1-7)] was prepared by the ethanol injection method followed by extrusion, as previously described (26, 27). Briefly, 97 mg of SPC was first added in 100 µL of absolute ethanol; after dissolution at 40°C, the resulting organic phase was injected using a fine needle syringe into 1 mL of phosphate-buffered saline (PBS) (0.15 M NaCl and 10 mM phosphate, pH 7.2) containing 1 mg of Ang-(1-7). The suspension was maintained at room temperature under magnetic stirring for 10 min. Empty liposomes (LEmp) were obtained using the same method but omitting Ang-(1-7). The resulting suspensions were then extruded (5×) through polycarbonate membranes with gradually reduced pore sizes (200 and 100 nm) using the Liposofast LF-12 device (Avestin, Canada) to achieve vesicles with calibrated size. Finally, liposome suspensions were subjected to dialysis using a 15-kDa MWCO membrane (Spectra/Por) for 2 hours at 4°C against PBS to remove ethanol and part of the non-encapsulated peptide. The Ang- (1-7)-containing and empty liposomal suspensions to be administered intranasally in animals were further concentrated (1.8-fold) using a 50-kDa Amicon Ultra0.5 filtration device at 14,000 × *g* for 30 min at 4°C. To determine the amount of encapsulated Ang-(1-7), the suspension was further dialyzed for 24 hours at 4°C against PBS.

Physicochemical characterization of liposomal formulation

The mean hydrodynamic diameter, polydispersity index (PDI), and zeta potential (ζ) of the liposomal formulations were determined using Zetasizer Nano ZS90 (Malvern Instruments, Malvern, UK). The samples were accurately diluted, i.e., 10 µL of liposomal suspensions in 990 µL of PBS for size and zeta potential measurements. The diluted samples were loaded into disposable cuvettes and analyzed at 25°C.

Determination of Ang-(1-7) in the liposomal formulation

Ang-(1-7) was quantified in the liposomal formulation exploiting the intrinsic fluorescence of the peptide, as previously described (22). Briefly, 50 µL of the liposome suspension was added to a quartz cuvette containing 2.2 mL of methanol, and fluorescence intensity was recorded with an excitation wavelength of 285 nm and emission at 300 nm, using a fluorescence spectrophotometer (Eclipse, Varian, USA). The peptide concentration was determined from a calibration curve. The fluorescence intensity vs concentration curve was found to be linear, and no significant interference of the lipid matrix was observed. The encapsulation efficiency of the peptide was calculated after recording the fluorescence intensity before (Fi) and after dialysis (Ff), as follows: EE% = 100 × (Ff − Fo)/(Fi − Fo), where Fo represents the fluorescence intensity of the peptide-free blank formulation.

Release kinetics of Ang-(1-7) from liposomes

The release study of Ang-(1-7) from liposomes was performed under dialysis conditions at 37°C. Just after the preparation of liposomal formulation, the resulting suspensions were divided into triplicates of 1 mL and added to Spectra-Por Float-A-Lyzer G2 MWCO 100 kDa maintained in beaker containing 50 mL of PBS under magnetic stirring at 37°C. A total of 50 µL of the dialyzed suspension was withdrawn at intervals of 0, 1, 2, 3, 6, and 24 hours and added to 2.2 mL of methanol for fluorescence reading as described above. The percentage of retained Ang-(1-7) was calculated at different time intervals. The data obtained with each formulation were fitted using monoexponential decay model, allowing the determination of the release half-time.

In vivo assays of liposomal Ang-(1-7) efficacy

Cells and mice

African green monkey kidney cells (Vero E6) were cultured in RPMI medium supplemented with 10% fetal bovine serum (FBS, GIBCO, Thermo Fisher Scientific), 100 U/mL

penicillin and streptomycin, and 0.25 µM amphotericin B and maintained in a 5% CO_2 incubator at 37°C. The SARS-CoV-2 gamma lineage P.1 (EPI_ISL_13017802) was kindly provided by Dr. Sergio Caldas from Fundação Ezequiel Dias-FUNED-MG and grown at the Biosafety Level 3 (BSL-3) laboratory of the Institute of Biological Sciences of Universidade Federal de Minas Gerais (UFMG). Viral stocks were cultured in Vero CCL81 cells in a humidified incubator at 37°C with 5% CO_2 and monitored daily for cytopathic effects for up to 72 hours. The viruses were titrated in Vero E6 cells using the plaque-forming units (PFU) assay (28), and viral aliquots were stored at −80°C for later use.

Transgenic C57BL/6j mice expressing the human ACE2 receptor, driven by the cytokeratin-18 gene promoter (K18-hACE2), were originally obtained from The Jackson Laboratory. Mice were group-housed at the Bioterio do Laboratório de Imunofarmacologia (Departamento de Bioquímica-Imunologia, ICB-UFMG), and experiments with SARS-CoV-2 were performed in the animal facility of the BSL-3 laboratory at UFMG. Mice were fed with standard diets, and maintained on a 12-hour light/dark cycle with 50%–58% humidity and a temperature of 25°C.

Infection and mice treatment

K18-hACE2 mice infected with SARS-CoV-2 were used as a preclinical model of COVID-19, as described previously (29, 30). Mice of different ages (11–12 weeks) of both sexes were infected with 6×10^4 PFU of SARS-CoV-2 intranasally. In the first experiment, treatment was initiated 8 hours post-infection with IN LAng (1-7) [0.73 mg of Ang-(1-7)/kg of body weight with 15 µL in each nostril], IN free Ang-(1-7) in PBS [same dose, volume, and route as LAng (1-7)], or IN PBS as vehicle (same volume and route as treated groups) and repeated every 12 hours for 6 days (n = 7–8/group). The dose of Ang-(1-7) was based on a previous work in which Ang-(1-7) was active in repressing inflammation in the murine model at 0.3 mg/kg of body weight (31). Mice were monitored daily for 15 days by measuring lethality rates. In a second set of experiments, treatment was initiated 8 hours post-infection with IP Veklury (20 mg/kg of body weight), IN LAng (1-7) [0.73 mg of Ang-(1-7)/kg of body weight, with 15 µL in each nostril], IN LEmp [same lipid dose as that in LAng (1-7)], and IN vehicle (PBS) and repeated every 12 hours for 5 days (n = 8/group). Uninfected mice (Mock) were acclimated for control purposes. Mice were monitored daily for 15 days by measuring body weight loss and lethality rates. In a parallel experiment with the same groups (except for the LEmp group), eight mice of each group were euthanized at 5 days post-infection. Lungs were harvested to assess viral load, production of inflammatory mediators, cell response, and histopathological changes. The kidney and brain were also collected for viral titer determination.

Viral loads by plaque assay

Mouse tissues were weighed and homogenized with magnetic beads (Thermo Fisher Scientific) in a TissueLyser LT equipment (Qiagen-Life Science Instruments) in 1 mL of RPMI medium supplemented with 2% FBS. Tissue homogenates were clarified by centrifugation at 10,000 × g for 5 min and stored at −80°C. Vero E6 cells were seeded at a density of 2.5×10^5 cells/well in 12-well flat-bottom tissue culture plates. The next day, the medium was removed and replaced with 100 µL of serial dilutions of the material to be titrated, diluted in RPMI with 1% FBS. One hour later, a fresh semisolid medium containing 1.5% carboxymethylcellulose was added. The plates were incubated for 72 hours and then fixed with 10% formaldehyde (final concentration) in PBS for 20 min. The plates were stained with 0.05% (wt/vol) crystal violet in 20% methanol and washed twice with distilled, deionized water. The results are expressed as PFU/g of tissue.

Viral loads by RT-qPCR

RNA was isolated from lung homogenates as described above and extracted using a QIAamp Viral RNA Mini Kit (QIAGEN, Inc., Valencia, USA) according to the manufacturer's instructions and quantified spectrophotometrically using the Nanodrop Lite (Thermo

Fisher Scientific). Subsequently, 500 ng of total RNA was subjected to cDNA synthesis with high-capacity cDNA reverse transcription kits (ThermoFisher Scientific) according to the manufacturer's instructions and stored at −20°C. Molecular diagnosis for SARS-CoV-2 detection (primer N1) was performed according to the manufacturer's instructions of the iTaq Universal Probes One-Step Kit. Real-time PCR was performed using the Quant Studio 3 (ThermoFisher Scientific). The PCR steps were as follows: 95°C for 3 min, followed by 40 cycles at 95°C for 15 s and 60°C for 1 min. Standard curves and negative controls were used to validate the method.

Immunofluorescence assay

To evaluate the presence of the virus in lung tissue by immunofluorescence, lungs from treated and control groups were collected for the preparation of cryosections of 5 µm thickness. Samples were stained with a specific antibody for SARS-CoV-2 (1:500, no. 40591-t62, 2019-nCoV Spike RBD Antibody, Sino Biological) and a secondary rabbit anti-goat Alexa Fluor 633 antibody (1:100, ThermoFisher Scientific, no. A-21052), and then incubated overnight at 4°C. Nuclei were stained with DAPI, and slides were mounted in Dako fluorescence mounting medium (Dako, Santa Clara, CA, USA). Images were acquired on a confocal microscope (Zeiss LSM 880, Germany) with a 63× immersion objective, using a 633 nm laser, at the Center for Image Acquisition and Processing (CAPI - UFMG).

ELISA assay of proinflammatory cytokines

Lung tissue was used to determine the concentration of secreted cytokines (TNF and IL-6). Homogenates were prepared and clarified by centrifugation at 2,500 rpm for 5 min. All samples were serially diluted, and standard curve and negative controls were used to validate the method. The assay was performed using mouse TNF and IL-6 DuoSet ELISA kits (R&D Systems, Inc., USA) according to the manufacturer's recommendations.

Flow cytometry assay of lymphoid and myeloid cells

Lungs were harvested, and lung homogenates previously digested with Collagenase I were cultured overnight in the presence of Brefeldin A (Golgi Stop, BD) to inhibit cytokine secretion in culture. Cells were washed twice with PBS, centrifuged at 300 × *g* for 10 min to remove soluble protein in the culture medium, and incubated with cell viability reagent (Live/Dead Fixable Dead Cell Stains) as recommended by the manufacturer (Invitrogen). The cell suspension was stained with two panels containing antibodies for the evaluation of activated T cells producing cytokines of the Th1, Th2, and Th17 profiles and cytokine-producing myeloid cells (Table S1). The panel for T cell evaluation consisted of antibodies against surface molecules diluted in PBS containing 0.1% BSA and 2 mM azide (FACS buffer): anti-CD45, anti-CD3, anti-CD4, anti-CD8, and their respective cytokines (Table S1). Incubation with the extracellular antibodies was performed for 20 min, and the cells were then washed twice by centrifugation for 4 min at 300 × *g* with FACS buffer (PBS, 0.1% BSA, and 2 mM azide). For myeloid cell characterization, the panel consisted of antibodies against surface molecules diluted in FACS buffer: anti-CD45, anti-CD11b, anti-F4/80, anti-Gr-1, and anti-CD206 (Table S1). Incubation with the extracellular antibodies was performed for 20 min, and the cells were then washed twice by centrifugation for 4 min at 300 × *g* with FACS buffer. Finally, the cell suspension previously stained with biotinylated anti-Gr-1 antibody was revealed. A new wash was performed for 4 min at 300 × *g*, and the cells were then incubated for 15 min with streptavidin. The cells were acquired on the LSR Fortessa cytometer (BD Pharmingen). FlowJo 10 (TreeStar) software was used for data analysis.

Histopathological evaluations

Histological changes related to the injury caused by SARS-CoV-2 and treatments were analyzed in the lungs of mice. Tissues of mice were fixed in 10 mL of 10%

neutral-buffered formalin. Paraffin blocks of collected tissues were prepared, cut into 5 µm thickness sections, and stained with hematoxylin and eosin for microphotograph analysis. Histopathological evaluation was performed using a score for each anatomical region. Lung samples were scored for acute inflammation in the lung parenchyma. Pleura and bronchi were scored for thickness and infiltrate, alveoli were scored for edema, thickness, and infiltrate, and vessels for thickness, infiltrate, and congestion. Score was established as: 0, for no alteration; 1, for discrete change (0%–25%); 2, for moderate changes (25%–50%); and 3, for intense changes (50%–100%).

Statistical analyses

Data are presented as means ± SEM or medians ± 95% confidence interval. Data normal distribution was checked with the following tests: Anderson–Darling test and D'Agostino and Pearson test. Statistical analysis of normally distributed data was performed using one-way ANOVA with Dunnett's multiple comparison post-test or two-way ANOVA with Tukey's multiple comparison post-test. For non-parametric data, Kruskal-Wallis's test followed by Dunn's multiple comparison post-test was used. Survival curves were analyzed using the Kaplan-Meier test and compared using log-rank (Mantel-Cox) test. Values of $P < 0.05$ were considered significant. The graphics and statistical analyses were performed using GraphPad Prism software (version 10, GraphPad Software, San Diego, CA, USA).

RESULTS

Preparation and characterization of liposomal Ang-(1-7) formulation

LAng (1-7) and LEmp liposomal formulations were prepared from soybean phosphatidylcholine by the ethanol injection method followed by extrusion. Table 1 displays the main characteristics of the final liposomal formulations. The formulations showed vesicles with a mean diameter of about 100 nm and essentially monodisperse (PDI < 0.1). The zeta potential was found to be close to zero, as expected from the zwitterionic character of phosphatidylcholine. The peptide encapsulation efficiency was about 13%. A study of the kinetics of release of Ang-(1-7) from liposomes at 37°C in dialysis conditions against PBS evidenced sustained peptide release from liposomes, with an estimated half-time of 9.3 ± 2.7 hours (Fig. 1).

Impact of treatment of infected mice with LAng (1-7) on animal survival

To evaluate the therapeutic efficacy of liposomal LAng (1-7) formulation given by IN instillation, K18-hACE2 transgenic mice infected with SARS-CoV-2 were used as a preclinical model. In the first experiment, a comparison was made with a free peptide solution at the same dose or the vehicle (PBS) given by the IN route. As shown in Fig. 2, treatment with LAng (1-7) significantly prolonged the survival of mice, compared to the vehicle, and 25% of treated mice survived at the end of the evaluation period. On the other hand, treatment with the free peptide did not prevent animal death, nor did it affect animal survival compared to the PBS control.

In the second experiment, a comparison was made with IP remdesivir (Veklury), as well as empty liposomes or PBS by IN route. Animals were treated every 12 hours for 5 days (Fig. 3A). A non-infected and non-treated group (Mock) was also used as a control. Figure 3 shows the survival rate (Fig. 3B) and body weight change (Fig. 3C and D)

TABLE 1 Characteristics of particle size, zeta potential, and peptide encapsulation efficiency of LAng (1-7) and LEmp formulations

Liposome	Size (nm) ± SD[a]	PDI ± SD[a]	Potential ζ (mV) ± SD[a]	EE% ± SD[a]
LAng (1–7)	99.9 ± 1.7	0.018 ± 0.009	−2.96 ± 0.04	13.4 ± 0.8
LEmp	101.1 ± 2.7	0.016 ± 0.006	−5.45 ± 0.08	N/A[b]

[a]Size, mean hydrodynamic diameter; PDI, polydispersity index; ζ, zeta potential (ζ); EE%, drug encapsulation efficiency; for liposomes containing Ang-(1-7) and empty liposomes (mean ± SD, $n = 3$).
[b]N/A, not applicable.

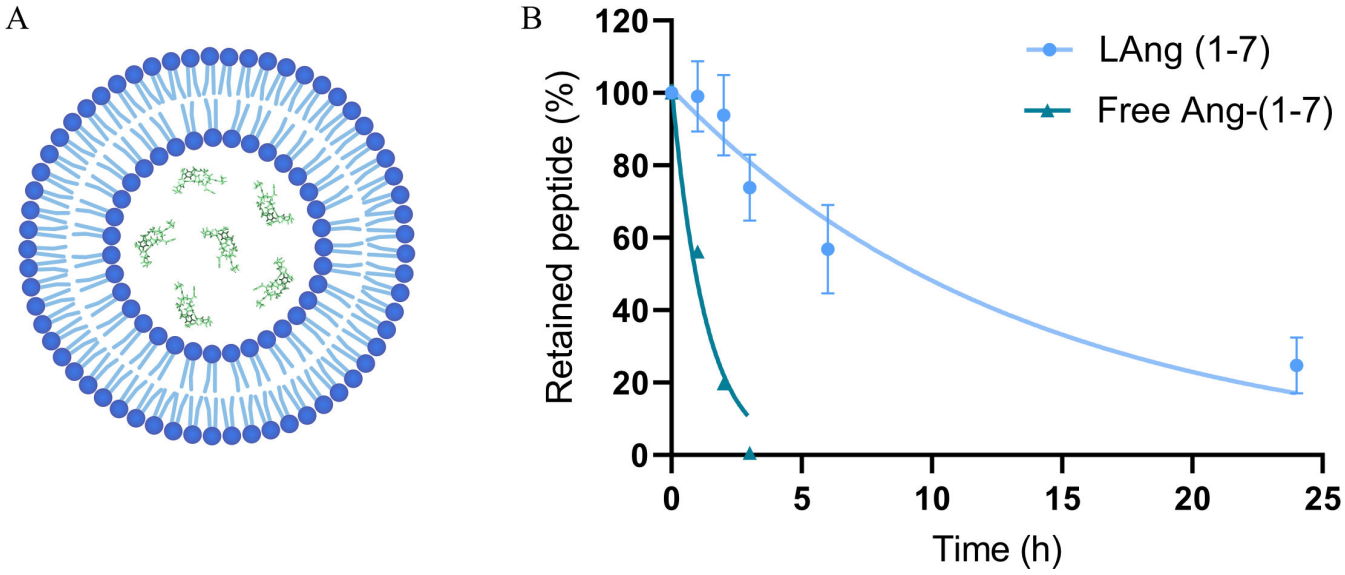

FIG 1 Kinetics of release of Ang-(1-7) from liposomes in dialysis condition against PBS at 37°C. Free (non-encapsulated) peptide was used as a control. (A) Schematic representation of a liposome incorporating the heptapeptide. (B) Data show the percentage of peptide retained in the dialysis tube as means ± SD of three independent experiments. Data were fitted according to monoexponential decay model.

of infected mice, during and after treatment. Treatments with LAng (1-7) and Veklury significantly prolonged the survival rate of mice with median survivals of 6 and 8 days, respectively, in comparison to LEmp and PBS groups (median survival of 5 days). Even if there was a difference between LAng (1-7) and Veklury groups regarding the final number of surviving animals (1 vs 3), suggesting higher efficacy of Veklury treatment, comparison of the survival curves between the two groups using log-rank (Mantel-Cox)

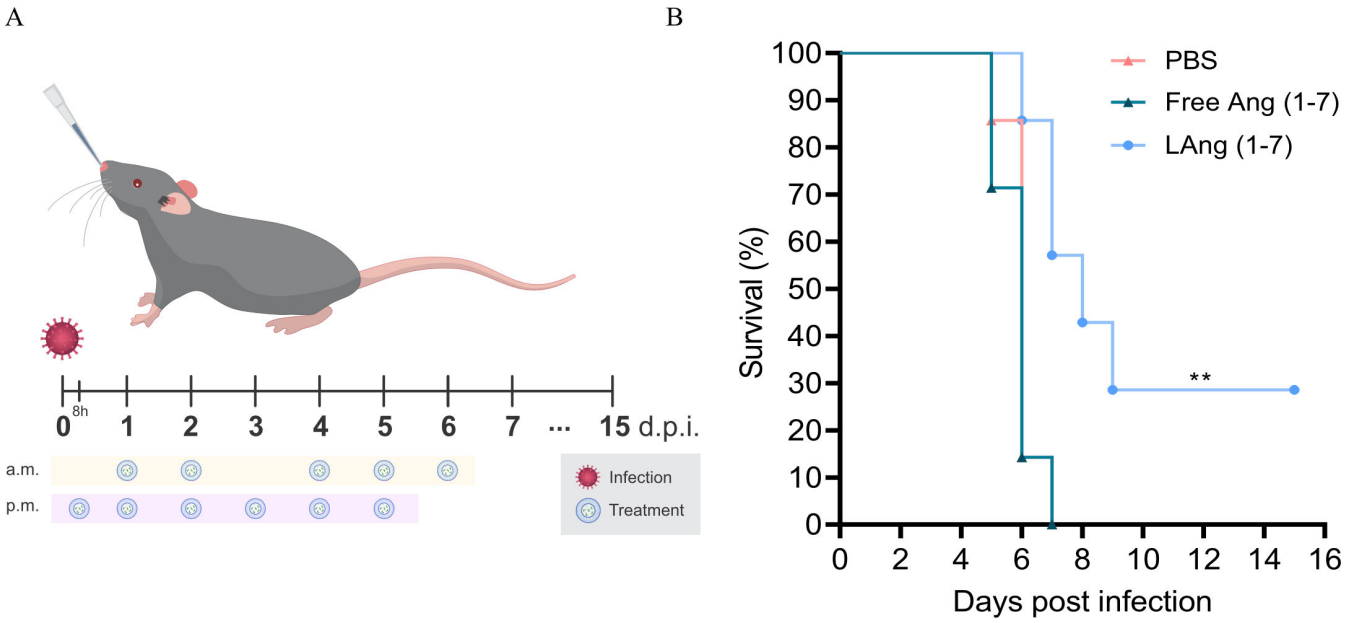

FIG 2 Survival rate of SARS-CoV-2-infected K18-hACE2 mice after treatment intranasally with LAng (1-7) or the free Ang-(1-7) peptide. K18-hACE2 transgenic mice were intranasally inoculated with SARS-CoV-2. (A) Schematic representation of the experimental protocol. (B) Survival rate. Treatment was started 8 hours after infection and carried out every 12 hours for 6 days. Experimental groups were (n = 7–8) LAng (1-7) at 0.73 mg of peptide/kg/dose IN, Ang-(1-7) in PBS at 0.73 mg of peptide/kg/dose IN and PBS IN control. Animal survival was registered on each day. Survival curves were analyzed using the Kaplan-Meier test and compared using log-rank (Mantel-Cox) test. $^{**}P < 0.01$.

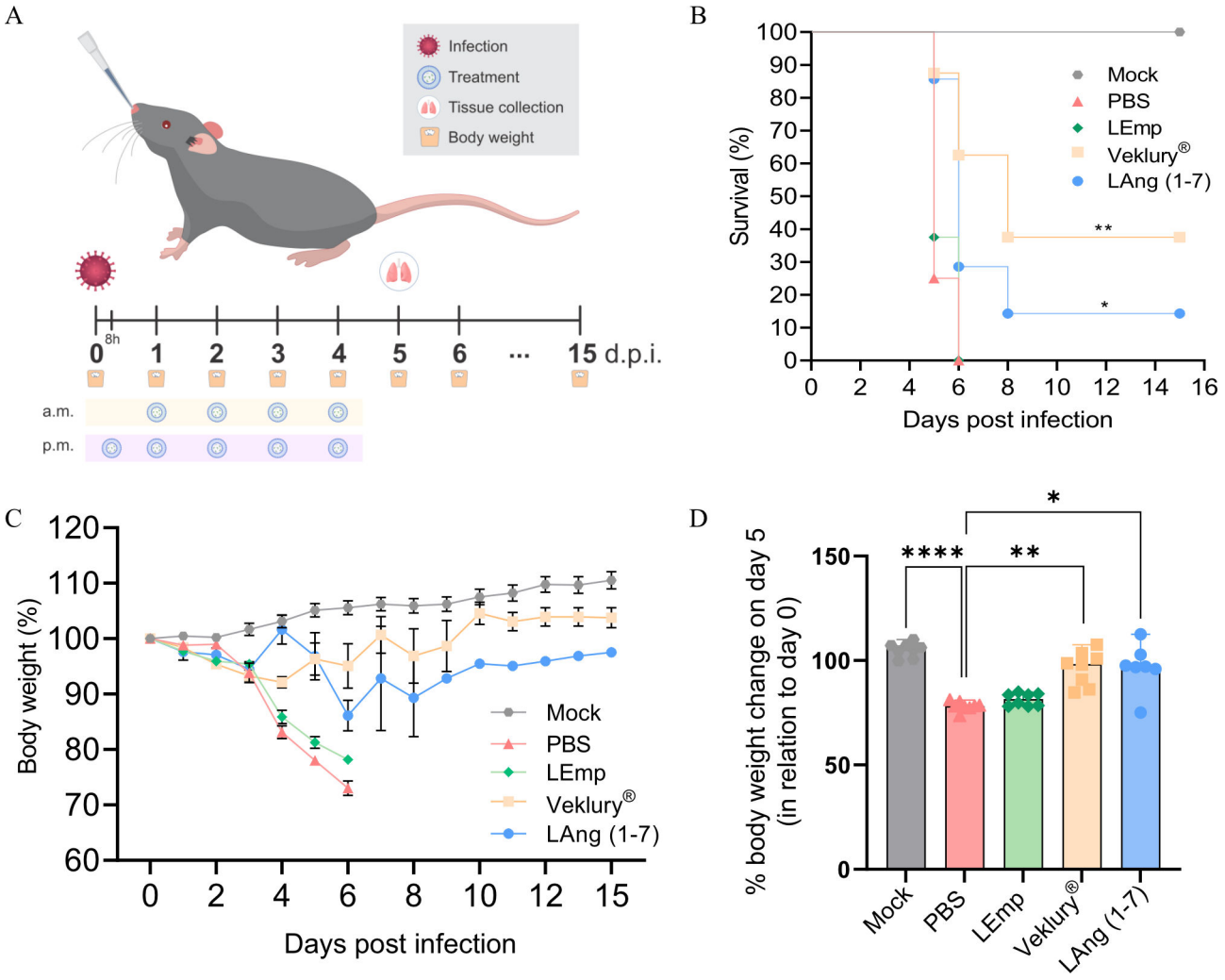

FIG 3 Clinical features of SARS-CoV-2-infected mice after treatment with intranasal LAng (1-7) or intraperitoneal remdesivir, in comparison with intranasal PBS and LEmp. (A) Schematic representation of the experimental protocol. Survival rate (B) and weight change (C and D) of SARS-CoV-2-infected mice during and after treatment. K18-hACE2 transgenic mice (n = 8) were intranasally inoculated with SARS-CoV-2. Treatment was started 8 hours after infection and carried out every 12 hours for 5 days. Experimental groups were LAng (1-7) at 0.73 mg of peptide/kg/dose IN, Veklury at 20 mg of remdesivir/kg/dose IP, LEmp IN at the same lipid dose as LAng (1-7), and PBS IN. A non-infected and non-treated group (Mock) was also used as a control. Animal survival and body weight were registered on each day. Survival curves were analyzed using the log-rank (Mantel-Cox) test. The average body weights were compared using two-way ANOVA followed by Dunnett's post-test. *P < 0.05; **P < 0.01; and ****P < 0.0001.

test showed no significant difference. LEmp and PBS groups showed marked weight loss during the 5 days following infection, in comparison with the Mock group. It is also noteworthy that treatments with LAng (1–7) and Veklury significantly decreased the body weight loss, in comparison to PBS (Fig. 3D). In addition to weight loss, the mice were lethargic and had difficulty breathing, in accordance with previous report (32). Thus, these first data demonstrate that treatment with LAng (1-7) promoted a significant clinical improvement of mice infected with SARS-CoV-2, compared to control animals, in a way comparable to Veklury-treated mice.

Impact of treatment of infected mice with LAng (1-7) on the viral load

Viral titers in the lung tissue of infected animals were next evaluated. Mice were treated as described above and submitted to euthanasia at 5 days post-infection, the peak of lung disease. Three different methods to assess viral titers were used: detection of viable

particles by plaque assay, RT-qPCR for viral RNA levels, and immunofluorescence of the viral S protein. As shown in Fig. 4, the plaque assay (Fig. 4A) and RT-qPCR (Fig. 4B) showed significant reductions of viral titers in LAng (1-7) and Veklury groups in comparison to the control PBS group. The immunofluorescence assay using a spike RBD antibody (Fig. 4C) revealed intense staining (pink spots) in PBS lung tissue samples and almost no staining in LAng (1-7) and Veklury samples, further supporting the reduction of the virus load. Evaluation of viral titers in the brain and kidney of animals showed high viral loads in the brain and low titers in the kidney. Furthermore, no significant effect of treatments on the viral titers in these tissues was observed (Fig. S1).

Impact of treatment of infected mice on inflammatory response in the lungs

Pro-inflammatory cytokines

To gain insight into the mechanism of the protective and antiviral actions of liposomal Ang-(1-7), we further evaluated the impact of treatment on the levels of pro-inflammatory cytokines IL-6 and TNF, which are known to be increased in the lungs of K18-hACE2 mice after infection with SARS-CoV-2 (29). As shown in Fig. 5, treatment with IN LAng (1-7), but not IP remdesivir, promoted a significant reduction in IL-6 level in comparison

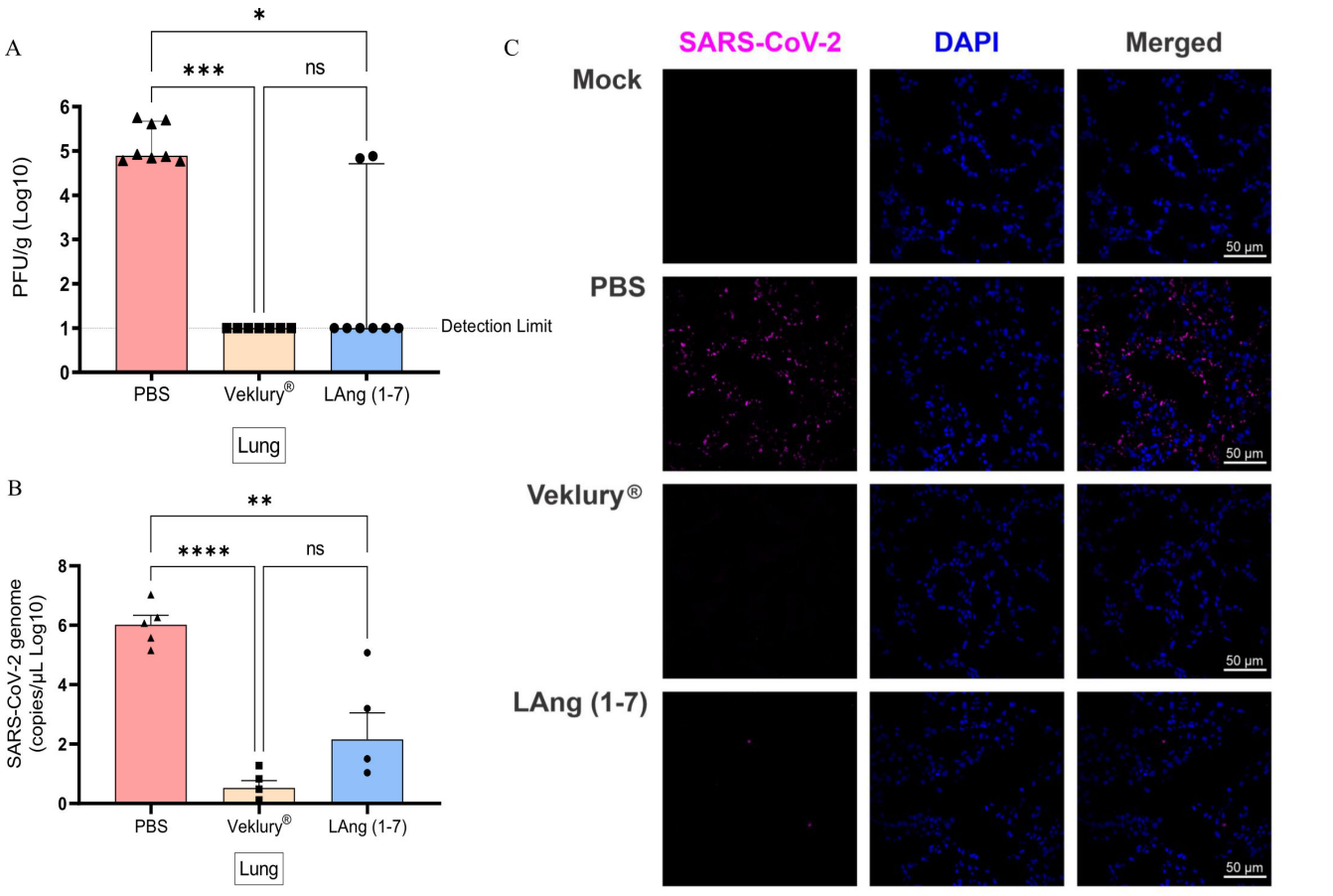

FIG 4 Viral titers in the lung of SARS-CoV-2-infected mice after treatment with intranasal LAng (1-7) or intraperitoneal remdesivir, in comparison with intranasal PBS. (A) Viral titers by limiting dilution plaque assay for viable virus (n = 8). (B) Viral loads by RT-qPCR for viral RNA levels (n = 5). (C) Representative immunofluorescence images of lungs. K18-hACE2 transgenic mice (n = 8) were intranasally inoculated with SARS-CoV-2. Treatment was started 8 hours post-infection and carried out every 12 hours for 5 days. Experimental groups were LAng (1-7) at 0.73 mg of peptide/kg/dose IN, Veklury at 20 mg of remdesivir/kg/dose IP, and PBS IN. Animals were euthanized 12 hours after the last dose. The dashed horizontal line indicates the detection limit. Data are shown as means ± SEM or medians ± 95% confidence intervals and are compared using one-way ANOVA followed by Tukey's post-test (RT-qPCR) or Kruskal-Wallis followed by Dunn's post-test (limiting dilution data), respectively. *P < 0.05; **P < 0.01; ***P < 0.001; and ****P < 0.0001.

to PBS control. On the other hand, both LAng (1-7) and remdesivir groups showed a reduction in TNF levels compared to the control. Thus, our data suggest that IN LAng (1-7) formulation is capable of attenuating the exacerbated pulmonary inflammatory response.

Myeloid and lymphoid cells

To further support the anti-inflammatory action of LAng (1-7) in the lungs, myeloid and lymphoid cells were investigated by cytometry. As shown in Fig. 6, myeloid cells ($CD45^+CD11b^+$) and inflammatory monocytes expressing $CD206^+$ and $iNOS^+$ ($CD45^+CD11b^+Gr^{-1}$-$F4\_80^+CD206^+$ and $CD45^+CD11b^+Gr^{-1}$-$F4\_80^+iNOS$) were significantly reduced in LAng (1-7) group, when compared to PBS. This is in contrast with Veklury, which produced no significant change. Accordingly, the level of leukocytes in LAng (1-7) was significantly lower than that in Veklury group. In T cell subsets, $CD8^+$ T cells showed a significantly lower recruitment and ability to secrete IL-4 and IL-17 in LAng (1-7) when compared to the Veklury group (Fig. S2). $CD4^+$ T cells releasing IL-4 and IL-17 were also significantly reduced in the LAng (1-7) group, when compared to PBS control. These data taken altogether further support the anti-inflammatory action of LAng (1-7).

Histopathological evaluations of the lung were also performed to establish a score. Accordingly, all infected groups showed discrete to moderate changes, including cell infiltrate and vessel congestion, whereas no change or discrete change was observed in non-infected mice (Fig. S3). No significant difference was found between PBS, LAng (1-7), and Veklury groups.

DISCUSSION

The present work reports the therapeutic efficacy of LAng (1-7) formulation by IN route in a well-established transgenic mouse model of COVID-19. This work describes the preparation of a liposomal Ang-(1-7) formulation from soybean phosphatidylcholine using the simple ethanol injection method. In a previous study, evidence was provided

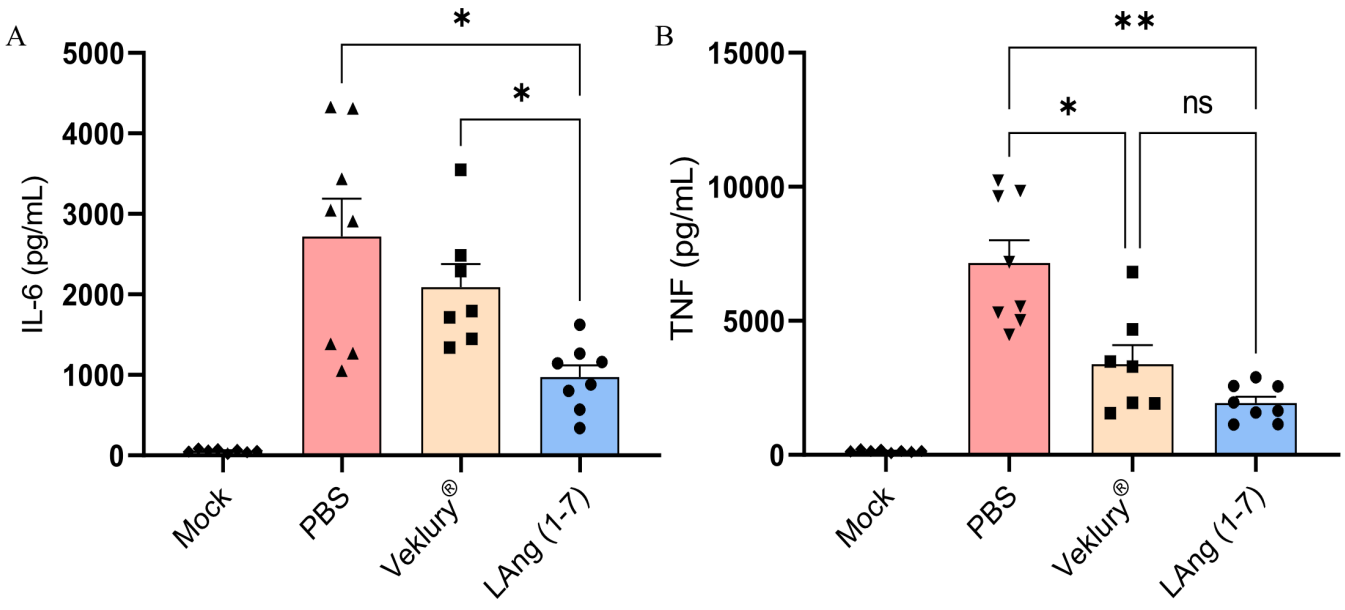

FIG 5 IL-6 (A) and TNF (B) levels in the lung of SARS-CoV-2-infected mice after treatment with intranasal LAng (1-7) or intraperitoneal remdesivir, in comparison with intranasal PBS. K18-hACE2 transgenic mice ($n = 8$) were intranasally inoculated with SARS-CoV-2. Treatment was started 8 hours post-infection and carried out every 12 hours for 5 days. Experimental groups were LAng (1-7) at 0.73 mg of peptide/kg/dose IN, Veklury at 20 mg of remdesivir/kg/dose IP, and PBS IN. A non-infected and non-treated group (Mock) was also used as a control. Animals were euthanized 12 hours after the last dose. The levels of IL-6 and TNF were determined by ELISA. Data are shown as means ± SEM and are compared using the Brown-Forsythe ANOVA test followed by Dunnett's T3 post-test. *$P < 0.05$ and **$P < 0.01$.

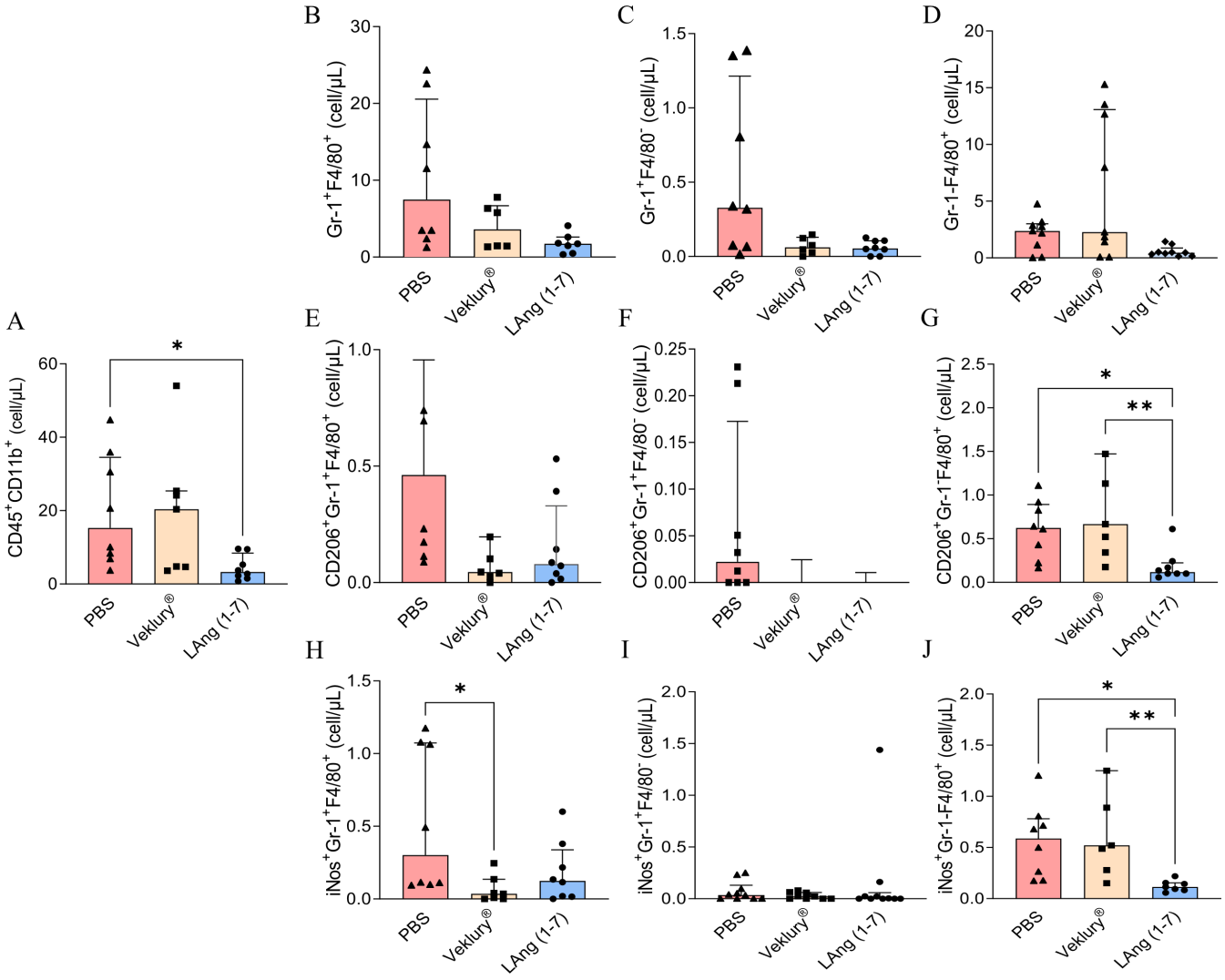

FIG 6 Myeloid cells' profile in the lung of SARS-CoV-2-infected mice after treatment with intranasal LAng (1-7) or intraperitoneal remdesivir, in comparison with intranasal PBS. K18-hACE2 transgenic mice (n = 8) were intranasally inoculated with SARS-CoV-2. Treatment was started 8 hours post-infection and carried out every 12 hours for 5 days. Experimental groups were LAng (1-7) at 0.73 mg of peptide/kg/dose IN, Veklury at 20 mg of remdesivir/kg/dose IP, and PBS IN. Animals were euthanized 12 hours after the last dose. Number of (A) myeloid cells, (B) monocytes, (C) neutrophils, (D) macrophages, (E–G) expressing CD206, and (H–J) iNOS. The panels of cells were determined by flow cytometry. Data are shown as medians ± 95% confidence intervals and are compared using Kruskal-Wallis followed by Dunn's post-test. *P < 0.05 and **P < 0.01.

that vesicles prepared from the same lipid using the same method showed colloidal stability when subjected to temperature stress (27).

The choice of intranasal route as a strategy to deliver the LAng (1-7) formulation to the lungs was based on a previous work, evidencing that the instillation of 15 µL of the compound solution into the nostrils delivered about 30% of the compound to the lungs (33). The dose of administered Ang-(1-7) is also consistent with that used in a previous study in a model of pneumonia caused by *Mycoplasma pneumoniae* (20).

Previous strategies for pulmonary administration of the peptide comprised nebulization of an Ang-(1-7)-cyclodextrin suspension, oropharyngeal instillation of Ang-(1-7) solution, and dry powder inhalation of spray dried trehalose-based microparticles/nanoparticles incorporating the peptide (19, 20, 34). Here, we evaluated for the first time the efficacy of intranasal instillation of liposomal Ang-(1-7), expecting that this strategy would have a greater impact on the control of inflammation due to the protection of the peptide from the action of proteolytic enzymes (22) and the local and sustained drug

release provided by the liposomal form in the lungs (24). The fact that our liposomes showed a slow peptide release with a half-time of 9 hours at 37°C further supports this approach. However, not all the amount of free external Ang-(1-7) was removed during the process of preparation of the liposomal sample for animal treatment. From the quantification of Ang-(1-7) in each step, we estimated that about one-third of the administered peptide dose was in the encapsulated form. Considering that treatment with the free peptide did not show an improvement in the survival of animals, it can be reasonably inferred that the effect of the formulation was essentially due to the encapsulated peptide. As a significant proportion of the administered formulation is also expected to reach the gastrointestinal tract (35), orally absorbed Ang-(1-7) may also exert activity. Thus, to get further insight into the mode of action of the formulation, future studies could investigate its efficacy by the oral route.

Our data show that treatment of SARS-CoV-2-infected K18-hACE2 mice through IN administration of LAng (1-7) significantly reduced the viral load in the lungs, promoted anti-inflammatory effects, and improved the animal survival, compared to PBS control. The 3–4 log reduction of lung virus titer in our study contrasts with the less than 1 log level of reduction achieved in the same animal model following IP Ang-(1-7) (18). This comparison further supports the benefits of local peptide delivery using a liposomal-controlled drug-release system. The antiviral activity of LAng (1-7) led us to compare its effectiveness with that of the antiviral remdesivir and not with that of an anti-inflammatory drug. Indeed, Chen et al. (36) reported that treatment of SARS-CoV-2-infected K18hACE2 mice with NSAID (meloxicam) impaired the production of proinflammatory cytokines and neutralizing antibodies but did not affect weight loss and viral burden in the lung (36). Of note, no direct Ang-(1-7) action against SARS-CoV-2 in human airway epithelial cells was previously observed *in vitro* (18). As a possible mechanism, the antiviral action of Ang-(1-7) may be related to the inhibition of the phosphorylation of JAK/STAT proteins (37), which are essential regulators of local and systemic antiviral innate immune response (38).

The benefits of treatment with LAng (1-7) were also associated with a marked anti-inflammatory effect, as evidenced by the reduced levels of IL-6 and TNF and the decrease of $CD11b^+$ myeloid cells and $CD8^+$ T cells infiltration in the lung. In addition, an impairment of the recruitment in $Gr\text{-}1^-F4/80^+$ cells expressing activation markers CD206 and iNos, as well as T cells secreting IL-4 and IL-17, was observed in the lung of mice treated with LAng (1-7). IL-17 reduction can be an important mechanism for controlling mucosal immunity by preventing neutrophils from migrating to the lungs (39). On the other hand, remdesivir did not significantly reduce IL-6 levels and showed elevated leukocyte infiltration, evidencing no anti-inflammatory effect, as expected from its distinct mechanism of action. The anti-inflammatory effect of LAng (1-7) is consistent with a previous *in vitro* study with alveolar epithelial cells exposed to SARS-CoV-2, showing that Ang-(1-7) attenuated SARS-CoV-2 spike protein-induced IL-6 and IL-8 production in alveolar epithelial cells through the activation of Mas (11). Furthermore, a recent report indicated that treatment of SARS-CoV-2-infected K18-hACE2 mice with IP Ang-(1-7) promoted the reduction of lung levels of IL-6, TNF, and CXCL1 in comparison to the vehicle-treated mice (18). Our data are also in agreement with previous reports on the protective and anti-inflammatory effects of Ang-(1-7) in different animal models of pulmonary diseases, including chronic asthma, sepsis-induced acute lung injury, pneumonia caused by *Mycoplasma pneumoniae,* and influenza virus (19–21, 31, 40). Regarding the possible role of inflammation in the level of infection, one may consider that the anti-inflammatory response to Ang-(1-7) resulted in the resolution of lung injury and provided normal or greater ability of the host to deal with infection (9). However, this relationship could not be established in our study, because no clear improvement in the lung histopathological score was found in the group treated with LAng (1-7), when compared to the control PBS group. The early time point used for this evaluation and the high intragroup variation in animal response in our experimental model probably explain the lack of evidence of lung injury resolution.

As an attempt to reconcile the still high lethality of treated animals with the low viral titer in the lungs, one can consider a previous study by Kumari et al. (41) that looked at the kinetics of SARS-CoV-2 invasion in the lungs and the brain of K18-hACE2 mice following intranasal infection at high inoculum (41). They observed that virus titers in the lungs were highest on the third day and decreased on days 5 and 6 after infection. In contrast, virus titers showed a peak in the brain on days 5 and 6. Several encephalitis markers were also identified. Therefore, these authors proposed that the main cause of death in this model may be neuroinvasion and encephalitis. The high viral load in the brains of mice in our study is consistent with this previous work. Although neither remdesivir nor LAng (1-7) significantly reduced virus titer in the brain, three out of eight mice in the LAng (1-7) group had virus titer below the detection limit. Such low virus titers were not observed in the control group. Therefore, in future work, it would be worth investigating the ability of IN liposomal Ang (1-7) to inhibit viral neuroinvasion. Whether the efficacy of LAng (1-7) can be further improved through adjustment in the dose and treatment regimen requires further investigation. As inflammation is a component of the host defense system and a protective response in the context of infectious diseases, it has been suggested that the greatest benefits of Ang-(1-7) may be achieved in the late stage of infection (9). Moreover, efficacy may be enhanced through manipulation of liposomal lipid composition. The conventional liposomes used in LAng (1-7) formulation are expected to be rapidly captured by the alveolar macrophages, thereby accelerating the peptide release *in vivo* (24, 42). In this context, the PEGylation of liposomes could promote a more sustained *in vivo* peptide release and greater activity (42).

Translation of the present data into clinical application also requires further studies, including a study of the viability of nebulization and evaluation of combination therapy with antiviral drugs.

In conclusion, this work demonstrates that treatment of SARS-CoV-2-infected mice with liposomal Ang-(1-7) through intranasal instillation significantly extended survival and reduced the viral load in the lung. Liposomal Ang-(1-7) emerges as a promising formulation to improve the treatment and decrease the severity of pulmonary infections.

ACKNOWLEDGMENTS

We thank the Biosafety Level 3 (BSL-3) laboratory at ICB/UFMG; Center for Image Acquisition and Processing (CAPI-UFMG); and Centro de Laboratórios Multiusuários, CELAM. We thank Prof. Vivian Vasconcelos Costa (Department of Morphology, ICB/UFMG) for the careful revision of the manuscript.

This work was supported by Conselho Nacional de Desenvolvimento Científico e Tecnológico (CNPq, Brazil), grant numbers 306198/2021-5 and 442731/2020-5; Fundação de Amparo a Pesquisa do Estado de Minas Gerais (FAPEMIG, Brazil), grant numbers TEC-RED-00282-16, RED-00202-22, RED-00028-23, APQ-00730-23, APQ-02618-23, and APQ-04650-23; Coordenação de Aperfeiçoamento de Pessoal de Nível Superior (CAPES, Brazil. No. 88887.506690/2020-00; 38/2022). This work received support from the National Institute of Science and Technology in Dengue and Host-Microorganism Interaction (INCT em Dengue), sponsored by CNPq (grant number 465425/2014-3) and FAPEMIG (grant number 25036), as well as the National Institute of Science and Technology in Nanobiopharmaceutics (INCT NanoBiofar) sponsored by CNPq (grant number 406792/2022-4).

F.F., P.P.G.G., M.M.T., and R.A.S.S. were recipients of a fellowship from CNPq. S.M. was a recipient of a studentship from CAPES.

AUTHOR AFFILIATIONS

[1]Department of Physiology and Biophysics, Institute of Biological Sciences, Universidade Federal de Minas Gerais, Belo Horizonte, Minas Gerais, Brazil
[2]Department of Biochemistry and Immunology, Universidade Federal de Minas Gerais, Belo Horizonte, Minas Gerais, Brazil

[3]State University of Minas Gerais, Divinopolis, Minas Gerais, Brazil

AUTHOR ORCIDs

Sabrina Mendes http://orcid.org/0000-0001-8553-9408
Clara Couto Fernandez http://orcid.org/0000-0002-0260-3564
Frédéric Frézard http://orcid.org/0000-0003-3783-5717

FUNDING

Funder	Grant(s)	Author(s)
Conselho Nacional de Desenvolvimento Científico e Tecnológico (CNPq)	306198/2021-5	Frédéric Frézard
Fundação de Amparo à Pesquisa do Estado de Minas Gerais (FAPEMIG)	TEC-RED-00282-16	Frédéric Frézard
Coordenação de Aperfeiçoamento de Pessoal de Nível Superior (CAPES)	88887.506690/2020-00	Frédéric Frézard
Coordenação de Aperfeiçoamento de Pessoal de Nível Superior (CAPES)	38/2022	Frédéric Frézard
Conselho Nacional de Desenvolvimento Científico e Tecnológico (CNPq)	406792/2022-4	Robson Augusto Souza dos Santos
Conselho Nacional de Desenvolvimento Científico e Tecnológico (CNPq)	465425/2014-3	Mauro Martins Teixeira
Conselho Nacional de Desenvolvimento Científico e Tecnológico (CNPq)	442731/2020-5	Pedro Pires Goulart Guimarães
Fundação de Amparo à Pesquisa do Estado de Minas Gerais (FAPEMIG)	RED-00202-22	Mauro Martins Teixeira
Fundação de Amparo à Pesquisa do Estado de Minas Gerais (FAPEMIG)	RED-00028-23	Frédéric Frézard
Fundação de Amparo à Pesquisa do Estado de Minas Gerais (FAPEMIG)	APQ-00730-23	Frédéric Frézard
Fundação de Amparo à Pesquisa do Estado de Minas Gerais (FAPEMIG)	APQ-02618-23	Mauro Martins Teixeira
Fundação de Amparo à Pesquisa do Estado de Minas Gerais (FAPEMIG)	APQ-04650-23	Mauro Martins Teixeira

AUTHOR CONTRIBUTIONS

Sabrina Mendes, Data curation, Formal analysis, Investigation, Methodology, Visualization, Writing – original draft, Writing – review and editing | Lays Cordeiro Guimarães, Data curation, Formal analysis, Methodology, Validation, Writing – review and editing | Pedro Augusto Carvalho Costa, Formal analysis, Methodology, Validation, Writing – review and editing | Clara Couto Fernandez, Formal analysis, Methodology, Visualization | Maria Marta Figueiredo, Data curation, Formal analysis, Methodology, Validation | Mauro Martins Teixeira, Funding acquisition, Methodology, Resources, Validation, Writing – review and editing | Robson Augusto Souza dos Santos, Funding acquisition, Methodology, Validation, Writing – review and editing | Pedro Pires Goulart Guimarães, Formal analysis, Investigation, Methodology, Supervision, Validation, Writing – review and editing | Frédéric Frézard, Conceptualization, Formal analysis, Funding acquisition, Investigation, Methodology, Project administration, Supervision, Validation, Writing – original draft, Writing – review and editing

DATA AVAILABILITY

Data are available to the public as AAC00835-24R1 "Intranasal Liposomal Angiotensin-(1-7) Administration Reduces Inflammation and Viral Load in the lungs during SARS-CoV-2 Infection in K18-hACE2 Transgenic Mice," through Figshare repository at DOI: https://doi.org/10.6084/m9.figshare.27089044.v1

ETHICS APPROVAL

In vivo experiments were conducted following the recommendations of the Guide for the Care and Use of Laboratory Animals from the National Council for Animal Experimentation Control (CONCEA). All protocols involving mice were approved by the UFMG Ethic Committee for Animal Use, under protocol number CEUA 147/2022. All experimental phases with SARS-CoV-2 were conducted by authorized personnel duly equipped and certified by the National Technical Biosafety Commission (CTNBio 8.094/2022).

ADDITIONAL FILES

The following material is available online.

Supplemental Material

Supplemental material (AAC00835-24-s0001.pdf). Figures S1 to S3; Table S1.

REFERENCES

1. Jefferson T, Dooley L, Ferroni E, Al-Ansary LA, van Driel ML, Bawazeer GA, Jones MA, Hoffmann TC, Clark J, Beller EM, Glasziou PP, Conly JM. 2023. Physical interventions to interrupt or reduce the spread of respiratory viruses. Cochrane Database Syst Rev 1:CD006207. https://doi.org/10.1002/14651858.CD006207.pub6
2. Jackson CB, Farzan M, Chen B, Choe H. 2022. Mechanisms of SARS-CoV-2 entry into cells. Nat Rev Mol Cell Biol 23:3–20. https://doi.org/10.1038/s41580-021-00418-x
3. Bos LDJ, Ware LB. 2022. Acute respiratory distress syndrome: causes, pathophysiology, and phenotypes. Lancet 400:1145–1156. https://doi.org/10.1016/S0140-6736(22)01485-4
4. Aboul-Fotouh S, Mahmoud AN, Elnahas EM, Habib MZ, Abdelraouf SM. 2023. What are the current anti-COVID-19 drugs? From traditional to smart molecular mechanisms. Virol J 20:241. https://doi.org/10.1186/s12985-023-02210-z
5. Aleem A, Kothadia JP. 2024. RemdesivirStatPearls. StatPearls Publishing, Treasure Island (FL).
6. Blair HA. 2023. Remdesivir: a review in COVID-19. Drugs (Abingdon Engl) 83:1215–1237. https://doi.org/10.1007/s40265-023-01926-0
7. Godwin PO, Polsonetti B, Caron MF, Oppelt TF. 2024. Remdesivir for the treatment of COVID-19: a narrative review. Infect Dis Ther 13:1–19. https://doi.org/10.1007/s40121-023-00900-3
8. Perico N, Cortinovis M, Suter F, Remuzzi G. 2023. Home as the new frontier for the treatment of COVID-19: the case for anti-inflammatory agents. Lancet Infect Dis 23:e22–e33. https://doi.org/10.1016/S1473-3099(22)00433-9
9. Sousa LP, Pinho V, Teixeira MM. 2020. Harnessing inflammation resolving-based therapeutic agents to treat pulmonary viral infections: what can the future offer to COVID-19? Br J Pharmacol 177:3898–3904. https://doi.org/10.1111/bph.15164
10. Luna P, Fernanda Pérez M, Castellar-Lopez J, Chang A, Montoya Y, Bustamante J, Rosales-Rada W, Mendoza-Torres E. 2023. Potential of angiotensin-(1-7) in COVID-19 treatment. Curr Protein Pept Sci 24:89–97. https://doi.org/10.2174/1389203724666221130140416
11. Shen Y-L, Hsieh Y-A, Hu P-W, Lo P-C, Hsiao Y-H, Ko H-K, Lin F-C, Huang C-W, Su K-C, Perng D-W. 2023. Angiotensin-(1-7) attenuates SARS-CoV2 spike protein-induced interleukin-6 and interleukin-8 production in alveolar epithelial cells through activation of Mas receptor. J Microbiol Immunol Infect 56:1147–1157. https://doi.org/10.1016/j.jmii.2023.09.003
12. Lobo SM, Plantefève G, Nair G, Joaquim Cavalcante A, Franzin de Moraes N, Nunes E, Barnum O, Berdun Stadnik CM, Lima MP, Lins M, et al. 2024. Efficacy of oral 20-hydroxyecdysone (BIO101), a MAS receptor activator, in adults with severe COVID-19 (COVA): a randomized, placebo-controlled, phase 2/3 trial. EClinMed 68:102383. https://doi.org/10.1016/j.eclinm.2023.102383
13. Issa H, Eid AH, Berry B, Takhviji V, Khosravi A, Mantash S, Nehme R, Hallal R, Karaki H, Dhayni K, Faour WH, Kobeissy F, Nehme A, Zibara K. 2021. Combination of angiotensin (1-7) agonists and convalescent plasma as a new strategy to overcome angiotensin converting enzyme 2 (ACE2) inhibition for the treatment of COVID-19. Front Med (Lausanne) 8:620990. https://doi.org/10.3389/fmed.2021.620990
14. Miesbach W. 2020. Pathological role of angiotensin II in severe COVID-19. TH Open 4:e138–e144. https://doi.org/10.1055/s-0040-1713678
15. Self WH, Shotwell MS, Gibbs KW, de Wit M, Files DC, Harkins M, Hudock KM, Merck LH, Moskowitz A, Apodaca KD, et al. 2023. Renin-angiotensin system modulation with synthetic angiotensin (1-7) and angiotensin II type 1 receptor-biased ligand in adults with COVID-19: two randomized clinical trials. JAMA 329:1170–1182. https://doi.org/10.1001/jama.2023.3546
16. Wagener G, Goldklang MP, Gerber A, Elisman K, Eiseman KA, Fonseca LD, D'Armiento JM. 2022. A randomized, placebo-controlled, double-blinded pilot study of angiotensin 1-7 (TXA-127) for the treatment of severe COVID-19. Crit Care 26:229. https://doi.org/10.1186/s13054-022-04096-9
17. Martins ALV, Annoni F, da Silva FA, Bolais-Ramos L, de Oliveira GC, Ribeiro RC, Diniz MML, Silva TGF, Pinheiro BD, Rodrigues NA, Dos Santos Matos AH, Motta-Santos D, Campagnole-Santos MJ, Verano-Braga T, Taccone FS, Santos RAS. 2024. Angiotensin-(1-7) infusion in COVID-19 patients admitted to the ICU: a seamless phase 1-2 randomized clinical trial. Ann Intensive Care 14:139. https://doi.org/10.1186/s13613-024-01369-0
18. Lima EB de S, Carvalho AFS, Zaidan I, Monteiro AHA, Cardoso C, Lara ES, Carneiro FS, Oliveira LC, Resende F, Santos FR da S, Souza-Costa LP, Chaves I de M, Queiroz-Junior CM, Russo RC, Santos RAS, Tavares LP, Teixeira MM, Costa VV, Sousa LP. 2024. Angiotensin-(1-7) decreases inflammation and lung damage caused by betacoronavirus infection in mice. Inflamm Res. https://doi.org/10.1007/s00011-024-01948-8
19. Magalhães GS, Gregório JF, Ramos KE, Cançado-Ribeiro ATP, Baroni IF, Barcelos LS, Pinho V, Teixeira MM, Santos RAS, Rodrigues-Machado MG, Campagnole-Santos MJ. 2020. Treatment with inhaled formulation of angiotensin-(1-7) reverses inflammation and pulmonary remodeling in a

model of chronic asthma. Immunobiology 225:151957. https://doi.org/10.1016/j.imbio.2020.151957
20. Collins KL, Younis US, Tanyaratsrisakul S, Polt R, Hay M, Mansour HM, Ledford JG. 2021. Angiotensin-(1-7) peptide hormone reduces inflammation and pathogen burden during *Mycoplasma pneumoniae* infection in mice. Pharmaceutics 13:1614. https://doi.org/10.3390/pharmaceutics13101614
21. Melo EM, Del Sarto J, Vago JP, Tavares LP, Rago F, Gonçalves APF, Machado MG, Aranda-Pardos I, Valiate BVS, Cassali GD, Pinho V, Sousa LP, A-Gonzalez N, Campagnole-Santos MJ, Bader M, Santos RAS, Machado AV, Ludwig S, Teixeira MM. 2021. Relevance of angiotensin-(1-7) and its receptor Mas in pneumonia caused by influenza virus and post-influenza pneumococcal infection. Pharmacol Res 163:105292. https://doi.org/10.1016/j.phrs.2020.105292
22. Silva-Barcellos NM, Frézard F, Caligiorne S, Santos RA. 2001. Long-lasting cardiovascular effects of liposome-entrapped angiotensin-(1-7) at the rostral ventrolateral medulla. Hypertension 38:1266–1271. https://doi.org/10.1161/hy1201.096056
23. Trapnell BC, Nakata K, Bonella F, Campo I, Griese M, Hamilton J, Wang T, Morgan C, Cottin V, McCarthy C. 2019. Pulmonary alveolar proteinosis. Nat Rev Dis Primers 5:16. https://doi.org/10.1038/s41572-019-0066-3
24. Krishna SS, Sudheesh MS, Viswanad V. 2023. Liposomal drug delivery to the lungs: a post covid-19 scenario. J Liposome Res 33:410–424. https://doi.org/10.1080/08982104.2023.2199068
25. Pulivendala G, Bale S, Godugu C. 2020. Inhalation of sustained release microparticles for the targeted treatment of respiratory diseases. Drug Deliv and Transl Res 10:339–353. https://doi.org/10.1007/s13346-019-00690-7
26. Jaafar-Maalej C, Diab R, Andrieu V, Elaissari A, Fessi H. 2010. Ethanol injection method for hydrophilic and lipophilic drug-loaded liposome preparation. J Liposome Res 20:228–243. https://doi.org/10.3109/08982100903347923
27. Cunha Matosinhos R, Frézard F, Mendes Silva Araújo S, Magalhães Barbosa A, de Souza IF, de Souza Filho JD, de Souza J, Corrêa Oliveira Bahia AP, Ietta F, Magnani A, Saúde-Guimarães DA. 2024. Development and characterization of liposomal formulations containing sesquiterpene lactones for the treatment of chronic gout. Sci Rep 14:6991. https://doi.org/10.1038/s41598-024-57663-1
28. Lin Y-C, Malott RJ, Ward L, Kiplagat L, Pabbaraju K, Gill K, Berenger BM, Hu J, Fonseca K, Noyce RS, Louie T, Evans DH, Conly JM. 2022. Detection and quantification of infectious severe acute respiratory coronavirus-2 in diverse clinical and environmental samples. Sci Rep 12:5418. https://doi.org/10.1038/s41598-022-09218-5
29. Winkler ES, Bailey AL, Kafai NM, Nair S, McCune BT, Yu J, Fox JM, Chen RE, Earnest JT, Keeler SP, Ritter JH, Kang L-I, Dort S, Robichaud A, Head R, Holtzman MJ, Diamond MS. 2020. SARS-CoV-2 infection of human ACE2-transgenic mice causes severe lung inflammation and impaired function. Nat Immunol 21:1327–1335. https://doi.org/10.1038/s41590-020-0778-2
30. da Silva Santos Y, Gamon THM, de Azevedo MSP, Telezynski BL, de Souza EE, de Oliveira DBL, Dombrowski JG, Rosa-Fernandes L, Palmisano G, de Moura Carvalho LJ, Luvizotto MCR, Wrenger C, Covas DT, Curi R, Marinho CRF, Durigon EL, Epiphanio S. 2023. Virulence profiles of wild-type, P.1 and delta SARS-CoV-2 variants in K18-hACE2 transgenic mice. Viruses 15:999. https://doi.org/10.3390/v15040999
31. El-Hashim AZ, Renno WM, Raghupathy R, Abduo HT, Akhtar S, Benter IF. 2012. Angiotensin-(1-7) inhibits allergic inflammation, via the MAS1 receptor, through suppression of ERK1/2- and NF-κB-dependent pathways. Br J Pharmacol 166:1964–1976. https://doi.org/10.1111/j.1476-5381.2012.01905.x
32. McCray PB, Pewe L, Wohlford-Lenane C, Hickey M, Manzel L, Shi L, Netland J, Jia HP, Halabi C, Sigmund CD, Meyerholz DK, Kirby P, Look DC, Perlman S. 2007. Lethal infection of K18-hACE2 mice infected with severe acute respiratory syndrome coronavirus. J Virol 81:813–821. https://doi.org/10.1128/JVI.02012-06
33. Southam DS, Dolovich M, O'Byrne PM, Inman MD. 2002. Distribution of intranasal instillations in mice: effects of volume, time, body position, and anesthesia. Am J Physiol Lung Cell Mol Physiol 282:L833–9. https://doi.org/10.1152/ajplung.00173.2001
34. Alabsi W, Acosta MF, Al-Obeidi FA, Hay M, Polt R, Mansour HM. 2021. Synthesis, physicochemical characterization, *in vitro* 2D/3D human cell culture, and *in vitro* aerosol dispersion performance of advanced spray dried and co-spray dried angiotensin (1-7) peptide and PNA5 with trehalose as microparticles/nanoparticles for targeted respiratory delivery as dry powder inhalers. Pharmaceutics 13:1278. https://doi.org/10.3390/pharmaceutics13081278
35. Eyles JE, Williamson ED, Alpar HO. 1999. Immunological responses to nasal delivery of free and encapsulated tetanus toxoid: studies on the effect of vehicle volume. Int J Pharm 189:75–79. https://doi.org/10.1016/s0378-5173(99)00239-2
36. Chen JS, Alfajaro MM, Chow RD, Wei J, Filler RB, Eisenbarth SC, Wilen CB. 2021. Non-steroidal anti-inflammatory drugs dampen the cytokine and antibody response to SARS-CoV-2 infection. J Virol 95:e00014-21. https://doi.org/10.1128/JVI.00014-21
37. Itcho K, Oki K, Kobuke K, Ohno H, Yoneda M, Hattori N. 2019. Angiotensin 1-7 suppresses angiotensin II mediated aldosterone production via JAK/STAT signaling inhibition. J Steroid Biochem Mol Biol 185:137–141. https://doi.org/10.1016/j.jsbmb.2018.08.007
38. Ezeonwumelu IJ, Garcia-Vidal E, Ballana E. 2021. JAK-STAT pathway: a novel target to tackle viral infections. Viruses 13:2379. https://doi.org/10.3390/v13122379
39. Miyamoto M, Prause O, Sjöstrand M, Laan M, Lötvall J, Lindén A. 2003. Endogenous IL-17 as a mediator of neutrophil recruitment caused by endotoxin exposure in mouse airways. J Immunol 170:4665–4672. https://doi.org/10.4049/jimmunol.170.9.4665
40. Chen X, Zhao B, Qu Y, Chen Y, Xiong J, Feng Y, Men D, Huang Q, Liu Y, Yang B, Ding J, Li F. 2020. Detectable serum SARS-CoV-2 viral load (RNAemia) is closely correlated with drastically elevated interleukin 6 level in critically Ill patients with COVID-19. Clin Infect Dis 71:1937–1942. https://doi.org/10.1093/cid/ciaa449
41. Kumari P, Rothan HA, Natekar JP, Stone S, Pathak H, Strate PG, Arora K, Brinton MA, Kumar M. 2021. Neuroinvasion and encephalitis following intranasal inoculation of SARS-CoV-2 in K18-hACE2 mice. Viruses 13:132. https://doi.org/10.3390/v13010132
42. Silva-Barcellos NM, Caligiorne S, dos Santos RAS, Frézard F. 2004. Site-specific microinjection of liposomes into the brain for local infusion of a short-lived peptide. J Control Release 95:301–307. https://doi.org/10.1016/j.jconrel.2003.12.010

3 MATERIAL SUPLEMENTAR (CAPÍTULO 1)

Supplemental material

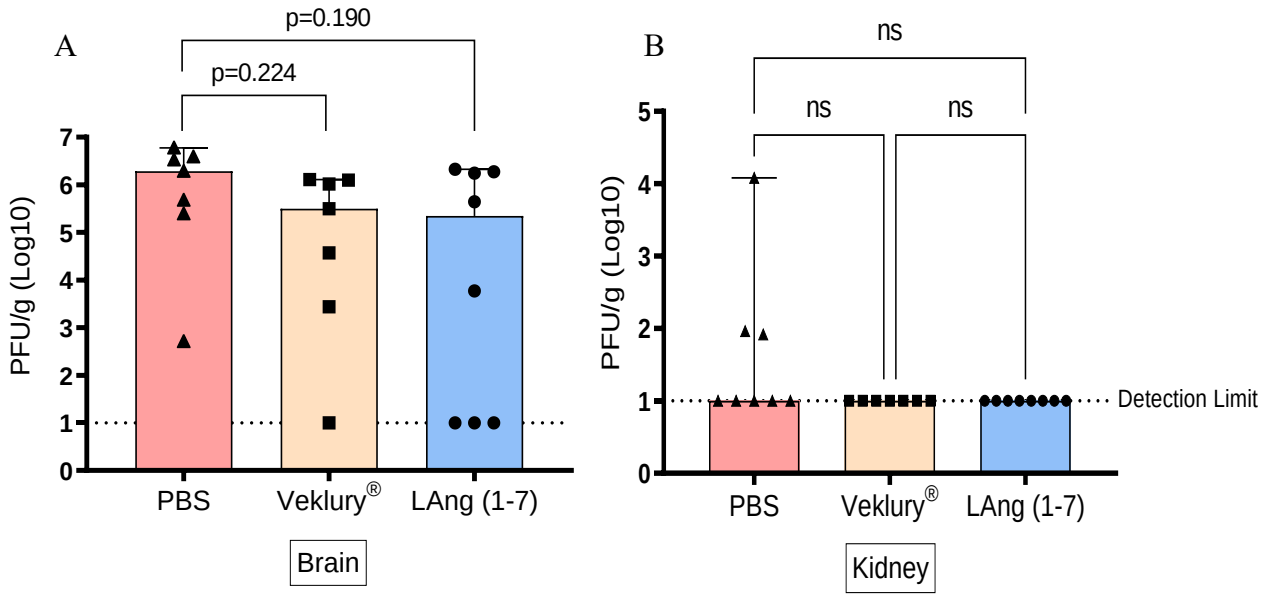

Figure S1. Viral loads in the brain (A) and kidney (B) of SARS-CoV-2-infected mice after treatment with intranasal LAng (1-7) or intraperitoneal remdesivir, in comparison with intranasal PBS. K18-hACE2 transgenic mice (n=8) were intranasally inoculated with SARS-CoV-2. Treatment was started 8 hours post-infection and carried out every 12 hours for 5 days. Experimental groups were: LAng (1-7) at 0.73 mg of peptide/kg/dose IN, Veklury® at 20 mg of remdesivir/kg/dose IP and PBS IN. Animals were euthanized 12 hours after the last dose. The titer of viable virus was determined by the limiting dilution plaque. The dashed horizontal lines indicate the detection limit. Data are shown as medians ± 95% confidence intervals and are compared using Kruskal-Wallis followed by Dunn's post-test. ns: no significant difference.

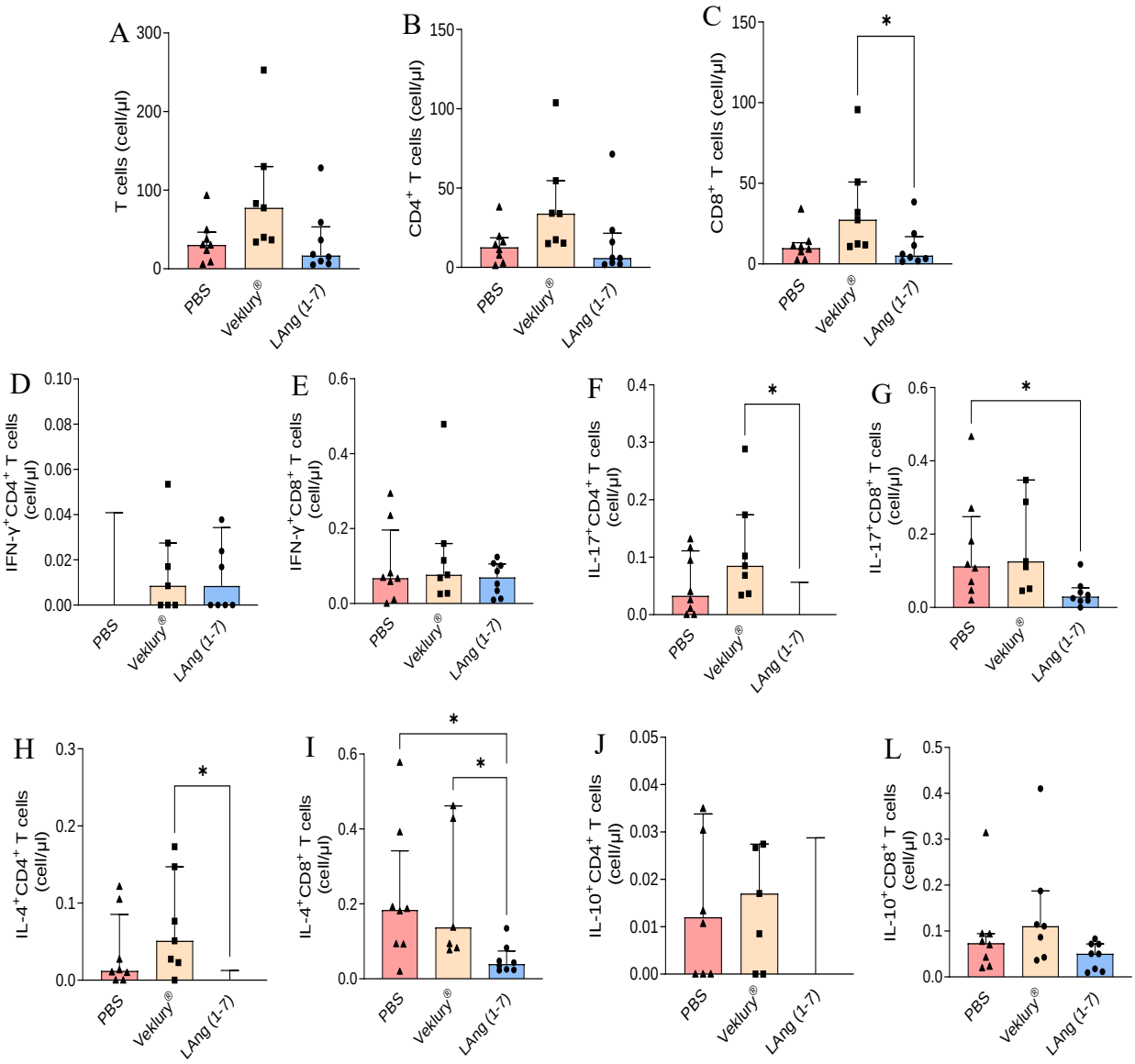

Figure S2. Lymphoid cells profile in the lungs of SARS-CoV-2-infected mice after treatment with intranasal LAng (1-7) or intraperitoneal remdesivir, in comparison with intranasal PBS. K18-hACE2 transgenic mice (n=8) were intranasally inoculated with SARS-CoV-2. Treatment was started 8 hours post-infection and carried out every 12 hours for 5 days. Experimental groups were: LAng (1-7) at 0.73 mg of peptide/kg/dose IN, Veklury® at 20 mg of remdesivir/kg/dose IP and PBS IN. Animals were euthanized 12 hours after the last dose. The panels of cells were determined

by flow cytometry. Data are shown as medians ± 95% confidence intervals and are compared using Kruskal-Wallis followed by Dunn's post-test. *p < 0.05 were considered significant.

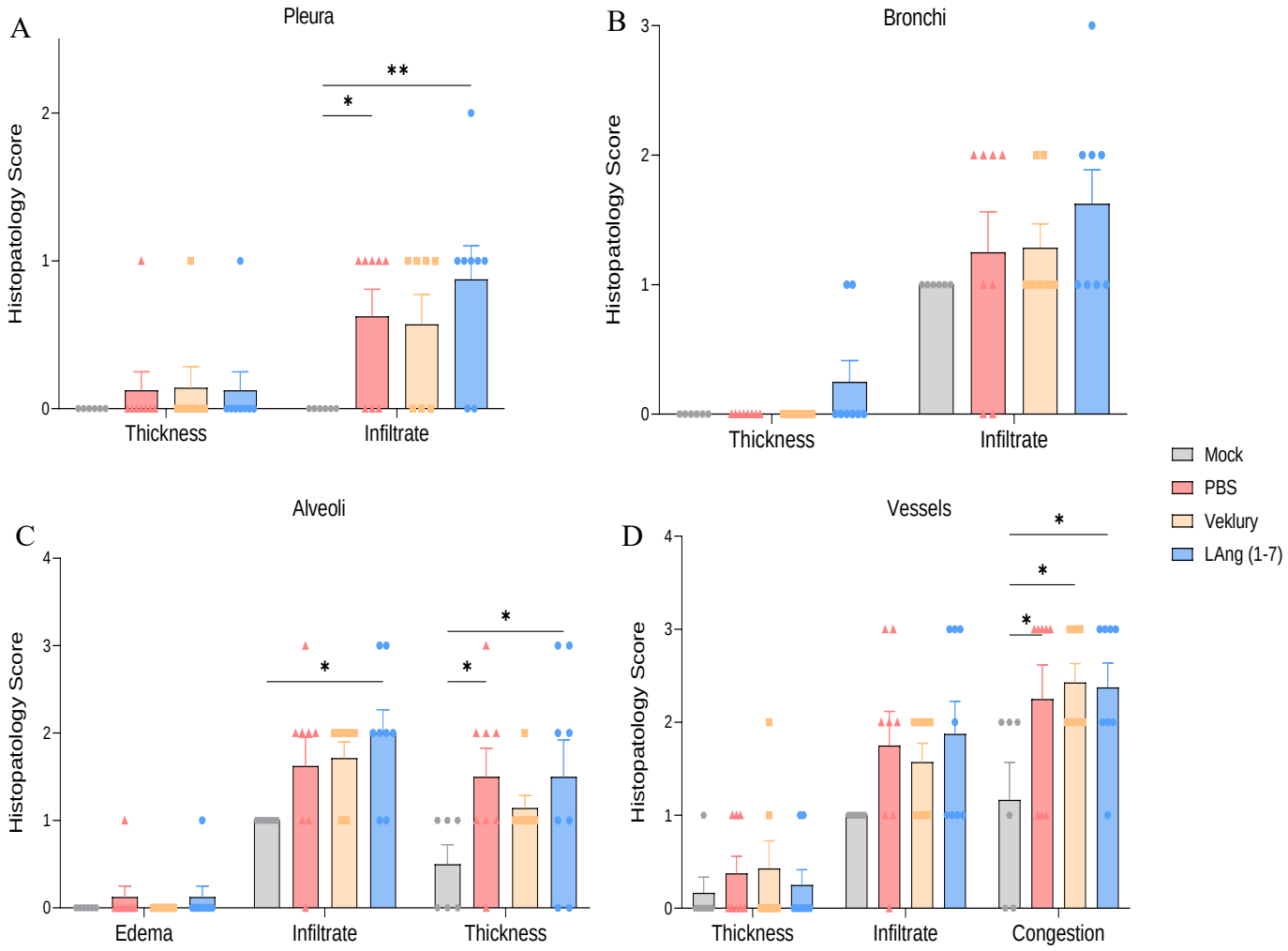

Figure S3. Histopathological scoring of lung tissue of SARS-CoV-2-infected mice after treatment with intranasal LAng (1-7) or intraperitoneal remdesivir, in comparison with intranasal PBS. Scoring for pleura (A), bronchi (B), alveoli (C) and vessels (D). K18-hACE2 transgenic mice (n=8) were intranasally inoculated with SARS-CoV-2. Treatment was started 8 hours post-infection and carried out every 12 hours for 5 days. Experimental groups were: LAng (1-7) at 0.73 mg of peptide/kg/dose IN, Veklury® at 20 mg of remdesivir/kg/dose IP and PBS IN. Animals were euthanized 12 hours after the last dose. Score was established as: 0, for no alteration; 1 for discrete

change (0-25%); 2, for moderate changes (25-50%); 3 for intense changes (50-100%). Data are shown as means ± SEM and compared using Two-way ANOVA followed by Tukey's multiple comparisons test. *p < 0.05; **P < 0.01.

Table S1. Antibodies used in flow cytometry analysis

Antigen	Fluorochrome	Clone	Concentration	Company
CD8a	eFluor 450	53-6.7	1/1300	Thermo
LIVE/DEAD	Acqua		1/1000	Thermo
Streptavidin	Pacific Orange		1/200	Thermo
CD45	Pacific Orange	30-F11	1/200	Thermo
CD11b	Super Bright600	M1/70	1/500	Thermo
CD206	PE	MR6F3	1/300	Thermo
IL-17	PE-eFluor610	eBio17B7	1/100	Thermo
iNos	PE-eFluor610	CXNFT	1/500	Thermo
CD45	PerCP-Cy5.5	Ly-5.2	1/200	BioLegend
CD4	PE-Cyanine7	GK1.5	1/3000	Thermo
F4/80	APC	BM8	1/200	Thermo
IL-10	AlexaFluor 700	JES5-16E3	1/100	Thermo
IFN-γ	APC-eFluor 780	XMG1.2	1/200	Thermo
Gr-1	Biotin	RB6-8C5	1/500	Biolegend

4 CAPÍTULO 2

INTRANASAL LIPOSOMAL REMDESIVIR INDUCES SARS-CoV-2 CLEARANCE IN K18-hACE2 MICE AND ENSURES SURVIVAL

Journal of Controlled Release 379 (2025) 558–573

Contents lists available at ScienceDirect

Journal of Controlled Release

journal homepage: www.elsevier.com/locate/jconrel

Intranasal liposomal remdesivir induces SARS-CoV-2 clearance in K18-hACE2 mice and ensures survival

Sabrina Mendes [a], Lays Cordeiro Guimarães [a], Leonardo Camilo de Oliveira [b], Pedro Augusto Carvalho Costa [a], Natália Jordana Alves da Silva [a], Gabriel Silva Alves Pessim Pereira [a], Clara Couto Fernandez [b], Maria Marta Figueiredo [c], Robson Augusto Souza dos Santos [a], Mauro Martins Teixeira [b], Vivian Vasconcelos Costa [d], Pedro Pires Goulart Guimarães [a], Frédéric Frézard [a,*]

[a] Department of Physiology and Biophysics, Institute of Biological Sciences, Universidade Federal de Minas Gerais, Belo Horizonte 31270-901, Minas Gerais, Brazil
[b] Department of Biochemistry and Immunology, Institute of Biological Sciences, Universidade Federal de Minas Gerais, Belo Horizonte 31270-901, Minas Gerais, Brazil
[c] State University of Minas Gerais, Divinopolis 35501-170, Minas Gerais, Brazil
[d] Department of Morphology, Institute of Biological Sciences, Universidade Federal de Minas Gerais, Belo Horizonte 31270-901, Minas Gerais, Brazil

ARTICLE INFO

Keywords:
COVID-19
Intranasal
Liposomes
K18-hACE2 mice
Remdesivir
SARS-CoV-2Parte superior do formulário

ABSTRACT

A huge challenge after the emergence of COVID-19 has been the discovery of effective antiviral drugs. Although remdesivir (RDV) emerged as one of the most promising drugs, its pharmaceutical formulation Veklury® is limited by moderate efficacy, high toxicity and need for parenteral administration. The aim of the present work was to develop a liposomal formulation of RDV for pulmonary administration and evaluate its efficacy in models of COVID-19. Liposomal RDV nanoformulation (LRDV) was selected based on high drug encapsulation efficiency, sustained drug release property and high *in vitro* selectivity index. A pharmacokinetic study of intranasal LRDV in mice demonstrated effective delivery of the drug to the lungs. LRDV was then evaluated for its efficacy in SARS-CoV-2-infected K18-hACE2 mice after repeated intranasal administration at 10 mg/kg/bid for 5 days. Veklury® given intraperitoneally at 20 mg/kg/bid was used for comparison. Mice receiving LRDV remained alive up to 15 days post-infection (dpi). On the other hand, the control groups receiving PBS and empty liposomes showed 100 % death at 6 dpi and the Veklury® group had 62.5 % death at 8 dpi. Intranasal LRDV also promoted a strong reduction in viral loads in the brain and lungs of mice and prevented the inflammatory response induced by SARS-CoV-2 in the lungs. This is in contrast with Veklury®, which did not significantly reduce the viral titer in the brain and was poorly effective in preventing the inflammatory response in the lungs. Intranasal LRDV emerges as a promising therapeutic strategy for COVID-19, including "Long COVID".

1. Introduction

Viral epidemics or pandemics of acute respiratory infections represent a global threat [1]. COVID-19, caused by SARS-CoV-2, is responsible for more than 7 million deaths worldwide, making it one of the deadliest viruses in human history (https://covid19.who.int/). After reaching the lower respiratory tract, SARS-CoV-2 often leads to severe acute respiratory syndrome (SARS), characterized by lung damage due to increased levels of proinflammatory cytokines and chemokines [2]. "Long COVID" also emerged as a post-acute infection syndrome in several patients reporting persistent manifestations, such as hyposmia, hypogeusia, sleep disturbances and substantial cognitive impairment, the latter affecting approximately one in four cases of COVID-19 [3–5].

A huge challenge after the emergence of COVID-19 has been the discovery or repurposing of effective antivirals [6]. Among antiviral candidates, remdesivir (RDV) or GS-5734, a nucleotide analogue prodrug and precursor of GS-441524, has emerged as one of the most promising [7–10]. RDV acts as an inhibitor of viral RNA-dependent RNA polymerase, targeting the viral genome replication process, with broad-spectrum activity against RNA viruses, including Ebolaviruses, Marburg virus, respiratory syncytial virus, Hepatitis C virus, several paramyxoviruses, MERS-CoV and SARS-CoV. The commercial drug known as

* Corresponding author.
E-mail address: frezard@icb.ufmg.br (F. Frézard).

https://doi.org/10.1016/j.jconrel.2025.01.044
Received 19 July 2024; Received in revised form 31 December 2024; Accepted 16 January 2025
Available online 24 January 2025

Veklury® consists of lyophilized powder, in which RDV is complexed with sulfobutylether β-cyclodextrin (SBE-β-CD) [10]. This pharmaceutical form allows intravenous administration of the lipophilic RDV molecule. Importantly, RDV has demonstrated antiviral activity against several variants of SARS-CoV-2, including Alpha, Beta, Gamma, Epsilon, Kappa, Lambda, Iota, Zeta, Delta, and Omicron [11]. In studies with mice infected with a chimeric variant of SARS-CoV, RDV significantly reduced viral load in the lungs and improved lung function [12]. RDV is currently the only antiviral approved for use in hospitalized patients with COVID-19 who are at high risk of progression to severe disease, with or without the need for supplemental oxygen. It is also recommended for non-hospitalized COVID-19 patients [13]. However, treatment with this antiviral can cause kidney and liver damage, in addition to cognitive dysfunction [14]. In this context, it has been proposed to improve the therapeutic index of RDV and patient adherence through its pulmonary administration, allowing greater local concentration of the drug and reducing its systemic side effects [15–17]. Another limitation of RDV regarding its potential for treating "Long COVID" is its low brain penetrance [18,19].

Recent progress in nanotechnology has brought the development of nanoparticles as advanced carrier systems to improve drug delivery to the lungs and brain [15,20–23]. In this context, liposomes have emerged as one of the most promising drug nanocarriers due to their excellent biocompatibility, ability to incorporate hydrophilic and lipophilic drugs and ease of surface modification to modulate their interactions with biological systems [24,25]. Moreover, liposomes can protect drugs from enzymatic degradation and prolong their residence time. The intranasal (IN) route has also been extensively investigated for systemic and brain drug delivery. After IN administration, liposomal drugs can enter the systemic circulation *via* absorption in the respiratory region, whereas they can be directly transported to the brain *via* the olfactory pathway [24]. Liposomal RDV formulations have been previously investigated for inhalation use [16,26]. A major challenge was achieving stable incorporation of RDV into vesicles. Liposomal RDV showed reduced *in vitro* cytotoxicity [26], however, its efficacy against SARS-CoV-2 has not yet been reported.

The aim of the present work was to develop a liposomal formulation of RDV and evaluate its therapeutic efficacy through *in vitro* and *in vivo* assays in COVID-19 models. A liposomal RDV nanoformulation was selected on the basis of high drug encapsulation efficiency, sustained drug release property and high *in vitro* selectivity index. Liposomal RDV administered intranasally to transgenic K18-hACE2 mice infected with SARS-CoV-2 resulted in virus clearance in the lungs and brain and 100 % animal survival. The therapeutic efficacy was much more pronounced than that of the commercial formulation of RDV (Verklury®) administered parenterally.

2. Material and methods

2.1. Reagents

Remdesivir (RDV) was acquired from MedChemExpress® (MCE) (NJ, USA). Soybean phosphatidylcholine (SPC, Phospholipon®90G), distearoylphosphatidylcholine (DSPC), dipalmitoylphosphatidylglycerol (DPPG), and distearoylphosphatidylethanolamine-polyethylene glycol2000 (DSPE-PEG2000) were obtained from Lipoid (Ludwigshafen, GER). Veklury® was imported by Gilead Sciences Farmacêutica do Brasil Ltda. Cholesterol (CHOL), ethanol 96°, methanol, hydroxypropyl-β-cyclodextrin (HP-β-CD), and sulfobutyl ether- β-cyclodextrin (SBE-β-CD) were acquired from Sigma-Aldrich (MO, USA).

2.2. Preparation of liposomal RDV formulations

Two different methods were evaluated for the preparation of liposomal RDV formulations.

The first method tested was the ethanol injection technique followed by extrusion, according to Jaafar-Maalej et al. [27], with the following modifications. To prepare RDV-containing conventional liposomes (LRDV), 73 mg of SPC were first dissolved in 75 μL of absolute ethanol at 40 °C and 7.5 mg of RDV was added and incubated until dissolution. The resulting organic phase was injected using a fine needle syringe into 0.75 mL of PBS (0.15 M NaCl, 10 mM phosphate, pH 7.2) at 25 °C under magnetic stirring. To prepare RDV-containing PEGylated liposomes (LRDV-PEG), 64 mg of SPC, 11.2 mg of DSPE-PEG, and 9 mg of CHOL were dissolved in 350 μL of ethanol and, after dissolution at 40 °C, 8 mg of RDV was added. The resulting organic phase was injected into 3 mL of PBS under magnetic stirring. Empty liposomes (LEmp and LEmp-PEG) were obtained using the same process but omitting RDV. The resulting suspensions were then extruded (5×) through polycarbonate membranes (Whatman®, USA) with gradually reduced pore sizes (200 and 100 nm), using the liposofast LF-12 device (Avestin®, CA). Finally, liposome suspensions were subjected to dialysis using 15 kDa MWCO membrane (Spectra/Por®) for 2 h at 4 °C against PBS to remove ethanol and non-encapsulated drug, leading to LRDV and LRDV-PEG formulations. LRDV formulation to be administered intranasally in animals was further concentrated (1.8-fold) using 50 kDa Amicon® Ultra0.5 filtration device at 14,000 ×g for 30 min at 4 °C.

The second preparation method is the dehydration-rehydration method (DRV), as first described by Kirby and Gregoriadis and modified by McCormack and Gregoriadis [28,29]. First, a complex between RDV and HP-β-CD was formed in water, by mixing 72 mg of HP-β-CD with 7.5 mg of RDV in 0.3 mL of water and heating at 60 °C for 5 min. Conventional liposomes were made from DSPC, DPPG and CHOL at molar ratio of 8:2:5, whereas PEGylated liposomes were composed of DSPC, DPPG, CHOL, and DSPE-PEG2000 at 8:2:5:0.8 mole ratio. Liposomes were initially prepared in water at 58.5 g/L of lipid, starting with the film hydration method to form multilamellar vesicles (MLVs) followed by five cycles of freezing (in liquid nitrogen) and thawing (water bath at 60 °C) to get FATMLVs and ending with extrusion through 200-nm (5×) and 100-nm (5×) polycarbonate membranes (10-mL Lipex® Extruder, Burnaby, BC, CA) to obtain monodisperse vesicles. The calibrated liposome suspension (2 mL) was then mixed with the RDV/HP-β-CD complex solution (0.3 mL) plus 40 mg of sucrose as cryoprotective sugar and, after homogenization, the suspension was immediately frozen in liquid nitrogen and lyophilized for 48 h, using an L101 lyophilizer (Liotop®, São Carlos/SP, BR). Empty liposomes were prepared using the same process and non-complexed HP-β-CD. Just before use, the lyophilizates were rehydrated with 0.4 mL of water, incubated at 60 °C for 30 min and vortexed every 10 min, leading to DRV liposome formulations.

2.3. Physicochemical characterization of liposomal RDV formulations

2.3.1. Particle size distribution and zeta potential

The average hydrodynamic diameter, polydispersity index and zeta potential (ζ) of the liposomal formulations were determined using a Zetasizer Nano ZS90 (Malvern Instruments, Malvern®, UK). The samples were accurately diluted, *i.e.*, 10 μL of liposomal suspensions in 990 μL of PBS for size and zeta potential analysis. The diluted samples were loaded into disposable cuvettes and analyzed at 25 °C. The liposomes were also characterized by the nanoparticle tracking analysis (NTA) technique, using LM14C Nanosight equipment (Malvern, UK).

2.3.2. Remdesivir concentration

RDV was quantified in the formulation by UV spectrophotometry, as previously described [30], except that measurements were performed in ethanol instead of water, to allow for lipid dissolution. Absorbance measurements were performed at 260 nm in a 96-well UV bottom plate (Corning®), using a Synergy™ HTX microplate reader (BioTek®, USA) after addition of 2.5 μL of the liposome formulation to 247.5 μL ethanol. A calibration curve was established. The absorbance *vs* concentration curve was found to be linear ($r^2 = 0.99$) and no significant interference

of the lipid matrix was observed. To determine the encapsulation efficiency of RDV (EE (%)) in LRDV and LRDV-PEG formulations, the absorbance was registered in the liposome suspension before (Ai) and after (Af) the extrusion/dialysis steps as follows: EE (%) = 100*(Af – Ao)/(Ai – Ao), where Ao represents the absorbance value of the blank formulation (prepared without RDV). To determine the encapsulation efficiency of RDV (EE (%)) in DRV formulations, 160 μL of the liposomal formulation was added to 800 μL of PBS and centrifuged at 22,000 ×*g* for 40 min at 15 °C. After pellet formation and complete removal of the supernatant, the liposome pellet was resuspended with 130 μL of PBS. The absorbance was registered in the liposomal suspension, before (Ai) and after (Af) centrifugation/resuspension as described above. The encapsulation efficiency of RDV was calculated as: EE (%) =100*(Af – Ao)/(Ai – Ao), where Ao represents the absorbance value of the blank formulation (without RDV).

2.3.3. Stability of liposomal RDV in suspension or under freeze-dried state

The LRDV formulation was prepared as three independent batches by the ethanol injection method, as described above, and dialyzed at 4 °C for 2 h against PBS to remove ethanol and unencapsulated drug. Each batch was divided into samples kept as aqueous suspensions or freeze-dried samples. The freeze-dried samples were obtained after addition of sucrose at 3:1 sugar/lipid mass ratio followed by immediate freezing in liquid nitrogen and freeze-drying for 48 h under light protection (Liotop® L101 lyophilizer). All samples were stored at 4 °C. At different time points for 60 days, a sample of each batch was assessed regarding particle size distribution, zeta potential and drug concentration, as described above. On each time point, the lyophilized samples were reconstituted with water, keeping the original volume.

2.3.4. Release kinetics of RDV from liposomal formulations

The release study of RDV from liposomes was performed under dialysis conditions at 37 °C, in the presence of HP-β-CD to ensure *sink* conditions. Just after preparation of the liposomal RDV formulations, HP-β-CD was added at a final concentration of 0.01 M and the resulting suspensions were divided into triplicates of 100 μL and added to Slide-A-Lyzer mini 10 kDa MWCO dialysis devices (Thermo Scientific®, BR) attached to an Eppendorf® tube containing 1.5 mL of PBS solution plus 0.01 M HP-β-CD under agitation in a ThermoMixer (Eppendorf®, BR) at 300 rpm/37 °C. A total of 2.5 μL of the dialyzed suspension (or 7.5 μL in the case of LRDV-PEG) was withdrawn at time intervals of 0, 0.5, 1, 2, 3, 4, 5, 6, and 24 h and diluted with 250 μL of ethanol for absorbance reading at 260 nm in a Synergy™ HTX microplate reader, with replacement of 2.5 μL of PBS solution containing 0.01 M HP-β-CD after collection of each sample (or 7.5 μL in the case of LRDV-PEG). Empty liposomes were dialyzed under the same conditions. The percentage of RDV retained was calculated at the different time intervals. The data obtained with each formulation was fitted using a monexponential decay model, allowing the determination of the RDV release half-time.

2.4. Cytotoxicity and antiviral activity

2.4.1. Cells and viruses

Human lung adenocarcinoma cells (Calu-3) and African green monkey kidney cells (Vero-E6 and Vero-CCL81) were obtained from the Rio de Janeiro cell bank (CALU-30264; VERO CCL81 0245; VERO E6 0407). Calu-3 were cultured in DMEM supplemented with 10 % fetal bovine serum (FBS) (GIBCO, Thermo Fisher Scientific®), 100 U/mL penicillin and streptomycin, and 0.25 μM amphotericin B. Vero E6 or Vero CCL-81 were cultured in RPMI medium supplemented with 10 % FBS, 100 U/mL penicillin and streptomycin, and 0.25 μM amphotericin B (Corning®). All cell lines were maintained in a 5 % CO_2 incubator at 37 °C. The SARS-CoV-2 gamma lineage P.1 (EPI_ISL_13017802) was kindly provided by Dr. Sergio Caldas from Fundação Ezequiel Dias - FUNED-MG and grown at the Biosafety Level 3 (BSL-3) at the Institute of Biological Sciences (ICB) of Universidade Federal de Minas Gerais (UFMG). Viral stocks were cultured in Vero CCL81 cells in a humidified incubator at 37 °C with 5 % CO_2 and monitored daily for cytopathic effects (CPE) for up to 72 h. Viruses were titrated in Vero E6 cells using the plaque-forming units (PFU) assay [31], and viral aliquots were stored at −80 °C for later use.

2.4.2. In vitro cytotoxicity assay

Vero-CCL81, Vero-E6 and Calu-3 cells were seeded at a density of 1×10^4 cells/well in 96-well clear bottom plate (Corning®) and incubated at 37 °C overnight. The medium in each well was removed, replaced with fresh medium containing RDV formulations at concentration ranging from 1 to 1500 μM, and incubated for 48 h. LRDV-CONV and LRDV-PEG were compared to free RDV and commercial RDV formulation (Veklury®) in the same experimental conditions, with concentration ranging from 1 to 1000 μM. LEmp and SBE-β-CD were also tested as controls. DMSO was used as a negative control. Cytotoxicity was determined using the MTT Assay Kit (Sigma-Aldrich®) according to the manufacturer's instructions.

2.4.3. In vitro antiviral activity assay

The antiviral assay of free and liposome-encapsulated RDV was performed as described previously [31]. Briefly, Vero E6 cells were seeded at 2.5×10^5 cells per well in 24-well plates and maintained to adhere for 16–24 h. The cells were adsorbed with SARS-CoV-2 at MOI = 0.01 PFU/cell in saline gel for 1 h at 37 °C. The plates were manually mixed every 10 min to redistribute the inoculum. The viral inoculum was removed and media containing dilutions of free or liposome-encapsulated RDV (concentration ranging from 0.01 to 10 μM) or vehicle (DMSO) were added. Veklury® was also used as positive control. The final concentration of DMSO was kept below 1 %. The cells were then incubated at 37 °C in a CO_2 incubator. At 48 h post-infection, the supernatants from the plates were collected and processed for titration. Virus titration was performed using the plaque formation assay. Vero E6 cells were seeded at 2.5×10^5 cells/well in 24-well plates and allowed to adhere for 16–24 h. A serial dilution (10^{-1}, 10^{-2}, 10^{-3} and 10^{-4}) of the viral suspensions (supernatants) was performed with RPMI medium containing 1 % FBS. After dilution, 100 μL of each solution was added to 24-well plates in triplicates. The cells were then incubated in a CO_2 incubator for 1 h, with mixing every 10 min. RPMI medium containing 1 % carboxymethylcellulose (CMC) was then added to all plates, which were further incubated in a CO_2 incubator at 37 °C for 4 days. After this interval, the plates were fixed with 10 % formaldehyde and stained with 0.05 % (*w/v*) crystal violet in 20 % methanol and washed twice with distilled, deionized water. Results are expressed as PFU/cell.

2.5. Pharmacokinetics of RDV

Pharmacokinetic studies of RDV were performed in the plasma and bronchoalveolar lavage (BAL) of C57BL/6 mice (male), using a spectrofluorimetric method previously validated by Elmansi et al. (2021) for RDV quantification [32]. The protocol was approved by the UFMG Ethic Committee for Animal Use (CEUA 28/2023).

In the plasma pharmacokinetic study, mice were randomly divided into three groups. A first group received a single dose of Veklury® at 20 mg RDV/kg by IP route. The two other groups received a single dose of LRDV or Veklury® at 10 mg RDV/kg by IN route (15 μL in each nostril). Mice were euthanized at different time intervals after drug administration (0, 4, 10, 20 and 60 min) and blood was collected *via* the orbital venous plexus in EDTA tubes and plasma was isolated ($n = 4$ per time point). To determine RDV plasma concentration, 0.1 mL of plasma was mixed with 0.5 mL of acetonitrile, the mixture was vortexed for 2 min and centrifuged at 3500 rpm for 30 min. 0.25 mL of the supernatant was then mixed with 2-mL of 0.04 M acetate buffer (pH 4.0). The resulting solution was then transferred to a quartz cuvette and the fluorescence intensity was recorded with excitation at 244 nm and emission at 405 nm, using a fluorescence spectrophotometer (Eclipse, Varian, USA).

Blank plasma samples were prepared similarly and used to establish a calibration curve of the fluorescence intensity *versus* RDV concentration.

In the pharmacokinetic study in the BAL, mice were divided into the following groups. The first group received IN Veklury® as a single dose of 10 mg RDV/kg (15 μL in each nostril). The second group received IN LRDV as a single dose of 10 mg RDV/kg (15 μL in each nostril). Mice were euthanized at different time intervals after drug administration (0, 4, 10, 15, 30 and 60 min) and the BAL was collected as described previously (n = 3–4 per time point) [33]. 0.5 mL of the recovered BAL volume was mixed with 2.5 mL of acetonitrile and the resulting solution was vortexed and then centrifuged at 3500 rpm for 30 min. In a quartz cuvette, 1 mL of the supernatant was mixed with 2 mL of acetate buffer (pH 4.0) and the fluorescence intensity was recorded with an excitation at 244 nm and emission at 405 nm. Blank BAL samples were prepared similarly and used to establish a calibration curve of the fluorescence intensity *versus* RDV concentration.

2.6. Liposome distribution in the brain

The distribution of liposomes in the brain after IN administration was evaluated in C57BL/6 mice using liposomes labeled with lipophilic fluorescent dye DiD, as described previously [34,35]. The protocol was approved by the UFMG Ethic Committee for Animal Use (CEUA 28/2023). Empty liposomes were prepared as described above and DiD was added from an ethanol stock solution (1 mM) at 1 % (*v*/v) to the final suspension. After 15-min incubation at 25 °C, DiD-labeled liposome suspension was instilled intranasally to mice as 15 μL in each nostril (n = 3). Empty liposomes and free DiD in PBS were used as controls. Four hours after administration, mice were euthanized, and the brains were fixed in OCT and rapidly frozen in liquid nitrogen. Brain sections were obtained using a cryostat, washed with PBS, and subsequently stained with DAPI (1:1000) for nuclear visualization. Images were acquired using a confocal microscope (Zeiss LSM 880, Germany), with a 40× immersion objective and a 633 nm laser, at the Center for Image Acquisition and Processing (CAPI-UFMG).

2.7. In vivo assays of antiviral and immunomodulatory activities

2.7.1. Animal model

Transgenic C57BL/6 J mice expressing the human angiotensin-converting enzyme 2 (hACE2) receptor, driven by the cytokeratin-18 gene promoter (K18-hACE2), were originally obtained from The Jackson Laboratory. Mice were group-housed at the Bioterio do Departamento de Bioquímica-Imunologia (ICB, UFMG) and experiments with SARS-CoV-2 performed at the animal facility of the BSL-3 laboratory at UFMG. Mice were fed with standard diets, and maintained on a 12-h light/dark cycle with 50–58 % humidity and temperature of 25 °C. *In vivo* experiments were conducted following the recommendations of the Guide for the Care and Use of Laboratory Animals from the National Council for Animal Experimentation Control (CONCEA). All protocols involving mice were approved by the UFMG Ethic Committee for Animal Use, under protocol number CEUA 147/2022.

2.7.2. Infection and treatment of mice

K18-hACE2 mice infected with SARS-CoV-2 were used as preclinical model of COVID-19, as described previously [36–38]. Intranasal exposure of K18-hACE2 mice to SARS-CoV-2 virus causes robust infection of the upper and lower airways followed by the brain and liver, that rapidly progresses into lethal disease. Mice of different ages (11–12 weeks) of both sexes were infected with 6×10^4 PFU of SARS-CoV-2 intranasally. Viral inoculations (20 μL) were performed under inhalational anesthesia with isoflurane. Liposomal formulations were freshly prepared before each administration. Treatment was initiated 8 h post-infection (n = 8/group) with IN LRDV (10 mg RDV/kg with 15 μL in each nostril), IN LEmp (same lipid dose as that in LRDV), IP Veklury® (20 mg RDV/kg) or IN PBS (vehicle), and repeated every 12 h for 5 days (total of 9 doses). Uninfected mice (Mock) were acclimated for control purposes. The therapeutic regimen with Veklury® (20 mg RDV/kg/bid for 5 days) was based on a previous study by Jeong et al. (2022) using the same animal model [19]. Mice were monitored daily for 15 days by measuring body weight and lethality rates. In a parallel experiment with the same groups (except for LEmp group), 8 mice of each group were euthanized at 5 days post-infection. Tissues were harvested to assess viral load, production of inflammatory mediators, cell response and histopathological changes. In another experiment, K18-hACE2 mice infected with SARS-CoV-2 as described above were subjected to treatment with IN LRDV or IN Veklury® at a dose of 10 mg RDV/kg/bid for 6 days to compare the impact of both treatments on animal survival (n = 8/group).

2.7.3. Viral titers by plaque assay

Mouse tissues, including lungs, brain and kidneys, were weighed and homogenized with magnetic beads (Thermo Fisher Scientific) in a TissueLyser LT equipment (QIAGEN - Life Science Instruments) in 1 mL of RPMI medium supplemented with 2 % FBS. Tissue homogenates were clarified by centrifugation at 10,000 ×g for 5 min and stored at −80 °C. Vero E6 cells were seeded at a density of 2.5×10^5 cells/well in 12-well flat-bottom tissue culture plates. The next day, the medium was removed and replaced with 100 μL of serial dilutions of the material to be titrated, diluted in RPMI 1 % FBS. One hour later, fresh semisolid medium containing 1.2 % CMC was added. Plates were incubated for 72 h and then fixed with 10 % formaldehyde (final concentration) in PBS for 20 min. The plates were stained with 0.05 % (*w*/*v*) crystal violet in 20 % methanol and washed twice with distilled, deionized water. Results are expressed as PFU/g of tissue.

2.7.4. Viral load by RT-qPCR

RNA was isolated from lung and brain homogenates as described above and extracted using a QIAamp Viral RNA Mini Kit (QIAGEN, Inc., Valencia, USA) according to the manufacturer's instructions, and quantified spectrophotometrically using the Nanodrop Lite (Thermo Fisher Scientific). Subsequently, 500 ng of total RNA was subjected to cDNA synthesis with high-capacity cDNA reverse transcription kits (ThermoFisher Scientific) according to the manufacturer's instructions and stored at −20 °C. Molecular diagnosis for SARS-CoV-2 detection (primer N1) was performed according to the manufacturer's instructions of the iTaq Universal Probes One-Step Kit. Real-time PCR was performed using the Quant Studio 3 (ThemoFisher Scientific). The PCR steps were as follows: 95 °C – 3 min, followed by 40 cycles 95 °C – 15 s, 60 °C – 1 min. Standard curve and negative controls were used to validate the method.

2.7.5. Immunofluorescence

To demonstrate the presence of the virus in the brain and lungs by immunofluorescence, tissues from treated and control groups were collected for preparation of cryosections of 5 μm thickness. Samples were stained with a specific antibody for SARS-CoV-2 (1:500, no:40591-t62, 2019-nCoV Spike RBD Antibody, Sino Biological) and a secondary rabbit anti-goat Alexa Fluor 633 antibody (1:100, ThermoFisher Scientific, no. A-21052), incubated overnight at 4 °C. Nuclei were stained with DAPI, and slides were mounted in Dako fluorescence mounting medium (Dako, Santa Clara, CA). Images were acquired on a confocal microscope (Zeiss LSM 880, Germany), with a 40× immersion objective, using a 633 nm laser, at the CAPI-UFMG. Six random fields from each sample were used for analysis.

2.7.6. Flow cytometry assay of myeloid and lymphoid cells

Lung and spleen homogenates previously digested with Collagenase I were cultured overnight in the presence of Brefeldin A (Golgi Stop, BD) to inhibit cytokine secretion in culture. Cells were washed twice with PBS, centrifuged at 300 ×g for 10 min to remove any soluble protein in the culture medium, and incubated with cell viability reagent (Live/Dead Fixable Dead Cell Stains) as recommended by the manufacturer

(Invitrogen). The cell suspension was stained with two panels containing antibodies for the evaluation of activated T cells producing cytokines of the Th1, Th2, and Th17 profiles and cytokine-producing myeloid cells (Table S1). The panel for myeloid cell characterization consisted of antibodies against surface molecules diluted in PBS containing 0.1 % BSA and 2 mM azide (FACS buffer): anti-CD45, anti-CD11b, anti-F4/80, anti-Gr-1, anti-CD206 (Table S2). The panel for T cell evaluation consisted of antibodies against surface molecules diluted in the FACS buffer: anti-CD45, anti-CD3, anti-CD4, anti-CD8, and their respective cytokines (Table S2). Incubation with the extracellular antibodies was performed for 20 min, and the cells were then washed twice by centrifugation for 4 min at 300 ×*g* with FACS buffer. Afterwards, cells were fixed for 35 min at 4 °C using eBiosciences Cytofix/Cytoperm buffer. Following this, cells were washed once with eBioscience Perm/Wash buffer. Subsequently, cells were stained with anti-iNos for 45 min at 4 °C. Finally, the cell suspension previously stained with biotinylated anti-Gr-1 antibody was revealed. A new washing was performed for 4 min at 300 ×g, and the cells were then incubated for 15 min with streptavidin. The cells were acquired on the LSR Fortessa cytometer (BD Pharmingen). FlowJo 10 (TreeStar) software was used for data analysis.

2.7.7. ELISA assay for proinflammatory cytokines

The level of secreted cytokines (TNF and IL-6) was determined in the lungs. Tissue homogenates were prepared and clarified by centrifugation at 2,500 ×*g* for 5 min. All samples were serially diluted, and a standard curve and negative controls were used. The assay was performed using mouse TNF and IL-6 DuoSet ELISA kits (R&D Systems, Inc. USA) according to the manufacturer's recommendations.

2.7.8. Histopathological analyses

Histopathological changes caused by SARS-CoV-2 and treatments were analyzed in the lung, liver and brain of mice. Mice tissues were fixed in 10 % neutral buffered formalin. Paraffin blocks of collected tissues were prepared and cut into 5-μm thickness sections and stained with hematoxylin and eosin (H&E) for microphotograph analysis. Histopathological evaluation was performed using a score for each anatomical region. Lung and liver samples were analyzed for lesions and acute inflammatory processes. Score was established as: 0, for no alteration; 1, for discrete change (0–25 %); 2, for moderate changes (25–50 %); 3, for intense changes (50–100 %).

2.8. Statistical analyses

Data are presented as means ± SEM or median ± 95 % confidence interval. Data normal distribution was checked with the following tests: Anderson–Darling test, D'Agostino and Pearson test. Statistical analysis of normally-distributed data was performed using One-way ANOVA with Dunnett's multiple comparison post-test or Two-way ANOVA with Tukey's multiple comparison post-test. For non-parametric data, Kruskal-Wallis's test followed Dunn's multiple comparison post-test was used. Survival curves were analyzed using the Kaplan-Meier test and compared using Logrank and Gehan-Beslow-Wilcoxon tests. Values of $p < 0.05$ were considered significant. The graphics and statistical analyses were performed using GraphPad Prism® (version 10) software (GraphPad Software, San Diego, CA, USA).

3. Results

3.1. Preparation and characterization of liposomal RDV formulations

Liposomal RDV formulations were first prepared by the ethanol injection method, taking advantage of the lipophilic character of RDV. Conventional (LRDV) and PEGylated (LRDV-PEG) liposomes were made from SPC as the main phospholipid. Characterization of the formulations by dynamic light scattering showed an average diameter in the range of 110 to 120 nm and a polydispersity index (PDI) below 0.1, indicating monodisperse vesicles (Table 1). The same trend was observed by NTA, showing diameter of 120.8 ± 44.8 for LRDV. LRDV and LRDV-PEG exhibited drug encapsulation efficiency close to 60 % and comparable encapsulated drug/lipid ratio. On the other hand, LRDV-PEG formulation was obtained with a final drug concentration 3.5-fold lower, due to the inclusion of cholesterol in the formulation and its limited solubility in ethanol.

A comparison of drug release profiles was performed under dialysis at 37 °C using HP-β-CD-containing PBS to ensure *sink* conditions. Fig. 1B exhibits the kinetics of RDV release and curve fitting according to monoexponential decay. Both liposomal formulations showed sustained drug release profiles when compared to the RDV/HP-β-CD complex. PEGylation resulted in significantly faster drug release. The most sustained drug release profile was achieved by the LRDV formulation, with a drug release half-time of 5.3 h.

The stability of LRDV was evaluated under storage at 4 °C, either as aqueous suspension or under the freeze-dried state in the presence of sucrose. The aqueous suspension was found to be stable for up to 5 days, regarding particle size distribution (diameter and polydispersity index), zeta potential and drug concentration (as absorbance). After 12 days of storage, a significant change in zeta potential and a decrease in drug concentration were observed (Fig. 1E,F). On the other hand, the lyophilized LRDV formulation was found to be stable up to 60 days of storage, with no change of particle size distribution, zeta potential or drug concentration, after reconstitution.

An alternative method was also evaluated for the preparation of liposomal RDV formulations. The method consisted in the prior formation of a drug-cyclodextrin inclusion complex, followed by incorporation of the water-soluble complex into DSPC/DPPG/CHOL liposomes containing or not DSPE-PEG2000, using the dehydration-rehydration process. The resulting conventional and PEGylated formulations were characterized regarding particle size distribution and zeta-potential, as well as drug encapsulation efficiency and kinetics of drug release. These formulations showed slightly greater liposome sizes and polydispersity indexes, compared to LRDV formulations, but lower drug encapsulation rate, ranging from 35 to 38 % (Table S1). Furthermore, the release half-times of RDV were found to be shorter than those of LRDV formulations (Fig. S1). Therefore, LRDV and LRDV-PEG formulations were selected for subsequent *in vitro* assays based on their higher drug encapsulation efficiency and more sustained drug release property.

3.2. In vitro cytotoxicity and antiviral activity

The impact of liposome encapsulation on RDV cytotoxicity has been evaluated in Vero CCL81, Calu-3 and Vero-E6 cells, through comparison with free RDV and RDV/SBE-β-CD complex (as Veklury®). As illustrated in Fig. 2A,B,C, both the LRDV and LRDV-PEG liposomal formulations were less cytotoxic than RDV alone or its complex with SBE-β-CD. Empty liposomes showed no cytotoxicity in the range of lipid concentration tested. The same profile was observed in all cell lines. The benefits of liposomes may be attributed to their sustained drug release properties, as evidenced above. This first data suggests that liposomal RDV formulations may be safer than the commercial cyclodextrin-based formulation Veklury® for *in vivo* application.

When evaluated for antiviral activity, LRDV and LRDV-PEG promoted a dose-dependent reduction in the production of infectious viruses with EC_{50} values of 0.9 and 1.2 μM, respectively, while RDV inhibited the virus with EC_{50} of 0.3 μM (Fig. 2D).

The cytotoxicity and antiviral activity data allowed the calculation of the selectivity index (SI) of each RDV formulation [39]. Interestingly, the encapsulation of RDV in liposomes improved the selectivity index, being the best result obtained for the LRDV formulation (Fig. 2D insert).

Table 1
Characteristics of conventional and PEGylated liposomal RDV formulations: particle size distribution, polydispersity index, zeta potential, and drug encapsulation efficiency.

Formulation	[a]Size (nm) ± SD	[a]PDI ± SD	[a]Potential ζ (mV) ± SD	Final RDV concentration (mg/mL) ± SD	[a]EE(%) ± SD	Encapsulated drug/lipid ratio (m/m)
LRDV	118.4 ± 3.2	0.047 ± 0.024	−2.14 ± 0.18	5.4 ± 0.4 (n = 5)	59.3 ± 4.4 (*n* = 5)	0.0610
LRDV-PEG	110.1 ± 1.8	0.026 ± 0.005	−8.97 ± 0.05	1.55 ± 0.21 (n = 2)	57.2 ± 7.2 (*n* = 2)	0.0543
[b]LEmp	102.7 ± 1.7	0.056 ± 0.036	−3.55 ± 0.07		–	–
[b]LEmp-PEG	104.2 ± 2.1	0.098 ± 0.016	−2.55 ± 0.09		–	–

[a] Means ± standard deviation (SD). Size: average hydrodynamic diameter; PDI: polydispersity index; potential ζ: zeta potential; EE(%): drug encapsulation efficiency.
[b] LEmp and LEmp-PEG were prepared by the same method as LRDV and LRDV-PEG, respectively, but omitting RDV.

3.3. Pharmacokinetics of RDV in the BAL and plasma and liposome distribution in the brain

LRDV was selected for subsequent *in vivo* studies on the basis of higher drug concentration and encapsulation efficiency, as well as its sustained drug release property. To get insight into the ability of LRDV to deliver RDV to the lungs, RDV levels were determined in the BAL of C57BL/6 mice at different time intervals after IN administration. Comparison was made with Veklury® administered by the same route and at the same dose (10 mg RDV/kg). As shown in Fig. 3A, IN instillation of LRDV resulted in rapid delivery of RDV to the lungs, with drug levels being detectable up to 15 min after administration. IN Veklury® showed a significantly lower level of RDV at 4 min compared to LRDV and no drug detected after 10 min. Thus, this data indicates that IN LRDV promoted more effective drug delivery and more sustained drug levels in the lungs, in comparison to IN Veklury®. A complementary question was whether IN LRDV would allow RDV to reach the blood circulation at a significant level. As shown in Fig. 3B, it was not possible to detect RDV in the plasma of mice after IN administration of LRDV. This is in contrast to Veklury® administered by IN or IP route, which resulted in a significant plasma level of RDV after 4 min.

The ability of our liposomal formulation to deliver a lipophilic compound to the brain was further investigated using empty liposomes (same lipid composition and concentration as LRDV) labeled with lipophilic fluorescent dye DiD. As illustrated in Fig. 3C, confocal microscopy images of brain sections showed red fluorescent regions, 4 h after IN instillation of the suspension. On the other hand, no fluorescence was observed after IN instillation of a solution of DiD in PBS or a suspension of non-labeled liposomes. Thus, the liposomes used in LRDV effectively delivered the lipophilic dye to the brain.

3.4. Impact of treatments on the survival of K18-hACE2 infected mice

The therapeutic efficacy of LRDV formulation was evaluated in K18-hACE2 mice infected with SARS-CoV-2, after IN administration every 12 h for 5 consecutive days. Comparison was performed with IP Veklury®, as well as empty liposomes or PBS by IN route. A non-infected and non-treated group (Mock) was also used as a control. Fig. 4 shows the survival rate and body weight change of infected mice during and after treatment. Remarkably, treatment with LRDV ensured 100 % animal survival (Fig. 4A,B). Veklury® prolonged the survival rate of mice with median survival of 8 days, compared to LEmp and PBS groups with median survival of 5 days. LEmp and PBS groups showed marked weight loss during the five days following infection (Fig. 4C). On the other hand, IN LRDV was significantly more effective than IP Veklury® in preventing body weight loss (Fig. 4C,D).

In another experiment, the efficacy of treatment with IN LRDV was compared to that with IN Veklury® at the same dose of RDV. The survival curves shown in Fig. S2A indicate that IN LRDV was significantly more effective than IN Veklury®. While 100 % animal survival was observed after IN LRDV, 50 % of animals died in IN Veklury® group.

3.5. Impact of treatments on viral loads in the lungs and brain

The viral loads were evaluated in the lungs and brain of infected animals, after treatment and euthanasia of mice at 5 dpi. Three different methods were used: the plaque assay for viable virus, RT-qPCR for viral RNA levels and immunofluorescence of the viral S protein.

As shown in Fig. 5A,B, plaque assay and RT-qPCR results indicated a significant reduction in viral titers in the lungs after treatments with IN LRDV and IP Veklury®, compared to the PBS control. Immunofluorescence assay of lung tissue using an RBD spike antibody (Fig. 5C) revealed intense staining (pink spots) in PBS samples, and almost no staining in LRDV and Veklury® samples, further supporting the reduction in virus load.

Determination of viral titers in the brain by plaque assay and RT-qPCR also showed significant virus suppression after treatment with IN LRDV, compared to PBS (Fig. 6A,B). Strikingly, no significant change in the viral titer was observed after IP Veklury®. The immunofluorescence images of the viral S protein, as illustrated in Fig. 6C, further supported the reduction in viral load.

Histopathological analysis of the brain of infected animals showed no apparent abnormalities in any experimental group, as illustrated in Fig. S3.

3.6. Impact of treatments of infected mice on inflammatory response in the lung

3.6.1. Pro-inflammatory cytokines

As IL-6 and TNF are known to be increased in the lungs of K18-hACE2 mice in response to SARS-CoV-2 infection and local inflammation is an important step towards tissue damage [36], the level of these pro-inflammatory cytokines was determined at 5 dpi. As shown in Fig. 7A, IL-6 level was significantly reduced in the LRDV group compared to the PBS and Veklury® groups, evidencing inhibition of the inflammatory response. Furthermore, treatments with IN LRDV and IP Veklury® significantly reduced the level of TNF compared to PBS.

3.6.2. Myeloid and lymphoid cells profiles

Treatment with IN LRDV also significantly reduced the numbers of infiltrated neutrophils and monocytes, including monocytes expressing $CD206^{+}$ and $iNOS^{+}$, when compared to PBS control (Fig. 8). This data further supports the inhibition of the inflammatory response by LRDV. It is also noteworthy that this effect was less pronounced after treatment with IP Veklury®.

On the other hand, comparison of the number of each lymphoid cell

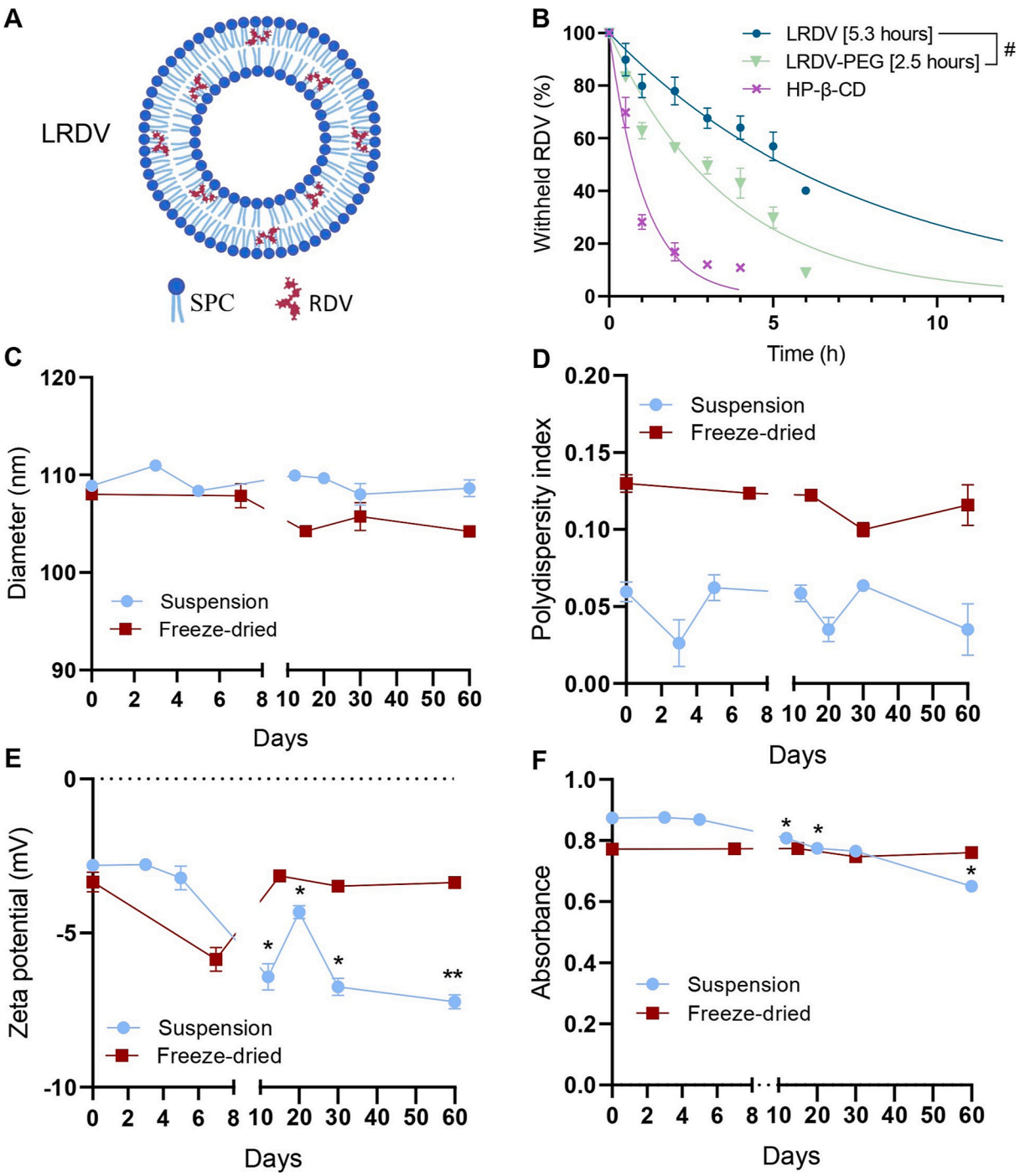

Fig. 1. Kinetics of RDV release from LRDV and LRDV-PEG formulations and stability of LRDV formulation under different storage conditions. **A**. Schematic representation of LRDV composition. **B**. Kinetics of RDV release under dialysis at 37 °C from conventional (LRDV) and PEGylated (LRDV-PEG) liposomes prepared by the ethanol injection method. Data were fitted according to monoexponential decay to determine RDV release half-time (values shown in bracket). The complex of RDV with HP-β-CD was used as a control. Data are shown as mean ± SEM obtained from three independent samples. $^{\#}p < 0.0001$ for comparison of the drug release half-time between LRDV and LRDV-PEG. Stability of LRDV regarding mean hydrodynamic diameter (**C**), polydispersity index (**D**), zeta potential (**E**) and absorbance at 260 nm (**F**) at different time intervals over a period of 60 days, after storage at 4 °C as suspension or under the freeze-dried state. On each time point, the freeze-dried samples were reconstituted with water and immediately analyzed. Data are presented as mean ± SEM from three independent formulation batches. *p < 0.05, **$p <$ 0.01 for comparison with time zero according to Repeated Measures One-way ANOVA followed by Dunnett's multiple comparisons test.

population in the lungs (CD45$^+$, CD3$^+$ T cells, CD4$^+$ T cells or CD8$^+$ T cells) between LRDV, Veklury® and PBS groups showed no significant differences (Fig. S4).

3.6.3. *Histopathological changes*

Histopathological evaluations of the lungs at 5 dpi were also performed to establish a score. Accordingly, all infected groups showed discrete to moderate changes, including cell infiltrate and vessels congestion, whereas no change or discrete change was observed in non-infected mice (Fig. S5). No significant difference was found between PBS, LRDV and Veklury® groups.

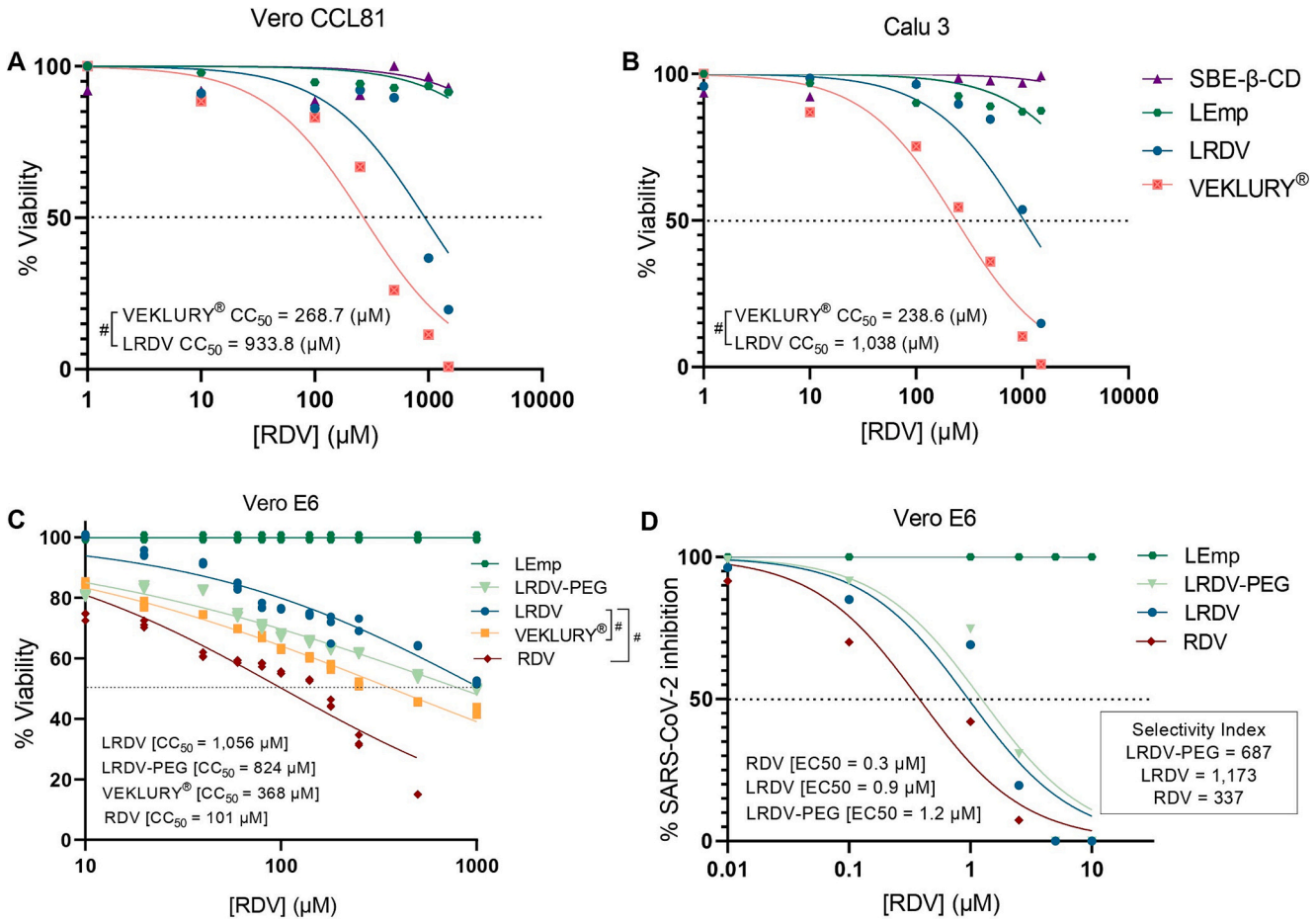

Fig. 2. Cytotoxicities and antiviral activities of LRDV and LRDV-PEG liposomal formulations in comparison to RDV alone or its complex with SBE-β-CD (Veklury®). **A**, **B**, **C**: viability (%) of Vero CCL81 (A) and Calu-3 (B) and Vero E6 (C) cells 48 h after exposition to the formulations at varying concentrations. Empty liposomes (LEmp) and SBE-β-CD were also used as controls. $^{\#}p < 0.0001$ for comparison of the CC_{50} between LRDV and Veklury® or RDV. **D**: inhibition (%) of SARS-CoV-2 production in Vero E6 cells. Graphs exhibit the means of % viability or % inhibition ($n = 2$–3) as a function of concentration, the non-linear least squares fitted curves, as well the values of the concentrations that reduce cell viability by 50 % (CC_{50}) and eliminates 50 % of the virus (EC_{50}) shown in bracket. The insert in D shows the selectivity index of LRDV and RDV, calculated as CC_{50}/EC_{50} ratio.

3.7. Systemic effects of treatments

To compare the systemic effects of LRDV and Veklury®, histopathological changes in the liver, virus titers in the kidney and profiles of lymphoid cells in the spleen were investigated.

Fig. 9 displays the results of histopathological evaluations of the liver of K18-hACE2 mice at 5 dpi. Animals treated with LRDV showed no histopathological change (Fig. 9A-B). On the other hand, the group treated with Veklury® presented marked hydropic degeneration in all treated animals (Fig. 9B). Some animals of the PBS group also showed hydropic degeneration, probably due to viral infection [40]. This data is consistent with the difference in the animals' body weight loss between the LRDV and Veklury® groups and corroborates the greater toxicity of RDV when administered parenterally, compared to the IN route.

In the kidney, no virus was detected in any of the animals receiving IN LRDV or IP Veklury®, in contrast to the PBS group in which 3 out of 8 animals showed viral titer (Fig. S6). This data suggests that both treatments were equally effective in reducing systemic viral titer.

The profile of lymphoid cells in the spleen was altered after treatment with Veklury®, showing an increase in $CD4^{+}$ cells secreting the anti-inflammatory cytokine IL-4 (Fig. S7). A similar trend was found after LRDV, although no significant differences were observed compared to the PBS group.

4. Discussion

The present work provides two major contributions. First, a liposomal RDV formulation was developed and selected based on high drug encapsulation efficiency, sustained drug release property and high *in vitro* selectivity index. Secondly, the antiviral efficacy of liposomal RDV was established *in vivo* after IN administration in a transgenic mouse model of COVID-19, showing strong reduction in SARS-CoV-2 titers in the brain and lungs and preventing the inflammatory response induced by the virus in the lungs. Notably, the liposomal formulation of RDV administered intranasally achieved 100 % animal survival in contrast to commercial Veklury® administered parenterally or intranasally.

Regarding the development of a liposomal RDV formulation, the ethanol injection method that resulted in the incorporation of RDV into the liposomal membrane proved to be more promising than the dehydration rehydration method that consisted of encapsulating the RDV-cyclodextrin complex in the internal aqueous compartment of liposomes. Indeed, higher drug encapsulation efficiency (Table 1) and slower drug release (Fig. 1B) were found from LRDV liposomes, compared to DRV formulations. Possibly, the RDV-cyclodextrin complex made RDV more readily available for permeation and release than LRDV, despite the more rigid membrane of DRV liposomes. Previous works have described the encapsulation of RDV in liposomes made from DPPC/cholesterol/DSPE-PEG2000 or DOPC using the lipid film hydration method [16,26]. It was also reported that liposomal RDV prepared

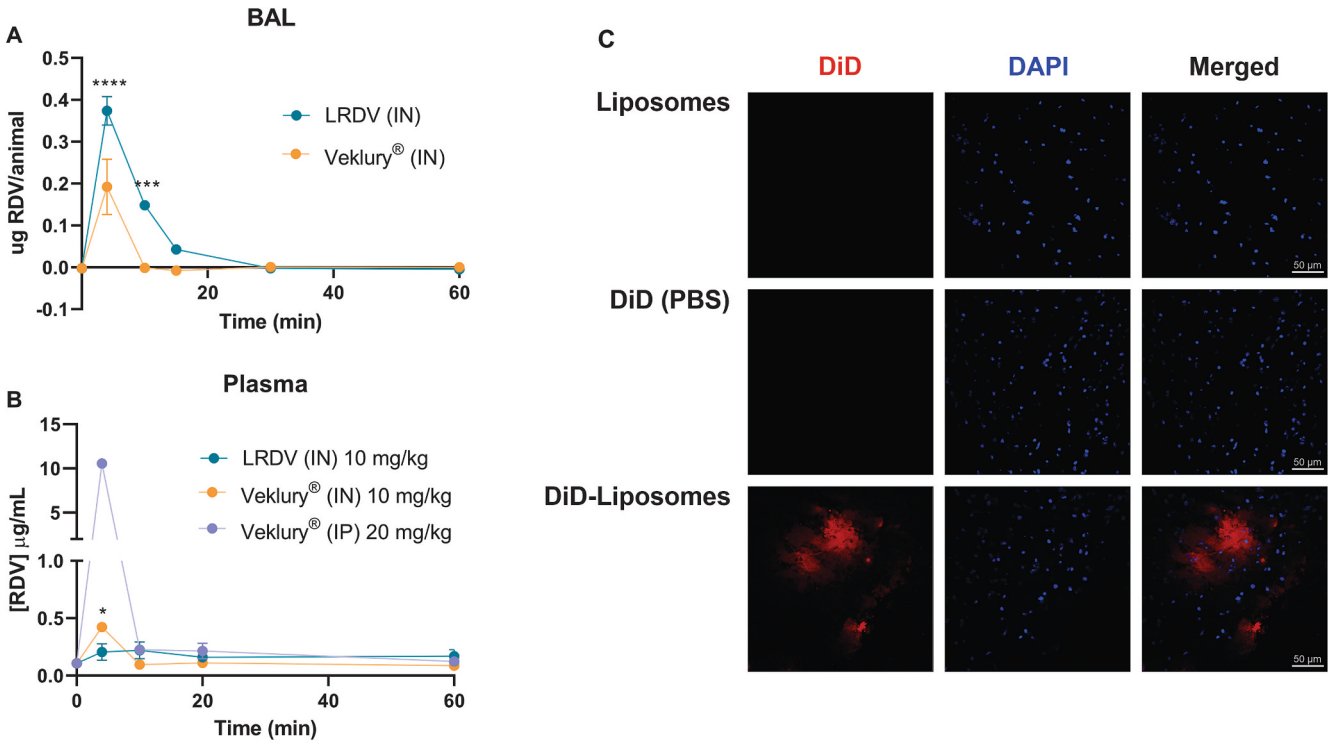

Fig. 3. Pharmacokinetics of RDV in the BAL (**A**) and plasma (**B**) after IN LRDV or Veklury® and liposome distribution in the brain (**C**). **A**: C57BL/6 mice received either IN LRDV or IN Veklury® at 10 mg of RDV/kg (15 µL in each nostril). Mice were euthanized at different time points ($n = 3$–4 per time), BAL were obtained and RDV concentrations were determined using a fluorimetric assay. Data are shown as means ± SEM. The value shown at time zero (−0.0024 ± 0.0078) was obtained from non-treated control mice. ***$p < 0.001$ and ****$p < 0.0001$ for comparison between LRDV and Veklury® by Two-way ANOVA and Tukey's multiple comparisons test. **B**: C57BL/6 mice received either IN LRDV or IN Veklury® at 10 mg of RDV/kg (15 µL in each nostril) or Veklury® intraperitoneally at 20 mg of RDV/kg. Mice were euthanized at different time points ($n = 4$ per time), plasma were collected and RDV concentrations were determined fluorimetrically. Data are shown as means ± SEM. The value shown at time zero (0.108 ± 0.021) was obtained from non-treated control mice. *$p < 0.05$ for comparison between IN LRDV and IN Veklury® by Two-way ANOVA and Tukey's multiple comparisons test. **C**: Representative confocal fluorescence microscopy images (amplification, 40×) of brain cryosections, 4 h after IN instillation in C57BL/6 mice of the suspension of empty liposomes labeled with lipophilic fluorescent dye DiD, non-labeled empty liposomes or free DiD in PBS (15 µL in each nostril).

by the ethanol injection method, as performed here, showed rapid precipitation of RDV [26]. Of note, precipitation was not observed with LRDV stored at 4 °C. Indeed, LRDV was stable for up to 5 days as aqueous suspension and at least 60 days under the freeze-dried state (Fig. 1C,D). Thus, our work represents a significant advance compared to previous studies, as a liposomal RDV formulation was achieved using a simple and scalable process (ethanol injection method) and low-cost lipid composition. Possible explanations for the greater stability of our formulation may be the use of natural phosphatidylcholine (instead of synthetic phospholipid), lower temperature (instead of 55 °C) and PBS (instead of water) during the injection process, as well as the liposome size calibration by extrusion (instead of probe sonication). The ability of the liposomes used in LRDV to migrate to the brain after IN administration (Fig. 3C) is in accordance with the literature. The effective size of nanocarriers for brain delivery has been reported to be up to 200 nm, which appears to be associated with the average diameter of olfactory exons [24]. Furthermore, the electrically neutral surface charge of our liposomes is expected to favor their distribution in the brain. Indeed, neutral liposomes displayed greater migration into the brain *via* the olfactory and trigeminal nerve pathways compared to cationic or anionic liposomes [41]. The rationale for evaluating the impact of including DSPE-PEG2000 in the liposome membrane was that PEGylated liposomes could promote a more sustained release of the drug *in vivo*, due to reduced cellular uptake compared to conventional liposomes [42]. Moreover, PEGylation of neutral liposomes has been found to further increase the efficiency of nose-to-brain delivery [41]. However, the inclusion of DSPE-PEG2000 in the membrane resulted in a suspension with lower final drug concentration (Table 1) and faster drug release (Fig. 1B). This agrees with previous observation [43] and may be attributed to the detergent and permeabilizing effect of DSPE-PEG2000. In future studies, it would be worth investigating a dry powder of liposomal RDV as an alternative dosage form for pulmonary administration by inhalation.

The Gamma (P.1) SARS-CoV-2 variant, used in the present work, was first identified in Manaus (AM, Brazil) in early December 2020, causing widespread infection despite the high seroprevalence against the wild-type (Wt) SARS-CoV-2 strain observed in the city [44]. This variant carries 17 amino acid changes, ten of which are located in its S protein, including three assigned as alarming (N501Y, E484K, and K417T) [45]. P.1 variant has been associated with an increased risk of reinfection compared to Wt SARS-CoV-2 [46] and a higher number of young patients developing severe complications [47]. Although the pandemic has lessened in severity, with the circulation of the omicron subvariants and their reduced pathogenicity, studies involving the more aggressive variants such as P.1 are still valuable, considering that new, more virulent variants could emerge and re-escalate the pandemic.

Our *in vitro* data confirmed that the antiviral activity of RDV was preserved upon incorporation into liposomes (Fig. 2D). Strikingly, liposomal encapsulation strongly reduced RDV cytotoxicity (Fig. 2A,B,C). This is an important result, considering the high local concentration of the drug in the nasal cavity and lungs after IN administration of LRDV. Interestingly, LRDV was also less cytotoxic than Veklury®, indicating that liposomes were more effective than cyclodextrins in reducing the drug cytotoxicity. The low cytotoxicity of LRDV is in agreement with a previous report for another liposomal formulation of RDV made from DOPC [26]. However, no direct comparison can be made, as the

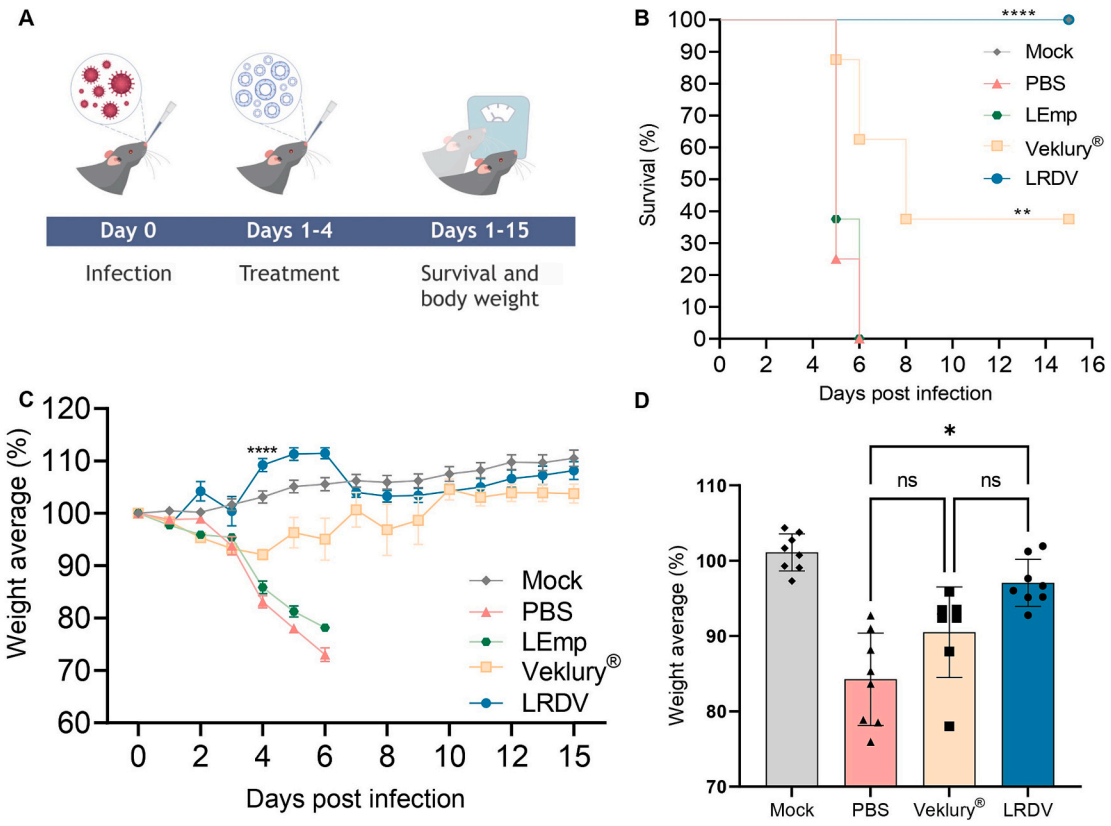

Fig. 4. Impact of intranasal treatment with liposomal RDV on survival (**B**) and body weight change (**C**, **D**) of K18-hACE2 mice infected with SARS-CoV-2. **A**: schematic representation of the experimental protocol. Treatment initiated 8 h after infection and was carried out every 12 h for 5 days. Experimental groups ($n = 8$/group) were: IN LRDV at 10 mg of RDV/kg/dose, IP Veklury® at 20 mg of RDV/kg/dose, IN LEmp at the same lipid dose as LRDV and IN PBS. An uninfected and untreated group (Mock) was also used as a control. **B**: animal survival registered on each day; survival curves were analyzed using the Kaplan-Meier test and compared using Logrank and Gehan-Beslow-Wilcoxon tests. $^{**}p < 0.01$, $^{****}p < 0.0001$ for comparison of LRDV with Veklury® and PBS, respectively. **C**: time course of body weight change in relation to day 0; means±SEM; ****p < 0.0001 for comparison with PBS group using Two-way ANOVA followed by Dunnett's post-test. **D**: body weight change at 5 dpi as means±SEM, compared with Kruskal-Wallis test followed by Dunn's post-test; $^{*}p < 0.05$ for comparison with PBS group. ns, no significant difference.

cytotoxicity assay carried out by these authors used a much shorter exposure time to the drug.

In line with other studies on intranasal drugs [24,25,48,49], our work had a dual objective: delivering RDV to the lungs to inhibit viral progression and SARS; and to reach the brain to prevent viral invasion and subsequent "Long COVID". The ability of LRDV to deliver RDV to the lungs after intranasal administration was confirmed by RDV pharmacokinetics in BAL (Fig. 3A). The short residence time of RDV in the BAL is consistent with a rapid capture of the non-PEGylated liposomes by pulmonary cells. Our pharmacokinetic and animal survival data (Fig. 3 and Fig. S2) also supported the idea that the liposomal carrier was more effective than cyclodextrin in controlling RDV release and delivery to the lungs. Three different factors may contribute to the higher efficacy of IN LRDV compared to IN Veklury®: i) the more sustained drug release property of liposomes (Fig. 1B); ii) the more effective delivery of RDV to the lung, as supported by pharmacokinetic data in the BAL (Fig. 3A); iii) the higher viscosity of the liposomal formulation leading to a prolonged residence time in the nasal cavity. On the other hand, plasma pharmacokinetic data indicated no detectable plasma level of RDV following IN instillation of LRDV (Fig. 3B), suggesting that the drug likely did not reach the brain after absorption into the systemic circulation. In contrast, RDV was detected in the plasma after IN and IP Veklury®, albeit for a very short period of time. The short half-life of RDV in the systemic circulation of mice is consistent with previous reports and was attributed to rapid degradation of the drug by carboxylesterases [10,50,51]. It has also been shown that RDV is intracellularly metabolized into an adenosine analog (GS-441524) and both RDV and GS-441524 are further metabolized into the active nucleoside triphosphate (GS-443902) by the host [10]. Previous pharmacokinetic study of inhaled RDV formulations at 10 mg RDV/kg in rats indicated very low plasma levels of RDV (below 1 ng/mL) and no detectable levels after 2 h of pulmonary dosing, in agreement with the data obtained here after IN LRDV and Veklury®. On the other hand, these authors reported much higher and more prolonged plasma levels of GS-441524 compared to RDV [51]. Considering that GS-441524 also exhibits antiviral activity, it has been proposed that this metabolite may contribute to the local and systemic antiviral actions of inhaled RDV formulations [51]. Indeed, the systemic effects of IN LRDV, likely mediated by metabolite GS-441524, are supported by the lack of histopathological changes in the liver (Fig. 9), the absence of virus in the kidney (Fig. S6), as well as the profile of lymphoid cells in the spleen (Fig. S7).

Few studies have demonstrated the efficacy of liposomal drug formulations in controlling pulmonary viral infections following IN administration. Reus et al. (2023) developed non-targeted and targeted PEGylated liposomes incorporating nafamostat and compared their efficacies by IP and IN routes in SARS-CoV-2-infected K18-hACE2 mice [52]. Interestingly, a significant reduction of the virus titer in lungs was achieved after IN administration of targeted liposomal nafamostat formulation. In a recent work, liposomal angiotensin-(1–7) administered intranasally promoted marked anti-inflammatory response, reduced virus titer in the lungs and slightly improved animal survival in the same experimental model of COVID-19 [53]. In another study, the delivery of neomycin to the upper and lower respiratory airways was recently achieved through nasal administration, resulting in effective

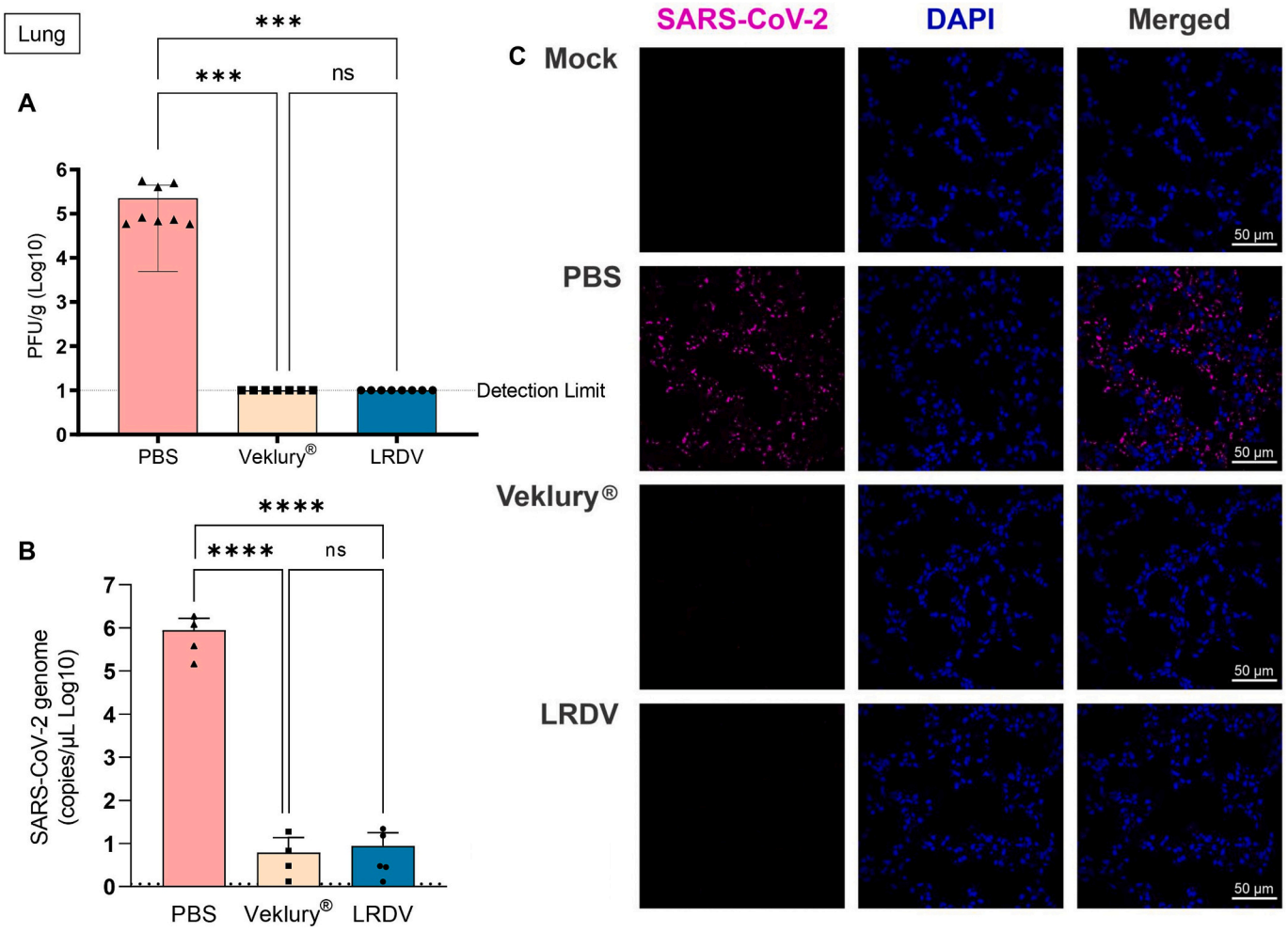

Fig. 5. Impact of intranasal treatment with liposomal RDV on the viral load in the lungs of mice infected with SARS-CoV-2. K18-hACE2 mice were intranasally inoculated with SARS-CoV-2. Treatment initiated 8 h after infection and was carried out every 12 h for 5 days. Experimental groups ($n = 8$/group) were: IN LRDV at 10 mg RDV/kg/dose, IP Veklury® at 20 mg of RDV/kg/dose and IN PBS. Animals were euthanized 12 h after the last dose. An uninfected and untreated group (Mock) was also used as a control. Viral loads were analyzed in the lungs at 5 dpi by plaque assay for viable virus (**A**) (n = 8) and RT-qPCR **(B)** ($n = 5$). **C**: representative immunofluorescence images using antibody against viral S protein. Blue colour represents cell nuclei, positive reaction with SARS-CoV-2 S protein appears in pink. The dashed horizontal line indicates the detection limit. Plaque assay data are shown as medians ±95 % confidence interval and compared using Kruskal-Wallis followed by Dunn's post-test. RT-qPCR data are shown as mean + SEM and compared using One-way ANOVA followed by Tukey's post-test. ***$p < 0.001$; ****$p < 0.0001$ for comparison with control PBS group. ns, no significant difference. (For interpretation of the references to colour in this figure legend, the reader is referred to the web version of this article.)

immunotherapeutic control of experimental respiratory virus infections [54]. Polymeric nanoparticles (NPs) have also been investigated for inhalation delivery of RDV. RDV-loaded nanocomposites, coated with supramolecular cell-penetrating peptide nanofibers to enhance cellular uptake, showed significantly higher *in vitro* activities against SARS-CoV-2 compared to those of free drug and uncoated RDV NPs [55]. Another polymeric nanovector has also been developed, which consisted of densely grafted NPs with a ligand to selectively bind to ACE2, showing promising *in vitro* antiviral activity [56]. RDV-loaded 2,2-bis(hydroxymethyl)propionic acid hyperbranched dendritic nanocarriers were also successfully prepared, showing low cytotoxicity on lung fibroblasts and alveolar macrophages [57].

Eliminating SARS-CoV-2 in the brain and lungs and preventing the exacerbated inflammatory response induced by the virus in the lungs are notable therapeutic actions of IN LRDV. To the best of our knowledge, this is the first report in a COVID-19 model of a drug effective in reducing viral load in the brain after IN administration (Fig. 6). This is in contrast to IP Veklury®, which also eliminated SARS-CoV-2 in the lungs but did not significantly affect virus load in the brain, in line with its low brain penetrance [18,19]. The prevention of lung inflammation by IN LRDV was evidenced by reduced levels of IL-6 and TNF (Fig. 7) and low numbers of infiltrated leukocytes, monocytes and neutrophils (Fig. 8). Thus, the outstanding efficacy of IN LRDV in comparison to IP Veklury® is also related to its greater ability to prevent an exacerbated inflammatory response in the lungs. Even though IN LRDV and IP Veklury® were as effective in reducing the virus titer in the lungs at 5 dpi (Fig. 5), LRDV may act earlier than Veklury® in suppressing the virus, thus preventing the onset of the inflammation process.

Histopathological changes were assessed in the liver (Fig. 9) to compare the systemic toxicities of IN LRDV and IP Veklury®. According to the literature, both SARS-CoV-2 infection [36] and RDV treatment [58–62] may lead to hepatic damage. The PBS group showed a highly variable response between animals, but no significant difference with the Mock group. This is in contrast with the Veklury® group that exhibited hepatic abnormalities in all animals. Thus, the lack of histopathological changes after LRDV treatment supports the systemic efficacy of IN treatment (likely mediated by metabolite GS-441524), as well as lower toxicity compared to IP Veklury®. Alternatively, the fast and effective delivery of RDV to the lungs from IN LRDV (Fig. 3A) may also prevent the systemic spread of the virus. Histopathological analysis of

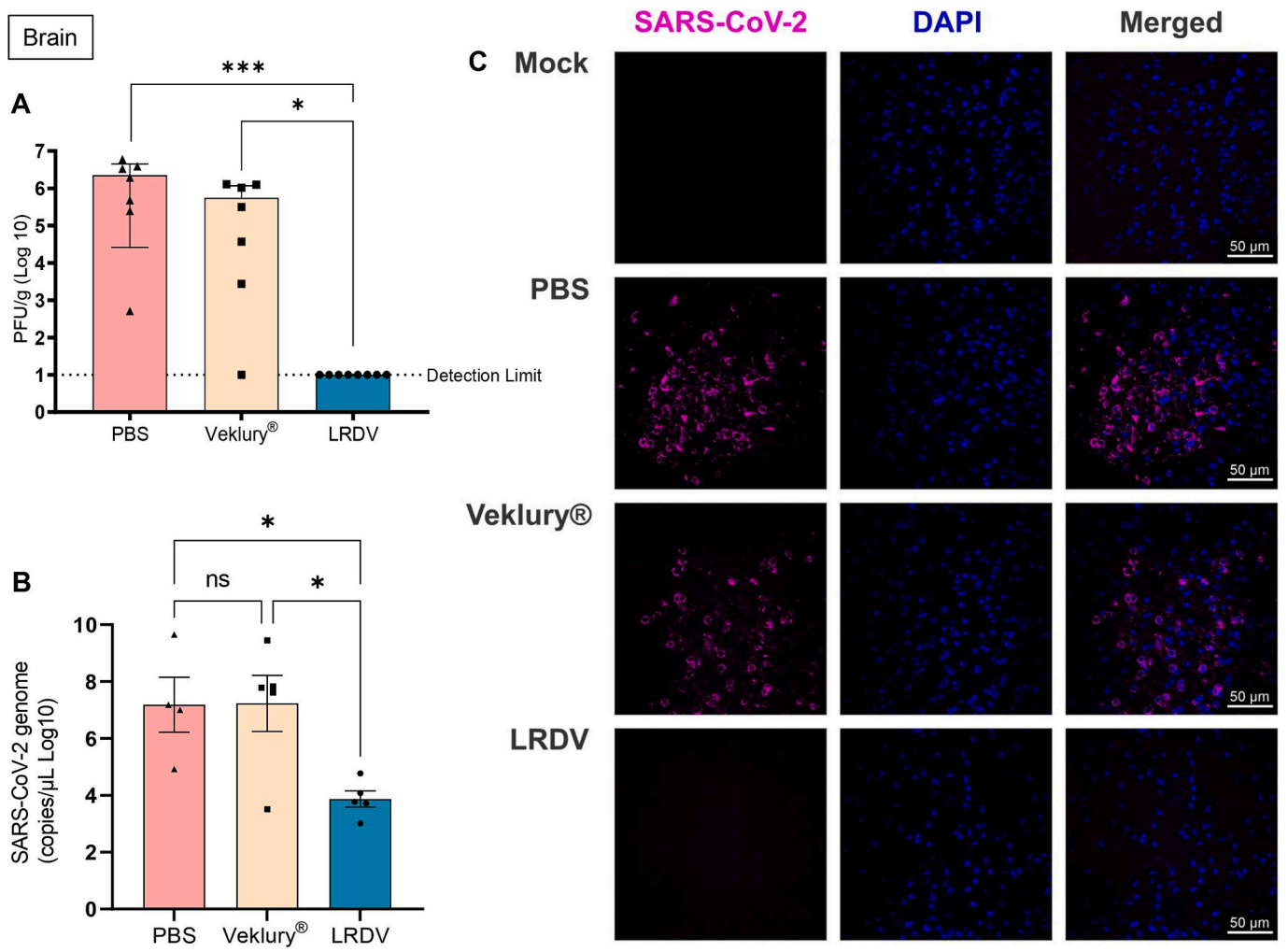

Fig. 6. Impact of intranasal treatment with liposomal RDV on the viral load in the brain of mice infected with SARS-CoV-2. K18-hACE2 mice were intranasally inoculated with SARS-CoV-2. Treatment initiated 8 h after infection and was carried out every 12 h for 5 days. Experimental groups (n = 8/group) were: IN LRDV at 10 mg RDV/kg/dose, IP Veklury® at 20 mg of RDV/kg/dose and IN PBS. Animals were euthanized 12 h after the last dose. An uninfected and untreated group (Mock) was used as a control. Viral loads were analyzed in the brain at 5 dpi by limiting dilution plaque assay for viable virus (**A**) (n = 8) and RT-qPCR (**B**) (n = 4–5). **C**: representative immunofluorescence images using antibody against viral S protein. Blue colour represents cell nuclei, positive reaction with SARS-CoV-2 S protein appears in pink. The dashed horizontal line indicates the detection limit. Plaque assay data are shown as medians +95 % confidence interval and compared using Kruskal-Wallis followed by Dunn's post-test. RT-qPCR data are shown as means ± SEM and compared using One-way ANOVA followed by Tukey's post-test. *p < 0.05; ***p < 0.001 for comparison with Veklury® and PBS groups. ns, no significant difference. (For interpretation of the references to colour in this figure legend, the reader is referred to the web version of this article.)

the brain of infected animals showed no abnormalities in any experimental group (Fig. S3), supporting no major toxicity of IN LRDV to the brain. On the other hand, all groups showed discrete to moderate histopathological changes in the lungs, including cell infiltrate and vessels congestion (Fig. S5), and no significant difference between LRDV and PBS groups was observed. Considering the early time point used for these assessments, it is difficult to distinguish between the effects of treatment and infection. Thus, future studies in uninfected animals would be important to further address the safety of liposomal RDV formulation.

Another remarkable difference between LRDV and Veklury® groups refers to the survival rate of animals. On day 8th post-infection, 62.5 % of Veklury® animals had died, whereas all LRDV animals remained alive up to 15th dpi (Fig. 4B). Three distinct factors may explain this difference. A previous study on the kinetics of SARS-CoV-2 invasion in K18-hACE2 mice has shown that virus titers in the lungs were highest on the third day and decreased on days 5 and 6 after infection [63]. In contrast, virus titers showed a peak in the brain on days 5 and 6, in line with our results (Fig. 6). Several encephalitis markers were also identified, and these authors proposed that the main cause of death in this model may be neuroinvasion and encephalitis. Thus, the lack of significant effect of IP Veklury® on viral load in the brain (Fig. 6) may be responsible for its lower therapeutic efficacy. Another possible contributing factor refers to the presence of the enzyme carboxylesterase 1c in the serum of mice, which markedly degrades RDV before reaching the tissues [10,50]. Therefore, the IN route and the protection provided by liposomes most probably prolonged the residence time and duration of action of the drug. Finally, Veklury® exhibited a greater drug toxicity following parenteral administration (Fig. 9) and lower ability to control the inflammatory process in the lung (Fig. 7 and Fig. 8). The latter factors may also contribute to the reduction in the survival rate of animals in the Veklury® group.

The high efficacy of the liposomal formulation of RDV after IN administration opens the way for a new therapeutic approach with RDV, until now restricted to IV treatment of hospitalized patients with COVID-19. Due to the delivery of RDV directly to the primary sites of infection, *i.e.*, nasal cavity, lungs and brain, as well as reduced systemic drug exposure and toxicity, IN liposomal RDV may enable effective and

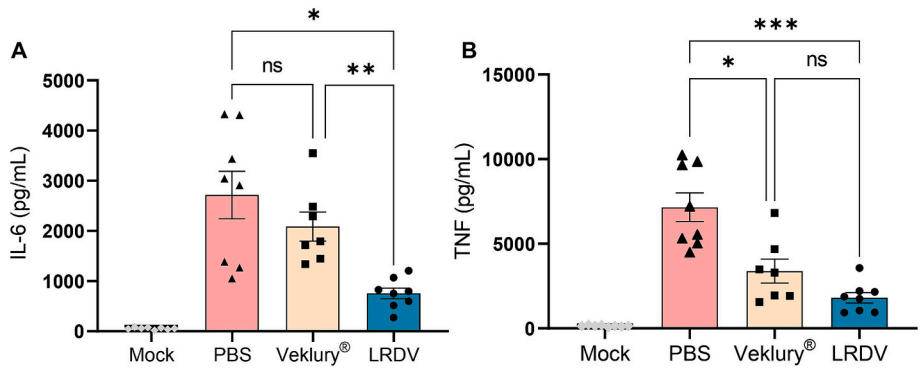

Fig. 7. Levels of cytokines IL-6 (**A**) and TNF (**B**) in the lung tissue of SARS-CoV-2-infected mice after treatment with RDV formulations. K18-hACE2 mice (n = 8) were intranasally inoculated with SARS-CoV-2. Treatment initiated 8 h after infection and was carried out every 12 h for 5 days. Experimental groups were: IN LRDV at 10 mg RDV/kg/dose, IP Veklury® at 20 mg of RDV/kg/dose and IN PBS. A non-infected and non-treated group (Mock) was also used as a control. Animals were euthanized 12 h after the last dose. The levels of IL-6 and TNF were determined by ELISA. Data are shown as means ± SEM and are compared using Brown-Forsythe ANOVA test followed by Dunnett's T3 post-test. *p < 0.05, **p < 0.01 and ***p < 0.001 for comparison with PBS and Veklury® groups. ns, no significant difference. (For interpretation of the references to colour in this figure legend, the reader is referred to the web version of this article.)

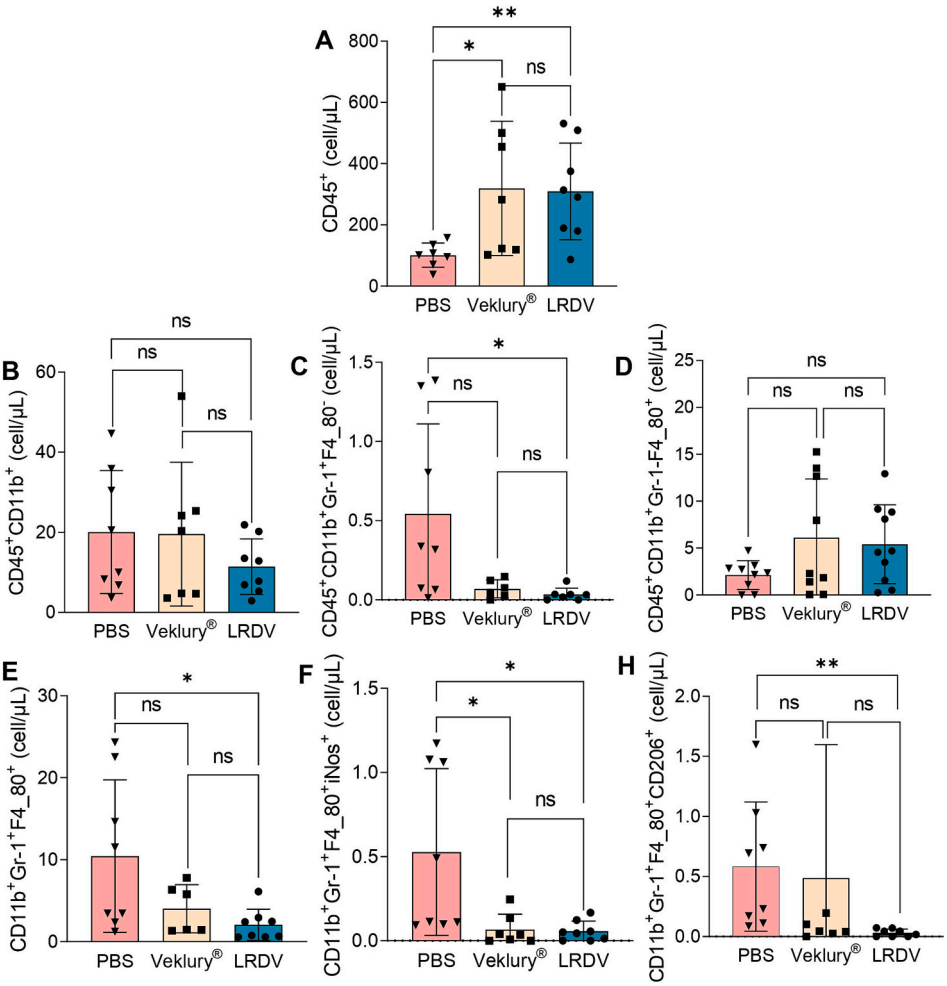

Fig. 8. Myeloid cells profile in the lungs of SARS-CoV-2-infected mice after treatment with intranasal LRDV or intraperitoneal Veklury®. K18-hACE2 mice (n = 8) were intranasally inoculated with SARS-CoV-2. Treatment initiated 8 h after infection and was carried out every 12 h for 5 days. Experimental groups were: IN LRDV at 10 mg RDV/kg/dose, IP Veklury® at 20 mg RDV/kg/dose and IN PBS. Animals were euthanized 12 h after the last dose. Number of (**A**) leucocytes, (**B**) myeloid cells, (**C**) neutrophils, (**D**) macrophages, (**E**) monocytes, (**F, G**) expressing $iNos^+$ or $CD206^+$. The panels of cells were determined by flow cytometry. Data are shown as medians ±95 % confidence intervals and are compared using Kruskal-Wallis followed by Dunn's post-test. *p < 0.05 and **p < 0.01 for comparison with PBS and Veklury® groups. ns, no significant difference.

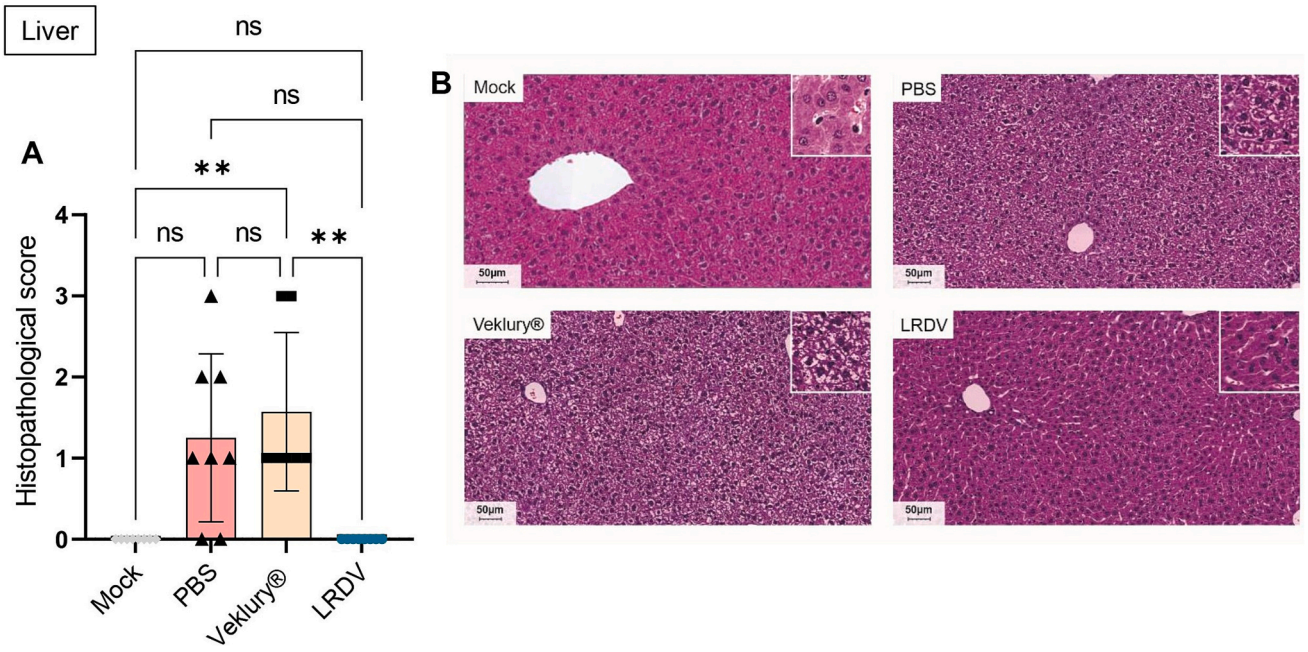

Fig. 9. Histopathology of the liver of K18-hACE2 mice 5 days after infection with SARS-CoV-2 and treatment with RDV formulations. A uninfected and untreated group (Mock) was used as a control. **A**: Graph reporting the histopathological score related to hydropic degeneration (0: no alteration; 1: discrete, 0–25 %; 2: moderate, 25–50 %; 3: intense, 50–100 %). **B**: Representative panoramic photomicrographs of liver parenchyma sections at 20× magnification, after hematoxylin and eosin staining. Mock, showing no lesion; PBS, showing hydropic degeneration in some hepatocytes; Veklury®, showing liver tissue with hydropic degeneration in virtually all hepatocytes; LRDV, showing liver parenchyma without lesion. Data were compared using the Kruskal-Wallis test *p < 0.05 and **$p < 0.01$. ns, no significant difference.

affordable early therapy in non-hospitalized patients. Its potential in preventing the onset of "Long COVID" also provides a significant advantage compared to conventional therapy.

5. Conclusions

In the present work, a liposomal RDV formulation was developed and selected based on high drug encapsulation efficiency, sustained drug release property and high *in vitro* selectivity index. The liposomal formulation effectively delivered RDV to the lungs after intranasal administration. The high therapeutic efficacy of liposomal RDV was established *in vivo*, after intranasal administration in a transgenic mouse model of COVID-19, showing SARS-CoV-2 clearance in the brain and lungs, preventing the inflammatory response in the lungs, as well as ensuring animal survival. This work is the first to report a nano-formulation capable of promoting effective delivery of RDV simultaneously to the brain and the lungs with a successful therapeutic outcome in a mouse model of COVID-19.

CRediT authorship contribution statement

Sabrina Mendes: Writing – review & editing, Writing – original draft, Visualization, Methodology, Investigation, Formal analysis, Data curation, Conceptualization. **Lays Cordeiro Guimarães:** Writing – review & editing, Visualization, Methodology, Investigation, Formal analysis, Data curation. **Leonardo Camilo de Oliveira:** Methodology, Investigation, Formal analysis, Data curation. **Pedro Augusto Carvalho Costa:** Writing – review & editing, Methodology, Investigation, Formal analysis, Data curation. **Natália Jordana Alves da Silva:** Writing – review & editing, Methodology, Investigation, Formal analysis. **Gabriel Silva Alves Pessim Pereira:** Investigation, Formal analysis, Data curation. **Clara Couto Fernandez:** Methodology, Investigation, Formal analysis. **Maria Marta Figueiredo:** Methodology, Investigation, Formal analysis. **Robson Augusto Souza dos Santos:** Writing – review & editing, Methodology, Funding acquisition. **Mauro Martins Teixeira:** Writing – review & editing, Methodology, Investigation, Funding acquisition. **Vivian Vasconcelos Costa:** Writing – review & editing, Methodology, Investigation, Funding acquisition. **Pedro Pires Goulart Guimarães:** Writing – review & editing, Methodology, Investigation, Funding acquisition, Formal analysis, Conceptualization. **Frédéric Frézard:** Writing – review & editing, Writing – original draft, Visualization, Validation, Supervision, Project administration, Methodology, Investigation, Funding acquisition, Formal analysis, Data curation, Conceptualization.

Declaration of competing interest

None.

Acknowledgements

We thank the animal biosafety level 3 laboratory (BSL-3) at UFMG; Center for Image Acquisition and Processing (CAPI-UFMG) and Centro de Laboratórios Multiusuários, CELAM. This work was supported by Conselho Nacional de Desenvolvimento Científico e Tecnológico (CNPq, Brazil) [grant number 306198/2021-5 and 442731/2020-5]; Fundação de Amparo a Pesquisa do Estado de Minas Gerais (FAPEMIG, Brazil) [grant numbers TEC-RED-00282-16, RED-00202-22, RED-00028-23, APQ-00730-23, APQ-02618-23 and APQ-04650-23]; Coordenação de Aperfeiçoamento de Pessoal de Nível Superior (CAPES, Brazil) [grant number 88887.506690/2020-00]. This work received support from the National Institute of Science and Technology in Dengue and Host-Microorganism Interaction (INCT em Dengue), sponsored by CNPq [grant number 465425/2014-3] and FAPEMIG [grant number 25036], as well as the National Institute of Science and Technology in Nanobiopharmaceutics (INCT NanoBiofar) sponsored by CNPq/MCTI [grant number 406792/2022-4]. FF, PPGG, VVC, RASS and MMT were recipients of fellowship from CNPq. SMSA was a recipient of a studentship from CAPES.

Appendix A. Supplementary data

Supplementary data to this article can be found online at https://doi.org/10.1016/j.jconrel.2025.01.044.

Data availability

Data will be made available on request.

References

[1] T. Jefferson, L. Dooley, E. Ferroni, L.A. Al-Ansary, M.L. van Driel, G.A. Bawazeer, M.A. Jones, T.C. Hoffmann, J. Clark, E.M. Beller, P.P. Glasziou, J.M, Conly, physical interventions to interrupt or reduce the spread of respiratory viruses, Cochrane Database Syst. Rev. (2023), https://doi.org/10.1002/14651858.CD006207.pub6.

[2] L.D.J. Bos, L.B. Ware, Acute respiratory distress syndrome: causes, pathophysiology, and phenotypes, Lancet 400 (2022) 1145–1156, https://doi.org/10.1016/S0140-6736(22)01485-4.

[3] A. Nalbandian, K. Sehgal, A. Gupta, M.V. Madhavan, C. McGroder, J.S. Stevens, J. R. Cook, A.S. Nordvig, D. Shalev, T.S. Sehrawat, N. Ahluwalia, B. Bikdeli, D. Dietz, C. Der-Nigoghossian, N. Liyanage-Don, G.F. Rosner, E.J. Bernstein, S. Mohan, A. A. Beckley, D.S. Seres, T.K. Choueiri, N. Uriel, J.C. Ausiello, D. Accili, D. E. Freedberg, M. Baldwin, A. Schwartz, D. Brodie, C.K. Garcia, M.S.V. Elkind, J. M. Connors, J.P. Bilezikian, D.W. Landry, E.Y. Wan, Post-acute COVID-19 syndrome, Nat. Med. 27 (2021) 601–615, https://doi.org/10.1038/s41591-021-01283-z.

[4] J. Aguado, A.A. Amarilla, A. Taherian Fard, E.A. Albornoz, A. Tyshkovskiy, M. Schwabenland, H.K. Chaggar, N. Modhiran, C. Gómez-Inclán, I. Javed, A. A. Baradar, B. Liang, L. Peng, M. Dharmaratne, G. Pietrogrande, P. Padmanabhan, M.E. Freney, R. Parry, J.D.J. Sng, A. Isaacs, A.A. Khromykh, G. Valenzuela Nieto, A. Rojas-Fernandez, T.P. Davis, M. Prinz, B. Bengsch, V.N. Gladyshev, T. M. Woodruff, J.C. Mar, D. Watterson, E.J. Wolvetang, Senolytic therapy alleviates physiological human brain aging and COVID-19 neuropathology, Nat. Aging (2023) 1–15, https://doi.org/10.1038/s43587-023-00519-6.

[5] S. Szabo, O. Zayachkivska, A. Hussain, V. Muller, What is really 'long COVID'? Inflammopharmacology 31 (2023) 551–557, https://doi.org/10.1007/s10787-023-01194-0.

[6] O. Abou-Arab, P. Huette, F. Debouvries, H. Dupont, V. Jounieaux, Y. Mahjoub, Inhaled nitric oxide for critically ill Covid-19 patients: a prospective study, Crit. Care 24 (2020) 645, https://doi.org/10.1186/s13054-020-03371-x.

[7] C.J. Gordon, E.P. Tchesnokov, J.Y. Feng, D.P. Porter, M. Götte, The antiviral compound remdesivir potently inhibits RNA-dependent RNA polymerase from Middle East respiratory syndrome coronavirus, J. Biol. Chem. 295 (2020) 4773–4779, https://doi.org/10.1074/jbc.AC120.013056.

[8] D.Z. Pan, P.M. Odorizzi, A. Schoenichen, M. Abdelghany, S. Chen, A. Osinusi, S. D. Patterson, B. Downie, K. Juneja, J.J. Wallin, Remdesivir improves biomarkers associated with disease severity in COVID-19 patients treated in an outpatient setting, Commun. Med. 3 (2023) 2, https://doi.org/10.1038/s43856-022-00232-2.

[9] A. Aleem, J.P. Kothadia, Remdesivir, in: StatPearls, StatPearls Publishing, Treasure Island (FL), 2024. http://www.ncbi.nlm.nih.gov/books/NBK563261/ (accessed October 9, 2024).

[10] J.J. Malin, I. Suárez, V. Priesner, G. Fätkenheuer, J. Rybniker, Remdesivir against COVID-19 and other viral diseases, Clin. Microbiol. Rev. 34 (2020), https://doi.org/10.1128/CMR.00162-20 e00162–20.

[11] H.A. Blair, Remdesivir: a review in COVID-19, Drugs 83 (2023) 1215–1237, https://doi.org/10.1007/s40265-023-01926-0.

[12] A.J. Pruijssers, A.S. George, A. Schäfer, S.R. Leist, L.E. Gralinksi, K.H. Dinnon, B. L. Yount, M.L. Agostini, L.J. Stevens, J.D. Chappell, X. Lu, T.M. Hughes, K. Gully, D.R. Martinez, A.J. Brown, R.L. Graham, J.K. Perry, V. Du Pont, J. Pitts, B. Ma, D. Babusis, E. Murakami, J.Y. Feng, J.P. Bilello, D.P. Porter, T. Cihlar, R.S. Baric, M.R. Denison, T.P. Sheahan, Remdesivir inhibits SARS-CoV-2 in human lung cells and chimeric SARS-CoV expressing the SARS-CoV-2 RNA polymerase in mice, Cell Rep. 32 (2020) 107940, https://doi.org/10.1016/j.celrep.2020.107940.

[13] P.O. Godwin, B. Polsonetti, M.F. Caron, T.F. Oppelt, Remdesivir for the treatment of COVID-19: a narrative review, Infect. Dis. Ther. 13 (2024) 1–19, https://doi.org/10.1007/s40121-023-00900-3.

[14] A. Izcovich, R.A. Siemieniuk, J.J. Bartoszko, L. Ge, D. Zeraatkar, E. Kum, A. Qasim, A.M. Khamis, B. Rochwerg, T. Agoritsas, D.K. Chu, S.L. McLeod, R.A. Mustafa, P. Vandvik, R. Brignardello-Petersen, Adverse effects of remdesivir, hydroxychloroquine and lopinavir/ritonavir when used for COVID-19: systematic review and meta-analysis of randomised trials, BMJ Open 12 (2022) e048502, https://doi.org/10.1136/bmjopen-2020-048502.

[15] G. Pulivendala, S. Bale, C. Godugu, Inhalation of sustained release microparticles for the targeted treatment of respiratory diseases, drug Deliv, Transl. Res. 10 (2020) 339–353, https://doi.org/10.1007/s13346-019-00690-7.

[16] J. Li, K. Zhang, D. Wu, L. Ren, X. Chu, C. Qin, X. Han, T. Hang, Y. Xu, L. Yang, L. Yin, Liposomal remdesivir inhalation solution for targeted lung delivery as a novel therapeutic approach for COVID-19, Asian, J. Pharm. Sci. 16 (2021) 772–783, https://doi.org/10.1016/j.ajps.2021.09.002.

[17] M.S. Vermillion, E. Murakami, B. Ma, J. Pitts, A. Tomkinson, D. Rautiola, D. Babusis, H. Irshad, D. Seigel, C. Kim, X. Zhao, C. Niu, J. Yang, A. Gigliotti, N. Kadrichu, J.P. Bilello, S. Ellis, R. Bannister, R. Subramanian, B. Smith, R. L. Mackman, W.A. Lee, P.J. Kuehl, J. Hartke, T. Cihlar, D.P. Porter, Inhaled remdesivir reduces viral burden in a nonhuman primate model of SARS-CoV-2 infection, Sci. Transl. Med. 14 (2022) eabl8282, https://doi.org/10.1126/scitranslmed.abl8282.

[18] P.J. Richardson, S. Ottaviani, A. Prelle, J. Stebbing, G. Casalini, M. Corbellino, CNS penetration of potential anti-COVID-19 drugs, J. Neurol. 267 (2020) 1880–1882, https://doi.org/10.1007/s00415-020-09866-5.

[19] J.H. Jeong, S. Chokkakula, S.C. Min, B.K. Kim, W.S. Choi, S. Oh, Y.S. Yun, S. H. Kang, O.J. Lee, E.G. Kim, J.H. Choi, J.Y. Lee, Y.K. Choi, Y.H. Baek, M.S. Song, Combination therapy with nirmatrelvir and molnupiravir improves the survival of SARS-CoV-2 infected mice, Antivir. Res. 208 (2022) 105430, https://doi.org/10.1016/j.antiviral.2022.105430.

[20] M. Chakravarty, A. Vora, Nanotechnology-based antiviral therapeutics, drug Deliv, Transl. Res. 11 (2021) 748–787, https://doi.org/10.1007/s13346-020-00818-0.

[21] M. Agrawal, S. Saraf, S. Saraf, S.G. Antimisiaris, M.B. Chougule, S.A. Shoyele, A. Alexander, Nose-to-brain drug delivery: an update on clinical challenges and progress towards approval of anti-Alzheimer drugs, J. Control. Release 281 (2018) 139–177, https://doi.org/10.1016/j.jconrel.2018.05.011.

[22] S.-H. Jeong, J.-H. Jang, Y.-B. Lee, Drug delivery to the brain via the nasal route of administration: exploration of key targets and major consideration factors, J. Pharm. Investig. 53 (2023) 119–152, https://doi.org/10.1007/s40005-022-00589-5.

[23] A. Rajput, P. Pingale, V. Dhapte-Pawar, Nasal delivery of neurotherapeutics via nanocarriers: facets, aspects, and prospects, Front. Pharmacol. 13 (2022) 979682, https://doi.org/10.3389/fphar.2022.979682.

[24] S.S. Hong, K.T. Oh, H.G. Choi, S.J. Lim, Liposomal formulations for nose-to-brain delivery: recent advances and future perspectives, Pharmaceutics 11 (2019) 540, https://doi.org/10.3390/pharmaceutics11100540.

[25] S.S. Krishna, M.S. Sudheesh, V. Viswanad, Liposomal drug delivery to the lungs: a post covid-19 scenario, J. Liposome Res. 33 (2023) 410–424, https://doi.org/10.1080/08982104.2023.2199068.

[26] R. Vartak, S.M. Patil, A. Saraswat, M. Patki, N.K. Kunda, K. Patel, Aerosolized nanoliposomal carrier of remdesivir: an effective alternative for COVID-19 treatment *in vitro*, Nanomed 16 (2021) 1187–1202, https://doi.org/10.2217/nnm-2020-0475.

[27] C. Jaafar-Maalej, R. Diab, V. Andrieu, A. Elaissari, H. Fessi, Ethanol injection method for hydrophilic and lipophilic drug-loaded liposome preparation, J. Liposome Res. 20 (2010) 228–243, https://doi.org/10.3109/08982100903347923.

[28] C. Kirby, G. Gregoriadis, Dehydration-rehydration vesicles: a simple method for high yield drug entrapment in liposomes, Bio/Technology 2 (1984) 979–984, https://doi.org/10.1038/nbt1184-979.

[29] B. McCormack, G. Gregoriadis, Entrapment of cyclodextrin-drug complexes into liposomes: potential advantages in drug delivery, J. Drug Target. 2 (1994) 449–454, https://doi.org/10.3109/10611869408996821.

[30] I. Bulduk, E. Akbel, A comparative study of HPLC and UV spectrophotometric methods for remdesivir quantification in pharmaceutical formulations, J. Taibah Univ. Sci. 15 (2021) 507–513, https://doi.org/10.1080/16583655.2021.1991737.

[31] Y.-C. Lin, R.J. Malott, L. Ward, L. Kiplagat, K. Pabbaraju, K. Gill, B.M. Berenger, J. Hu, K. Fonseca, R.S. Noyce, T. Louie, D.H. Evans, J.M. Conly, Detection and quantification of infectious severe acute respiratory coronavirus-2 in diverse clinical and environmental samples, Sci. Rep. 12 (2022) 5418, https://doi.org/10.1038/s41598-022-09218-5.

[32] H. Elmansi, A.E. Ibrahim, I.E. Mikhail, F. Belal, Green and sensitive spectrofluorimetric determination of Remdesivir, an FDA approved SARS-CoV-2 candidate antiviral; application in pharmaceutical dosage forms and spiked human plasma, Anal. Methods 13 (2021) 2596–2602, https://doi.org/10.1039/d1ay00469g.

[33] L. Van Hoecke, E.R. Job, X. Saelens, K. Roose, Bronchoalveolar lavage of murine lungs to analyze inflammatory cell infiltration, J. Vis. Exp. 123 (2017) 55398, https://doi.org/10.3791/55398.

[34] M. Rodriguez, Y. Soler, K.M.K. Muthu, Y. Zhao, E.V. Batrakova, N. El-Hage, Targeting Beclin1 as an adjunctive therapy against HIV using Mannosylated Polyethylenimine nanoparticles, Pharmaceutics 13 (2021) 223, https://doi.org/10.3390/pharmaceutics13020223.

[35] Q. Du, Y. Liu, M. Fan, S. Wei, M. Ismail, M. Zheng, PEG length effect of peptide-functional liposome for blood brain barrier (BBB) penetration and brain targeting, J. Control. Release 372 (2024) 85–94, https://doi.org/10.1016/j.jconrel.2024.06.005.

[36] E.S. Winkler, SARS-CoV-2 infection of human ACE2-transgenic mice causes severe lung inflammation and impaired function, Nat. Immunol. 21 (2020) 1327–1335, https://doi.org/10.1038/s41590-020-0778-2.

[37] M. Carossino, P. Montanaro, A. O'Connell, D. Kenney, H. Gertje, K.A. Grosz, M. Ericsson, B.R. Huber, S.A. Kurnick, S. Subramaniam, T.A. Kirkland, J.R. Walker, K.P. Francis, A.D. Klose, N. Paragas, M. Bosmann, M. Saeed, U.B.R. Balasuriya, F. Douam, N.A. Crossland, Fatal neuroinvasion and SARS-CoV-2 tropism in K18-hACE2 mice is partially independent on hACE2 expression, Preprint 2021 (01) (2021) 13.425144, https://doi.org/10.1101/2021.01.13.425144.

[38] Y. da Silva Santos, T.H.M. Gamon, M.S.P. de Azevedo, B.L. Telezynski, E.E. de Souza, D.B.L. de Oliveira, J.G. Dombrowski, L. Rosa-Fernandes, G. Palmisano, L. J. de Moura Carvalho, M.C.R. Luvizotto, C. Wrenger, D.T. Covas, R. Curi, C.R. F. Marinho, E.L. Durigon, S. Epiphanio, Virulence profiles of wild-type, P.1 and Delta SARS-CoV-2 variants in K18-hACE2 transgenic mice, Viruses 15 (2023) 999, https://doi.org/10.3390/v15040999.

[39] R. Cavalli, M. Donalisio, A. Bisazza, A. Civra, E. Ranucci, P. Ferruti, D. Lembo, Enhanced antiviral activity of acyclovir loaded into nanoparticles, Methods

Enzymol. 509 (2012) 1–19, https://doi.org/10.1016/B978-0-12-391858-1.00001-0.
[40] H. Akbari, F. Taghizadeh-Hesary, COVID-19 induced liver injury from a new perspective: mitochondria, Mitochondrion 70 (2023) 103–110, https://doi.org/10.1016/j.mito.2023.04.001.
[41] T. Kurano, T. Kanazawa, A. Ooba, Y. Masuyama, N. Maruhana, M. Yamada, S. Iioka, H. Ibaraki, Y. Kosuge, H. Kondo, T. Suzuki, Nose-to-brain/spinal cord delivery kinetics of liposomes with different surface properties, J. Control. Release 344 (2022) 225–234, https://doi.org/10.1016/j.jconrel.2022.03.017.
[42] M.C. Woodle, Sterically stabilized liposome therapeutics, Adv. Drug Deliv. Rev. 16 (1995) 249–265, https://doi.org/10.1016/0169-409X(95)00028-6.
[43] E.G. Azevedo, R.R. Ribeiro, S.M. da Silva, C.S. Ferreira, L.E. de Souza, A. A. Ferreira, R.A. de Oliveira, E. Castro, C. Demicheli, S.A. Rezende, F. Frézard, Mixed formulation of conventional and pegylated liposomes as a novel drug delivery strategy for improved treatment of visceral leishmaniasis, Expert Opin. Drug Deliv. 11 (2014) 1551–1560, https://doi.org/10.1517/17425247.2014.932347.
[44] N.R. Faria, T.A. Mellan, C. Whittaker, I.M. Claro, D.D.S. Candido, S. Mishra, M.A. E. Crispim, F.C.S. Sales, I. Hawryluk, J.T. McCrone, R.J.G. Hulswit, L.A.M. Franco, M.S. Ramundo, J.G. de Jesus, P.S. Andrade, T.M. Coletti, G.M. Ferreira, C.A. M. Silva, E.R. Manuli, R.H.M. Pereira, P.S. Peixoto, M.U.G. Kraemer, N. Jr, C.D. C. Gaburo, H. Camilo, W.M. Hoeltgebaum, E.C. Souza, L.M. Rocha, M.C. de Souza, L.I.T. de Pinho, F.S.V. Araujo, A.B. de Malta, J.D.P. Silva Lima, D.A.G. Zauli, A.C. S. Ferreira, R.P. Schnekenberg, D.J. Laydon, P.G.T. Walker, H.M. Schlüter, A.L. P. Dos Santos, M.S. Vidal, V.S. Del Caro, R.M.F. Filho, H.M. Dos Santos, R. S. Aguiar, J.L. Proença-Modena, B. Nelson, J.A. Hay, M. Monod, X. Miscouridou, H. Coupland, R. Sonabend, M. Vollmer, A. Gandy, C.A. Jr, V.H. Prete, M. A. Nascimento, T.A. Suchard, S.L.K. Bowden, C.H. Pond, O. Wu, N.M. Ratmann, C. Ferguson, N.J. Dye, P. Loman, A. Lemey, N.A. Rambaut, M.D.P.S.S. Carvalho Fraiji, O.G. Pybus, S. Flaxman, S. Bhatt, E.C., Sabino, genomics and epidemiology of the P.1 SARS-CoV-2 lineage in Manaus, Brazil, Science 372 (2021) 815–821, https://doi.org/10.1126/science.abh2644.
[45] S. Tosta, M. Giovanetti, V.B. Nardy, L.R.O. da Silva, M.K.A. Gomez, J.G. Lima, C. W. Cardoso, T.O. Silva, M.S.P.L. de Souza, P.H.P. Dias, V. Fonseca, T. de Oliveira, J. Lourenço, L.C.J. Alcantara, F. Pereira, A. Leal, Short report: early genomic detection of SARS-CoV-2 P.1 variant in Northeast Brazil, PLoS Negl. Trop. Dis. 15 (2021) e0009591, https://doi.org/10.1371/journal.pntd.0009591.
[46] K. Tao, P.L. Tzou, J. Nouhin, R.K. Gupta, T. de Oliveira, S.L.K. Pond, D. Fera, R. W. Shafer, The biological and clinical significance of emerging SARS-CoV-2 variants, Nat. Rev. Genet. 22 (2021) 757–773, https://doi.org/10.1038/s41576-021-00408-x.
[47] C.K.V. Nonaka, T. Gräf, C.A.L. Barcia, V.F. Costa, J.L. de Oliveira, R.D.H. da Passos, I.N. Bastos, M.C.B. de Santana, I.M. Santos, K.A.F. de Sousa, T.G.L. Weber, I. C. Siqueira, C.A.G. Rocha, A.V.A. Mendes, B.S.F. Souza, SARS-CoV-2 Variant of Concern P.1 (Gamma) Infection in Young and Middle-Aged Patients Admitted to the Intensive Care Units of a Single Hospital in Salvador, Northeast Brazil, Int. J. Infect. Dis. 111 (2021) 47–54, https://doi.org/10.1016/j.ijid.2021.08.003.
[48] L.-A. Keller, O. Merkel, A. Popp, Intranasal drug delivery: opportunities and toxicologic challenges during drug development, Drug Deliv. Transl. Res. 12 (2022) 735–757, https://doi.org/10.1007/s13346-020-00891-5.
[49] V.A. Duong, T.T. Nguyen, H.J. Maeng, Recent advances in intranasal liposomes for drug, gene, and vaccine delivery, Pharmaceutics 15 (2023) 207, https://doi.org/10.3390/pharmaceutics15010207.
[50] T.P. Sheahan, A.C. Sims, S.R. Leist, A. Schäfer, J. Won, A.J. Brown, S. A. Montgomery, A. Hogg, D. Babusis, M.O. Clarke, J.E. Spahn, L. Bauer, S. Sellers, D. Porter, J.Y. Feng, T. Cihlar, R. Jordan, M.R. Denison, R.S. Baric, Comparative therapeutic efficacy of remdesivir and combination lopinavir, ritonavir, and interferon beta against MERS-CoV, Nat. Commun. 11 (2020) 222, https://doi.org/10.1038/s41467-019-13940-6.
[51] S. Sahakijpijarn, C. Moon, J.J. Koleng, D.J. Christensen, R.O. Williams III, Development of remdesivir as a dry powder for inhalation by thin film freezing, Pharmaceutics 12 (2020) 1002, https://doi.org/10.3390/pharmaceutics12111002.
[52] P. Reus, H. Guthmann, N. Uhlig, M. Agbaria, L. Issmail, V. Eberlein, M.M. Nordling-David, D. Jbara-Agbaria, S. Ciesek, D. Bojkova, J. Cinatl, A. Burger-Kentischer, S. Rupp, A. Zaliani, T. Grunwald, P. Gribbon, A. Kannt, G. Golomb, Drug repurposing for the treatment of COVID-19: targeting nafamostat to the lungs by a liposomal delivery system, J. Control. Release 364 (2023) 654–671, https://doi.org/10.1016/j.jconrel.2023.10.050.
[53] S. Mendes, L.C. Guimarães, P.A.C. Costa, C.C. Fernandez, M.M. Figueiredo, M. M. Teixeira, R.A.S. Dos Santos, P.P.G. Guimarães, F. Frézard, Intranasal liposomal angiotensin-(1-7) administration reduces inflammation and viral load in the lungs during SARS-CoV-2 infection in K18-hACE2 transgenic mice, Antimicrob. Agents Chemother. 68 (2024) e0083524, https://doi.org/10.1128/aac.00835-24.
[54] T. Mao, J. Kim, M.A. Peña-Hernández, G. Valle, M. Moriyama, S. Luyten, I.M. Ott, M.L. Gomez-Calvo, J.R. Gehlhausen, E. Baker, B. Israelow, M. Slade, L. Sharma, W. Liu, C. Ryu, A. Korde, C.J. Lee, V. Silva Monteiro, C. Lucas, H. Dong, Y. Yang, S. Gopinath, C.B. Wilen, N. Palm, C.S. Dela Cruz, A. Iwasaki, Intranasal neomycin evokes broad-spectrum antiviral immunity in the upper respiratory tract, Proc. Natl. Acad. Sci. USA 121 (2024) e2319566121, https://doi.org/10.1073/pnas.2319566121.
[55] U. Chintapula, S.U. Karim, P.R. Iyer, H. Asokan-Sheeja, B. Neupane, F. Nazneen, H. Dong, F. Bai, K.T. Nguyen, A novel nanocomposite drug delivery system for SARS-CoV-2 infections, Nanoscale Adv. 6 (2024) 3747–3758, https://doi.org/10.1039/d4na00361f.
[56] V. Sanna, S. Satta, T. Hsiai, M. Sechi, Development of targeted nanoparticles loaded with antiviral drugs for SARS-CoV-2 inhibition, Eur. J. Med. Chem. 231 (2022) 114121, https://doi.org/10.1016/j.ejmech.2022.114121.
[57] E. Halevas, B. Mavroidi, C. Kokotidou, A. Moschona, M. Sagnou, A. Mitraki, G. Litsardakis, M. Pelecanou, Remdesivir-loaded bis-MPA hyperbranched dendritic nanocarriers for pulmonary delivery, J. Drug Deliv. Sci. Technol. 75 (2022) 103625, https://doi.org/10.1016/j.jddst.2022.103625.
[58] N. DeFoor, S. Paul, S. Li, E.K.G. Basso, V. Stevenson, J.L. Browning, A.K. Prater, S. Brindley, G. Tao, A.M. Pickrell, Remdesivir increases mtDNA copy number causing mild alterations to oxidative phosphorylation, Sci. Rep. 13 (2023) 15339, https://doi.org/10.1038/s41598-023-42704-y.
[59] M. Rana, R.M. Ahmad, M. Al-Sammak, Histological assessment of remdesivir on kidney and liver of albino rats in different doses and their withdrawal, Mil. Med. Sci. Lett. (Voj. Zdrav. Listy) 93 (2024) 10–18, https://doi.org/10.31482/mmsl.2023.022.
[60] R. Zampino, F. Mele, L.L. Florio, L. Bertolino, R. Andini, M. Galdo, R. De Rosa, A. Corcione, E. Durante-Mangoni, Liver injury in remdesivir-treated COVID-19 patients, Hepatol. Int. 14 (2020) 881–883, https://doi.org/10.1007/s12072-020-10077-3.
[61] K. Liu, S. Stern, E.L. Heil, L. Li, R. Khairi, S. Heyward, H. Wang, Dexamethasone mitigates remdesivir-induced liver toxicity in human primary hepatocytes and COVID-19 patients, Hepatol. Commun. 7 (2023) e0034, https://doi.org/10.1097/HC9.0000000000000034.
[62] C. Carothers, K. Birrer, M. Vo, Acetylcysteine for the treatment of suspected Remdesivir-associated acute liver failure in COVID-19: a case series, Pharmacotherapy 40 (2020) 1166–1171, https://doi.org/10.1002/phar.2464.
[63] P. Kumari, H.A. Rothan, J.P. Natekar, S. Stone, H. Pathak, P.G. Strate, K. Arora, M. A. Brinton, M. Kumar, Neuroinvasion and encephalitis following intranasal inoculation of SARS-CoV-2 in K18-hACE2 mice, Viruses 13 (2021) 132, https://doi.org/10.3390/v13010132.

5 MATERIAL SUPLEMENTAR (CAPÍTULO 2)

Supplementary Data

for "Intranasal liposomal remdesivir induces SARS-CoV-2 clearance in K18-hACE2 mice and ensures survival" by Mendes et al. (2025)

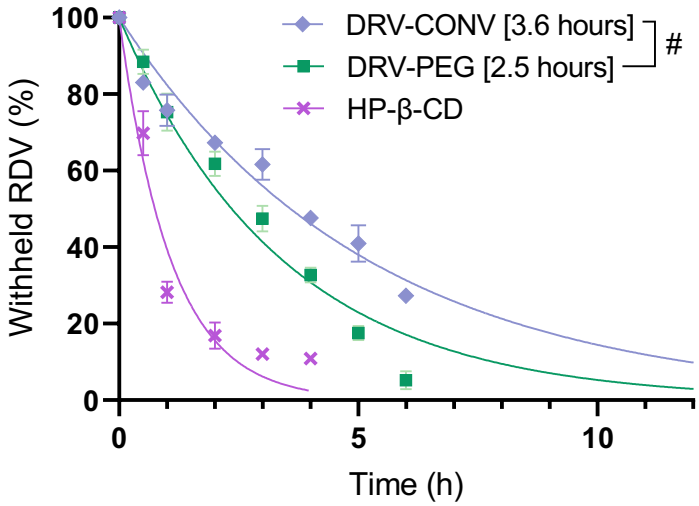

Figure S1 – Kinetics of RDV release from different liposomal formulations under dialysis conditions at 37°C. The formulations consisted in DSPC/DPPG/CHOL liposomes containing (DRV-PEG) or not (DRV-CONV) DSPE-PEG2000, prepared using the dehydration-rehydration method. Data were fitted according to monoexponential decay, allowing the determination of half-time of RDV release (values shown in bracket). The complex of RDV with HP-β-CD was used as a control in the experiment. Data are shown as mean ± SEM obtained from three independent samples. $^{\#}p<0.0001$ for comparison of half-time of drug release between DRV-CONV and DRV-PEG.

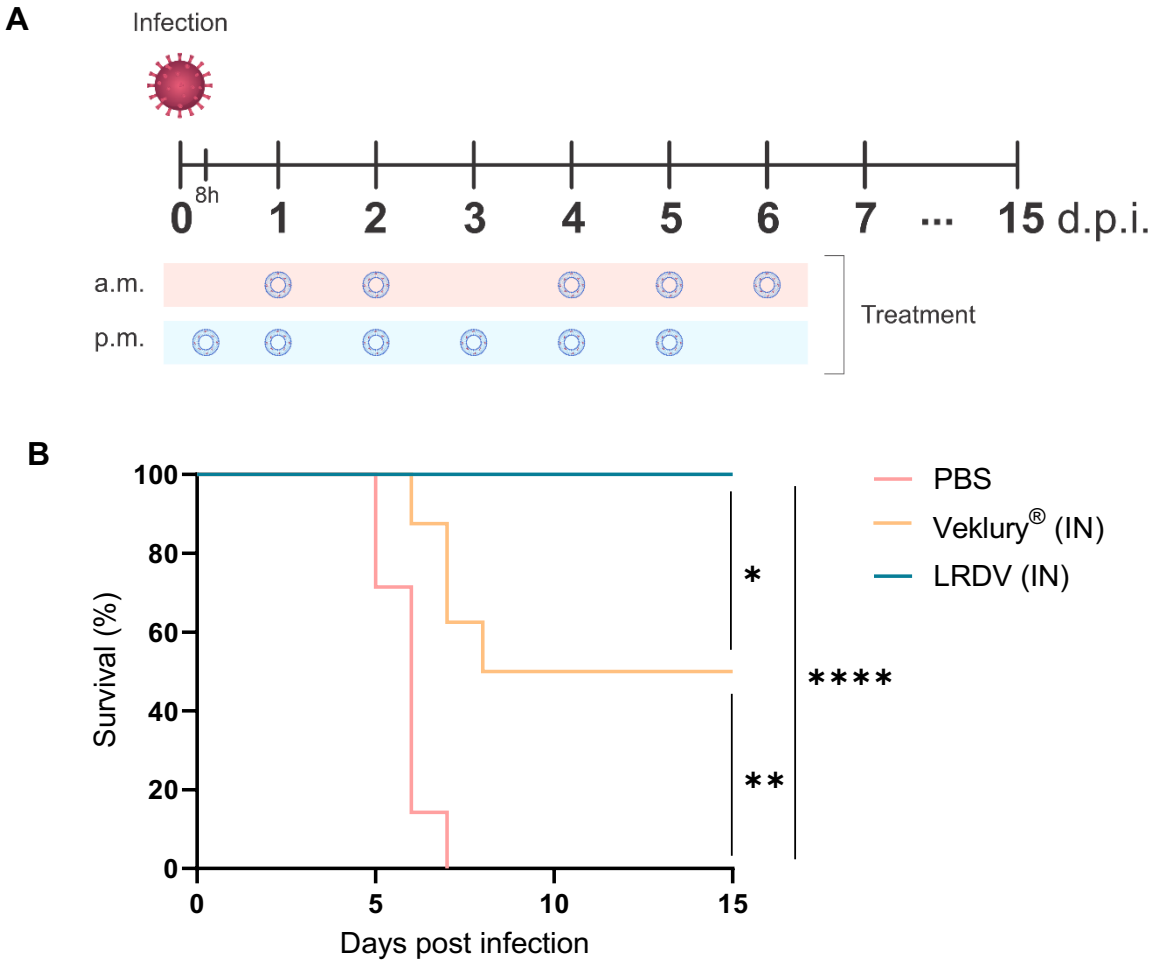

Figure S2 – Impact of intranasal treatment with liposomal RDV versus Veklury® on survival of K18-hACE2 mice infected with SARS-CoV-2. **A:** schematic representation of the experimental protocol. Treatment was initiated 8 hours after infection and was carried out every 12 hours for 6 days. Experimental groups (n=8/group) were: IN LRDV at 10 mg RDV/kg/dose, IN Veklury® at 10 mg RDV/kg/dose and IN PBS. **B:** animal survival was registered on each day. Survival curves were analyzed using the Kaplan-Meier test and compared using Logrank and Gehan-Beslow-Wilcoxon tests. *p<0.05, **p<0.01, ****p<0.0001.

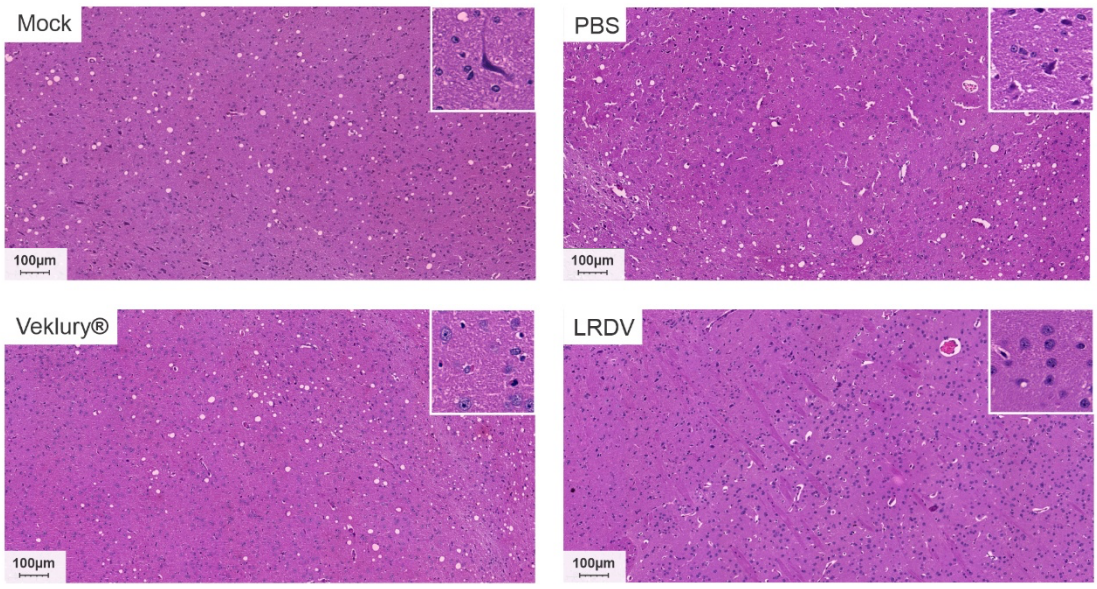

Figure S3. Histopathology of the brain of SARS-CoV-2 infected K18-hACE2 mice after treatment with intranasal LRDV or intraperitoneal Veklury®, compared to intranasal PBS. A non-infected and non-treated group (Mock) was also used as a control. A representative panoramic photomicrograph is shown for each group, after hematoxylin and eosin staining. Sections at 20x magnification. The histopathological analysis of the brain of animals in each experimental group (n = 8) showed no alteration.

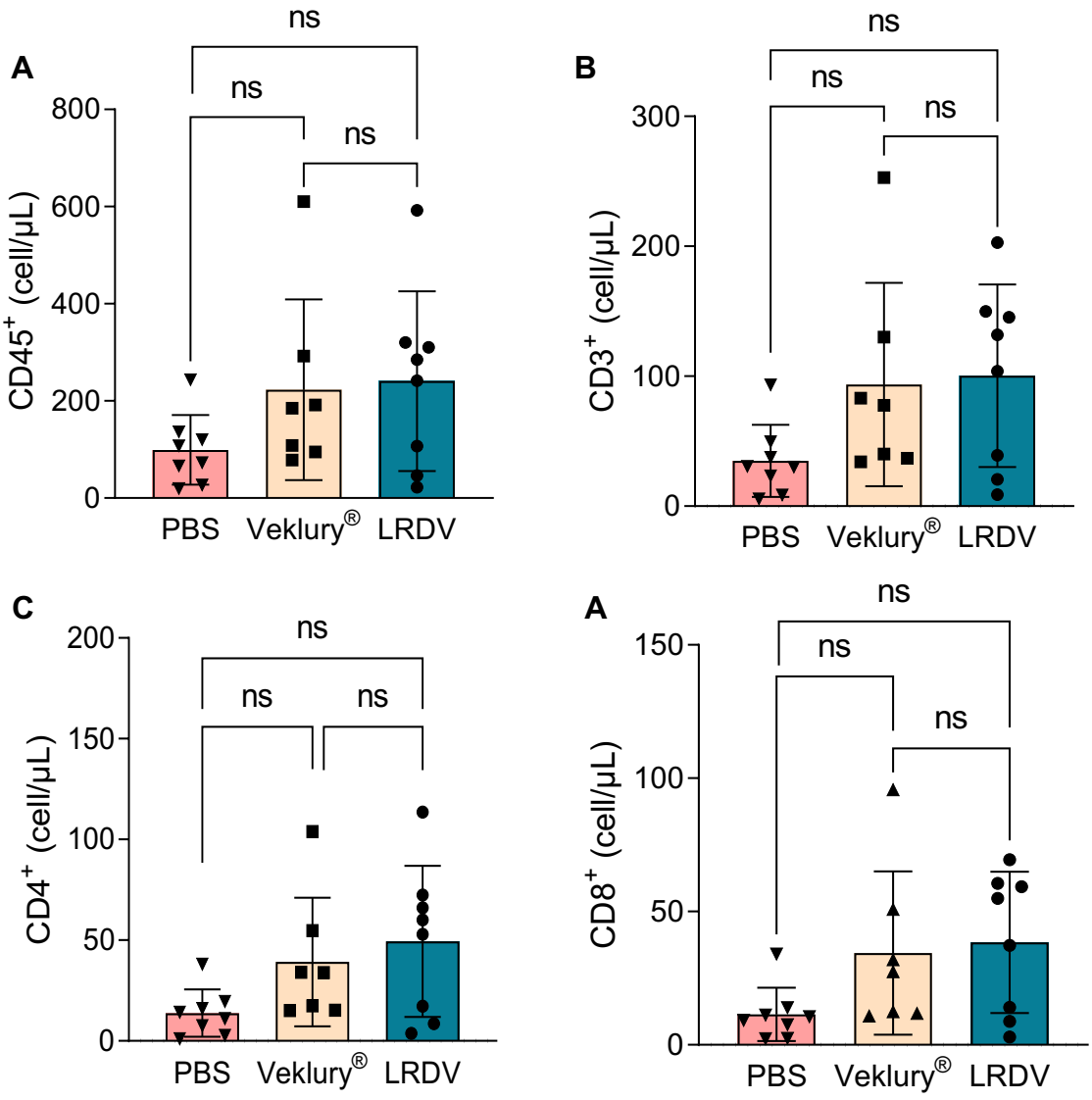

Figure S4 – Lymphoid cell profile in the lungs of mice infected with SARS-CoV-2 after treatment with intranasal LRDV or intraperitoneal Veklury®. K18-hACE2 mice (n=8) were inoculated intranasally with SARS-CoV-2. Treatment was initiated 8 hours after infection and performed every 12 hours for 5 days. The experimental groups were: IN LRDV at 10 mg RDV/kg/dose, IP Veklury® at 20 mg RDV/kg/dose and IN PBS. The animals were sacrificed 12 hours after the last dose. Number of (**A**) $CD45^+$ cells, **(B)** $CD3^+$ T cells, **(C)** $CD4^+$ T cells and **(D)** $CD8^+$ T cells. Cell panels were determined by flow cytometry. Data are presented as medians ± 95% confidence intervals and are compared using Kruskal-Wallis followed by Dunn's post-test. ns, no significant difference.

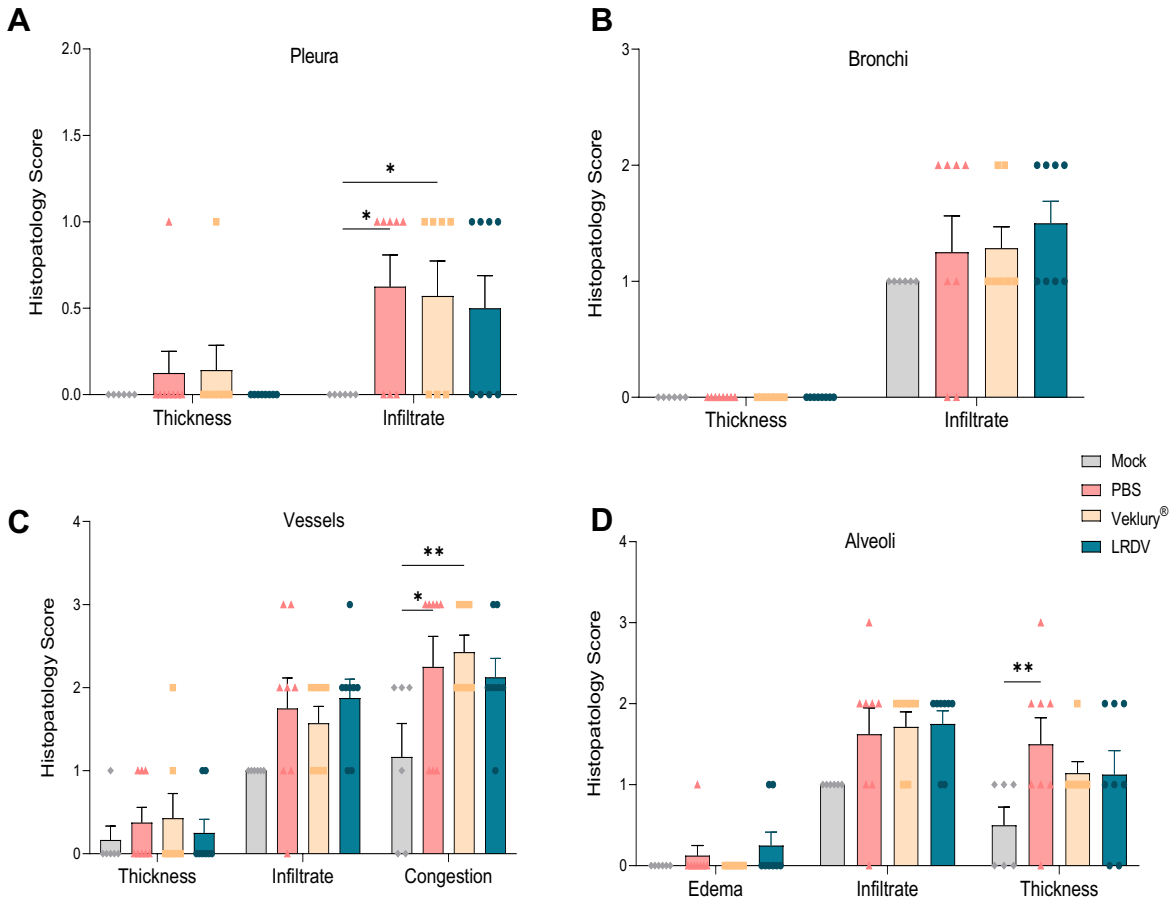

Figure S5 – Histopathological scoring of lung tissue of SARS-CoV-2 infected mice after treatment with intranasal LRDV or intraperitoneal remdesivir, in comparison with intranasal PBS. Scoring for pleura **(A)**, bronchi **(B)**, vessels **(C)** and alveoli **(D)**. K18-hACE2 transgenic mice (n=8) were intranasally inoculated with SARS-CoV-2. Treatment was started 8 hours post-infection and carried out every 12 hours for 5 days. Experimental groups were: LRDV at a dose of 10 mg/kg IN, Veklury® at 20 mg of remdesivir/kg/dose IP and PBS IN. Animals were euthanized 12 hours after the last dose. Score was established as: 0, for no alteration; 1 for discrete change (0-25%); 2, for moderate changes (25-50%); 3 for intense changes (50-100%). Data are shown as means ± SEM and compared using Two-way ANOVA followed by Tukey's multiple comparisons test. *$p < 0.05$; **$P < 0.01$.

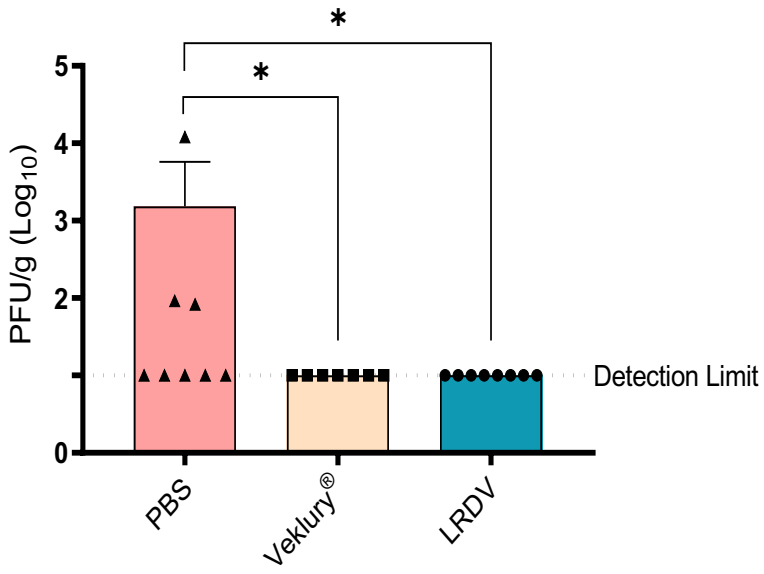

Figure S6. Impact of intranasal treatment with liposomal RDV on the viral load in the kidney of mice infected with SARS-CoV-2. K18-hACE2 mice were intranasally inoculated with SARSCoV-2. Treatment was initiated 8 hours after infection and was carried out every 12 hours for 5 days. Experimental groups (n=8/group) were: IN LRDV at 10 mg RDV/kg/dose, IP Veklury® at 20 mg of RDV/kg/dose and IN PBS. Animals were euthanized 12 hours after the last dose. Viral loads were analyzed in the lungs at 5 dpi by limiting dilution plaque assay for viable viruses. The dashed horizontal line indicates the detection limit. Data were compared using Kruskal-Wallis followed by two-stage linear step-up procedure of Benjamini, Krieger and Yekutieli. *represents the discovery of a significant difference.

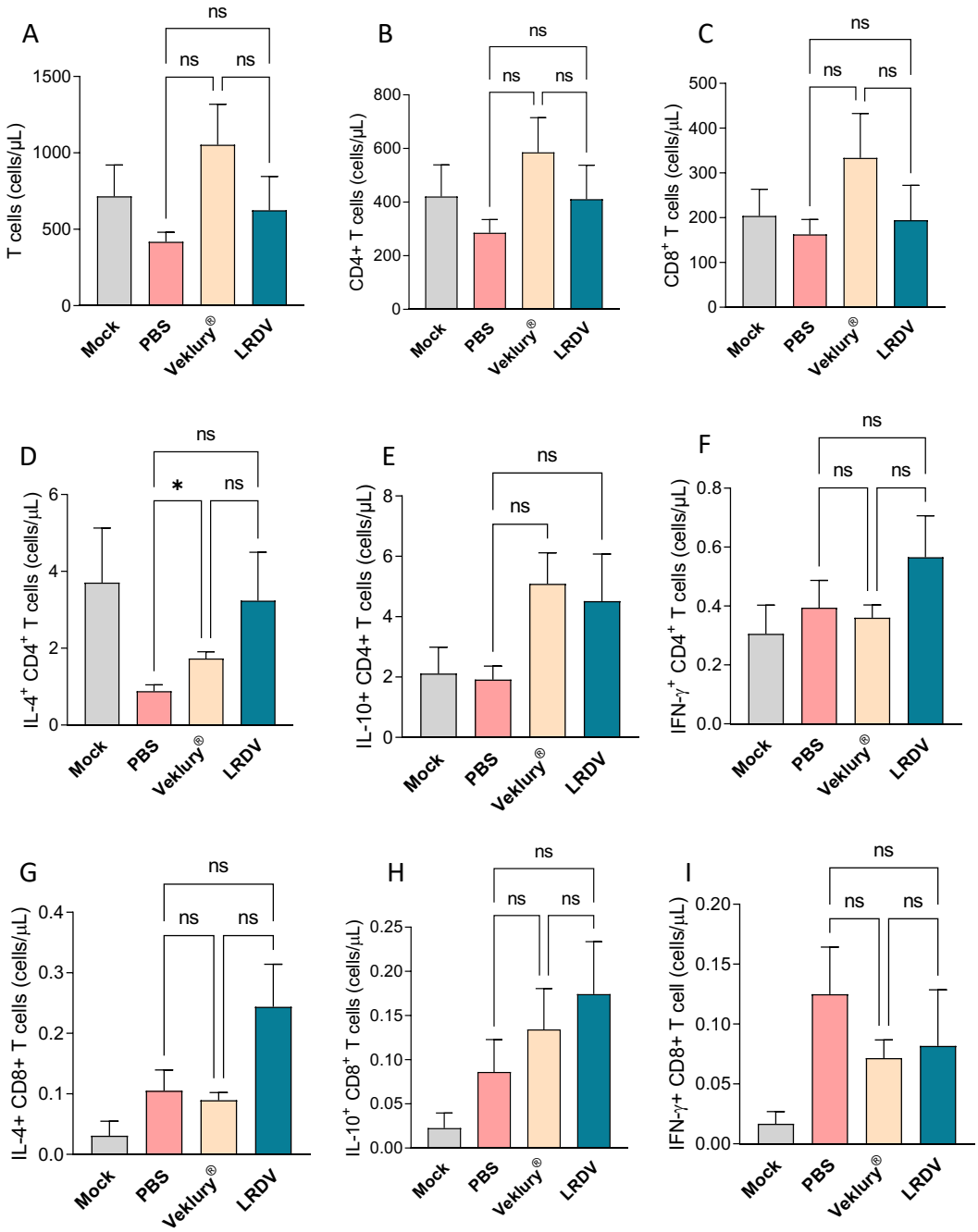

Figure S7. Lymphoid cell profile in the spleen of mice infected with SARS-CoV-2 after treatment with intranasal LRDV or intraperitoneal Veklury®. K18-hACE2 mice (n=8/group) were inoculated intranasally with SARS-CoV-2. Treatment was initiated 8 hours after infection and performed every 12 hours for 5 days. The experimental groups were: IN LRDV at 10 mg RDV/kg/dose, IP Veklury® at 20 mg RDV/kg/dose and IN PBS. Mock: non-infected and non-treated group. The animals were sacrificed 12 hours after the last dose. Number of T cells (A), $CD4^+$ T cells (B); $CD8^+$ T cells (C), $CD4^+$ T cells secreting IL-4 (D), IL-10 (E) and IFN-γ (F); $CD8^+$ T cells secreting IL-4 (G), IL-10 (H) and IFN-γ (I). Cell panels were determined by flow cytometry. Data are presented as means ± SEM and compared using Welch's ANOVA test followed by Dunnett's T3 multiple comparisons test. *$p<0.05$; ns, no significant difference.

Table S1. Characteristics of liposomal RDV formulations prepared from DSPC, DPPG and CHOL, in the absence (DRV-CONV) or presence (DRV-CONV) of DSPE-PEG2000, using the dehydration-rehydration method.

Formulation	[a]Size (nm) ± SD	[a]PDI ± SD	[a]Potential ζ (mV) ± SD	Final RDV concentration (mg/mL)	[a]EE(%) ± SD	Encapsulated drug/lipid ratio (m/m)
DRV-CONV	127.1±2.8	0.189 ±0.022	-5.09 ±0.12	6.3	35.1 (n = 1)	0.0225
DRV-PEG	130.3±3.4	0.122 ±0.021	- 4.53 ±0.06	7.0±0.9	38.3±5.4 (n = 2)	0.0245
[b]Empty DRV	112.8±3.2	0.062 ±0.030	- 3.39 ±0.14		-	

[a]Means ± standard deviation (SD). Size: average hydrodynamic diameter; PDI: polydispersity index; potential ζ: zeta potential; EE (%): drug encapsulation efficiency.

[b]Empty DRV were prepared by the same method as DRV-CONV, in the presence of HP-β-CD but no drug.

Table S2. Antibodies used in flow cytometry analysis.

Antigen	Fluorochrome	Clone	Concentration	Company
CD8a	eFluor 450	53-6.7	1/1300	Thermo
LIVE/DEAD	Acqua		1/1000	Thermo
Streptavidin	Pacific Orange		1/200	Thermo
CD45	Pacific Orange	30-F11	1/200	Thermo
CD11b	Super Bright600	M1/70	1/500	Thermo
CD206	PE	MR6F3	1/300	Thermo
IL-17	PE-eFluor610	eBio17B7	1/100	Thermo
iNos	PE-eFluor610	CXNFT	1/500	Thermo
CD45	PerCP-Cy5.5	Ly-5.2	1/200	BioLegend
CD4	PE-Cyanine7	GK1.5	1/3000	Thermo
F4/80	APC	BM8	1/200	Thermo
IL-10	AlexaFluor 700	JES5-16E3	1/100	Thermo
IFN-γ	APC-eFluor 780	XMG1.2	1/200	Thermo
Gr-1	Biotin	RB6-8C5	1/500	Biolegend

4 CONCLUSÃO GERAL

Em conclusão, este conjunto de estudos possibilitou o desenvolvimento de nanoformulações lipossomais contendo Ang-(1–7) e Remdesivir, bem como a demonstração de seu potencial terapêutico para o tratamento da COVID-19 por via intranasal. No modelo de camundongos transgênicos K18-hACE2 infectados com o SARS-CoV-2, o tratamento com lipossomas contendo Ang-(1–7) [LAng(1–7)] resultou em reduções significativas da carga viral e da inflamação pulmonar. De forma complementar, a formulação lipossomal de Remdesivir (LRDV) apresentou desempenho superior à formulação comercial, prevenindo a mortalidade, diminuindo a carga viral nos pulmões e no cérebro e atenuando a resposta inflamatória pulmonar. Em conjunto, esses achados reforçam o potencial da terapia lipossomal administrada por via intranasal como uma estratégia inovadora, eficaz e promissora para o tratamento da COVID-19 e para o manejo das sequelas associadas à condição pós-COVID-19.

5 REFERÊNCIAS BIBLIOGRÁFICAS

AHMAD, Anam; ZAHEER, Muhammad; BALIS, Fred J. Baricitinib. *In*: **StatPearls**. Treasure Island (FL): StatPearls Publishing, 2025.

ALEEM, Abdul *et al.* Hepatic manifestations of COVID-19 and effect of remdesivir on liver function in patients with COVID-19 illness. **Proceedings (Baylor University. Medical Center)**, v. 34, n. 4, p. 473–477, 2021.

ALEEM, Abdul; KOTHADIA, Jiten P. Remdesivir. *In*: **StatPearls**. Treasure Island (FL): StatPearls Publishing, 2025.

ANTIMISIARIS, S. G. *et al.* Overcoming barriers by local drug delivery with liposomes. **Advanced Drug Delivery Reviews**, v. 174, p. 53–86, 1 jul. 2021.

ATTIQ, Ali *et al.* The triumvirate of NF-κB, inflammation and cytokine storm in COVID-19. **International Immunopharmacology**, v. 101, p. 108255, dez. 2021.

ATTIQ, Ali *et al.* Cytokine Storm-Induced Thyroid Dysfunction in COVID-19: Insights into Pathogenesis and Therapeutic Approaches. **Drug Design, Development and Therapy**, v. 18, p. 4215–4240, 20 set. 2024.

CARABELLI, Alessandro M. *et al.* SARS-CoV-2 variant biology: immune escape, transmission and fitness. **Nature Reviews Microbiology**, v. 21, n. 3, p. 162–177, mar. 2023.

CHAKRAVARTY, Malobika; VORA, Amisha. Nanotechnology-based antiviral therapeutics. **Drug Delivery and Translational Research**, v. 11, n. 3, p. 748–787, 2021.

CHATTERJEE, Bhaswati; THAKUR, Suman S. Remdesivir and Its Combination With Repurposed Drugs as COVID-19 Therapeutics. **Frontiers in Immunology**, v. 13, p. 830990, 12 maio 2022.

CHATURVEDI, Mayank; KUMAR, Manish; PATHAK, Kamla. A review on mucoadhesive polymer used in nasal drug delivery system. **Journal of Advanced Pharmaceutical Technology & Research**, v. 2, n. 4, p. 215–222, 2011.

Coronavirus disease (COVID-19): Corticosteroids, including dexamethasone. Disponível em: <https://www.who.int/news-room/questions-and-answers/item/coronavirus-disease-covid-19-dexamethasone>. Acesso em: 4 fev. 2025.

COVID-19 deaths | WHO COVID-19 dashboard. Disponível em: <https://data.who.int/dashboards/covid19/cases>. Acesso em: 29 jan. 2025.

COVID-19 variants | WHO COVID-19 dashboard. Disponível em: <https://data.who.int/dashboards/covid19/variants>. Acesso em: 29 jan. 2025.

DUONG, Van-An; NGUYEN, Thi-Thao-Linh; MAENG, Han-Joo. Recent Advances in Intranasal Liposomes for Drug, Gene, and Vaccine Delivery. **Pharmaceutics**, v. 15, n. 1, p. 207, 6 jan. 2023.

ELSAYED, Nourhan; HOW, Chee Wun; FOO, Jhi Biau. Development and characterization of pH-sensitive zerumbone-encapsulated liposomes for lung fibrosis via

inhalation route. **European Journal of Pharmaceutics and Biopharmaceutics**, v. 207, p. 114599, 1 fev. 2025.

FILIP, Roxana *et al.* Global Challenges to Public Health Care Systems during the COVID-19 Pandemic: A Review of Pandemic Measures and Problems. **Journal of Personalized Medicine**, v. 12, n. 8, p. 1295, 7 ago. 2022.

FORMICA, María L. *et al.* On a highway to the brain: A review on nose-to-brain drug delivery using nanoparticles. **Applied Materials Today**, v. 29, p. 101631, 1 dez. 2022.

FOUNTAIN, John H.; KAUR, Jasleen; LAPPIN, Sarah L. Physiology, Renin Angiotensin System. *In*: **StatPearls**. Treasure Island (FL): StatPearls Publishing, 2025.

FRÉZARD, Frédéric *et al.* Lipossomas: propriedades físico-químicas e farmacológicas, aplicações na quimioterapia à base de antimônio. **Química Nova**, v. 28, p. 511–518, jun. 2005.

FURBISH, Amelia *et al.* First analytical confirmation of drug-induced crystal nephropathy in felines caused by GS-441524, the active metabolite of Remdesivir. **Journal of Pharmaceutical and Biomedical Analysis**, v. 247, p. 116248, 1 set. 2024.

GILEAD, Remdesivir. Summary on compassionate use. 2020.

GORDON, Calvin J. *et al.* The antiviral compound remdesivir potently inhibits RNA-dependent RNA polymerase from Middle East respiratory syndrome coronavirus. **The Journal of Biological Chemistry**, v. 295, n. 15, p. 4773–4779, 10 abr. 2020.

HARVEY, William T. *et al.* SARS-CoV-2 variants, spike mutations and immune escape. **Nature Reviews. Microbiology**, v. 19, n. 7, p. 409–424, 2021.

HOFFMANN, Markus; KLEINE-WEBER, Hannah; PÖHLMANN, Stefan. A Multibasic Cleavage Site in the Spike Protein of SARS-CoV-2 Is Essential for Infection of Human Lung Cells. **Molecular Cell**, v. 78, n. 4, p. 779- 784.e5, 21 maio 2020.

HONG, Soon-Seok *et al.* Liposomal Formulations for Nose-to-Brain Delivery: Recent Advances and Future Perspectives. **Pharmaceutics**, v. 11, n. 10, p. 540, 17 out. 2019.

HU, Ben *et al.* Characteristics of SARS-CoV-2 and COVID-19. **Nature Reviews. Microbiology**, v. 19, n. 3, p. 141–154, 2021.

HUANG, Xiangang *et al.* Nanotechnology-based strategies against SARS-CoV-2 variants. **Nature Nanotechnology**, v. 17, n. 10, p. 1027–1037, out. 2022.

IMAI, Yumiko *et al.* Angiotensin-converting enzyme 2 protects from severe acute lung failure. **Nature**, v. 436, n. 7047, p. 112–116, jul. 2005.

ISSA, Hawraa *et al.* Combination of Angiotensin (1-7) Agonists and Convalescent Plasma as a New Strategy to Overcome Angiotensin Converting Enzyme 2 (ACE2) Inhibition for the Treatment of COVID-19. **Frontiers in Medicine**, v. 8, p. 620990, 18 mar. 2021.

JEONG, Seung-Hyun; JANG, Ji-Hun; LEE, Yong-Bok. Drug delivery to the brain via the nasal route of administration: exploration of key targets and major consideration factors. **Journal of Pharmaceutical Investigation**, v. 53, n. 1, p. 119–152, 2023.

JOHNSON, Donavon B.; LOPEZ, Michael J.; KELLEY, Brendan. Dexamethasone. *In*: **StatPearls**. Treasure Island (FL): StatPearls Publishing, 2025.

KATIYAR, Harshita *et al.* SARS-CoV-2 Assembly: Gaining Infectivity and Beyond. **Viruses**, v. 16, n. 11, p. 1648, 22 out. 2024.

KHAN, Abdur Rauf *et al.* Progress in brain targeting drug delivery system by nasal route. **Journal of Controlled Release**, v. 268, p. 364–389, 28 dez. 2017.

KSIAZEK, Sara H. *et al.* Renin–Angiotensin–Aldosterone System: From History to Practice of a Secular Topic. **International Journal of Molecular Sciences**, v. 25, n. 7, p. 4035, 4 abr. 2024.

KUBA, Keiji *et al.* A crucial role of angiotensin converting enzyme 2 (ACE2) in SARS coronavirus–induced lung injury. **Nature Medicine**, v. 11, n. 8, p. 875–879, 2005.

LANZA, Katharina *et al.* Covid-19: the renin–angiotensin system imbalance hypothesis. **Clinical Science (London, England : 1979)**, v. 134, n. 11, p. 1259–1264, jun. 2020.

LI, Jingjing *et al.* Liposomal remdesivir inhalation solution for targeted lung delivery as a novel therapeutic approach for COVID-19. **Asian Journal of Pharmaceutical Sciences**, v. 16, n. 6, p. 772–783, nov. 2021.

LI, Xi *et al.* SARS-CoV-2: pathogenesis, therapeutics, variants, and vaccines. **Frontiers in Microbiology**, v. 15, p. 1334152, 13 jun. 2024.

LI, Xiao C.; ZHANG, Jianfeng; ZHUO, Jia L. The vasoprotective axes of the renin-angiotensin system: physiological relevance and therapeutic implications in cardiovascular, hypertensive and kidney diseases. **Pharmacological research**, v. 125, n. Pt A, p. 21–38, nov. 2017.

LIMA, Erick Bryan de Sousa *et al.* Angiotensin-(1–7) decreases inflammation and lung damage caused by betacoronavirus infection in mice. **Inflammation Research**, v. 73, n. 11, p. 2009–2022, 1 nov. 2024.

LIU, Peng; CHEN, Guiliang; ZHANG, Jingchen. A Review of Liposomes as a Drug Delivery System: Current Status of Approved Products, Regulatory Environments, and Future Perspectives. **Molecules**, v. 27, n. 4, p. 1372, 17 fev. 2022.

LUO, Zhilin *et al.* Inhalation Lenalidomide-Loaded Liposome for Bleomycin-Induced Pulmonary Fibrosis Improvement. **AAPS PharmSciTech**, v. 24, n. 8, p. 235, 16 nov. 2023.

MARQUES, Fúlvia D. *et al.* An Oral Formulation of Angiotensin-(1-7) Produces Cardioprotective Effects in Infarcted and Isoproterenol-Treated Rats. **Hypertension**, v. 57, n. 3, p. 477–483, mar. 2011.

Medicamentos aprovados. Disponível em: <https://www.gov.br/anvisa/pt-br/assuntos/campanhas/coronavirus/medicamentos/medicamentos-aprovados>. Acesso em: 29 jan. 2025.

MIESBACH, Wolfgang. Pathological Role of Angiotensin II in Severe COVID-19. **TH Open: Companion Journal to Thrombosis and Haemostasis**, v. 4, n. 2, p. e138–e144, 26 jun. 2020.

O'TOOLE, Áine *et al.* Pango lineage designation and assignment using SARS-CoV-2 spike gene nucleotide sequences. **BMC Genomics**, v. 23, n. 1, p. 121, 11 fev. 2022.

PAN, David Z. *et al.* Remdesivir improves biomarkers associated with disease severity in COVID-19 patients treated in an outpatient setting. **Communications Medicine**, v. 3, n. 1, p. 1–6, 3 jan. 2023.

(PDF) LIPOSOMES: TYPE, PREAPRATION AND EVALUATION. **ResearchGate**, 22 out. 2024.

PREUSS, Charles V.; ANJUM, Fatima. Tocilizumab. *In*: **StatPearls**. Treasure Island (FL): StatPearls Publishing, 2025.

RICHARDSON, Peter J. *et al.* CNS penetration of potential anti-COVID-19 drugs. **Journal of Neurology**, v. 267, n. 7, p. 1880–1882, 2020.

SALIE, Faatiema; SAIDI, Trust. Nanomedicine drug delivery in South Africa: a retrospective study on research, funding and collaboration. **Frontiers in Pharmacology**, v. 14, p. 1317137, 3 jan. 2024.

SHARMA, Abhay. Inferring molecular mechanisms of dexamethasone therapy in severe COVID-19 from existing transcriptomic data. **Gene**, v. 788, p. 145665, 1 jul. 2021.

TAY, Matthew Zirui *et al.* The trinity of COVID-19: immunity, inflammation and intervention. **Nature Reviews. Immunology**, v. 20, n. 6, p. 363–374, 2020.

Therapeutics and COVID-19: living guideline. Disponível em: <https://app.magicapp.org/#/guideline/nBkO1E>. Acesso em: 4 fev. 2025.

Tracking SARS-CoV-2 variants. Disponível em: <https://www.who.int/activities/tracking-SARS-CoV-2-variants>. Acesso em: 29 jan. 2025.

TRAPNELL, Bruce C. *et al.* Pulmonary alveolar proteinosis. **Nature Reviews Disease Primers**, v. 5, n. 1, p. 1–17, 7 mar. 2019.

TRIEBEL, Hannah; CASTROP, Hayo. The renin angiotensin aldosterone system. **Pflugers Archiv**, v. 476, n. 5, p. 705, 17 jan. 2024.

TROUGAKOS, Ioannis P. *et al.* Insights to SARS-CoV-2 life cycle, pathophysiology, and rationalized treatments that target COVID-19 clinical complications. **Journal of Biomedical Science**, v. 28, p. 9, 12 jan. 2021.

VARTAK, Richa *et al.* Aerosolized nanoliposomal carrier of remdesivir: an effective alternative for COVID-19 treatment in vitro. **Nanomedicine**, p. 10.2217/nnm-2020–0475, 2021.

V'KOVSKI, Philip *et al.* Coronavirus biology and replication: implications for SARS-CoV-2. **Nature Reviews Microbiology**, v. 19, n. 3, p. 155–170, mar. 2021.

WAGENER, Gebhard *et al.* A randomized, placebo-controlled, double-blinded pilot study of angiotensin 1–7 (TXA-127) for the treatment of severe COVID-19. **Critical Care**, v. 26, n. 1, p. 229, 28 jul. 2022.

WU, Di *et al.* The blood–brain barrier: Structure, regulation and drug delivery. **Signal Transduction and Targeted Therapy**, v. 8, n. 1, p. 1–27, 25 maio 2023.

YU, Qingyuan *et al.* Cytokine Storm in COVID-19: Insight into Pathological Mechanisms and Therapeutic Benefits of Chinese Herbal Medicines. **Medicines**, v. 11, n. 7, p. 14, 18 jul. 2024.

ZHU, Na *et al.* A Novel Coronavirus from Patients with Pneumonia in China, 2019. **The New England Journal of Medicine**, v. 382, n. 8, p. 727–733, 20 fev. 2020.

6 ANEXOS

6.1 – PATENTE DEPOSITADA – COMPOSIÇÃO LIPOSSOMAL MISTA DE REMDESIVIR COM UM PEPTÍDEO ANGIOTENSINÉRGICO, PROCESSO E USO

870250009148
04/02/2025 13:10
29409162330076378

Pedido nacional de Invenção, Modelo de Utilidade, Certificado de Adição de Invenção e entrada na fase nacional do PCT

Número do Processo: BR 10 2025 002202 8

Dados do Depositante (71)

Depositante 1 de 1

Nome ou Razão Social: UNIVERSIDADE FEDERAL DE MINAS GERAIS
Tipo de Pessoa: Pessoa Jurídica
CPF/CNPJ: 17217985000104
Nacionalidade: Brasileira
Qualificação Jurídica: Instituição de Ensino e Pesquisa
Endereço: Av. Antônio Carlos, 6627 - Unidade Administrativa II - 2º andar- sala 2011
Cidade: Belo Horizonte
Estado: MG
CEP: 31270-901
País: Brasil
Telefone: (31) 3409-6430
Fax:
Email: patentes@ctit.ufmg.br

6.2 - PATENTE DEPOSITADA – PROCESSO PARA OBTENÇÃO DE LIPOSSOMAS COM ALTOS TEORES DE ENCAPSULAÇÃO DE PRINCÍPIOS ATIVOS HIDROSSOLÚVEIS E USO

INSTITUTO NACIONAL DA PROPRIEDADE INDUSTRIAL

870240076536
06/09/2024 11:25
29409162322522631

Pedido nacional de Invenção, Modelo de Utilidade, Certificado de Adição de Invenção e entrada na fase nacional do PCT

Número do Processo: BR 10 2024 018382 7

Dados do Depositante (71)

Depositante 1 de 1

Nome ou Razão Social: UNIVERSIDADE FEDERAL DE MINAS GERAIS
Tipo de Pessoa: Pessoa Jurídica
CPF/CNPJ: 17217985000104
Nacionalidade: Brasileira
Qualificação Jurídica: Instituição de Ensino e Pesquisa
Endereço: Av. Antônio Carlos, 6627 - Unidade Administrativa II - 2º andar- sala 2011
Cidade: Belo Horizonte
Estado: MG
CEP: 31270-901
País: Brasil
Telefone: (31) 3409-6430
Fax:
Email: patentes@ctit.ufmg.br

6.3 PREMIAÇÕES

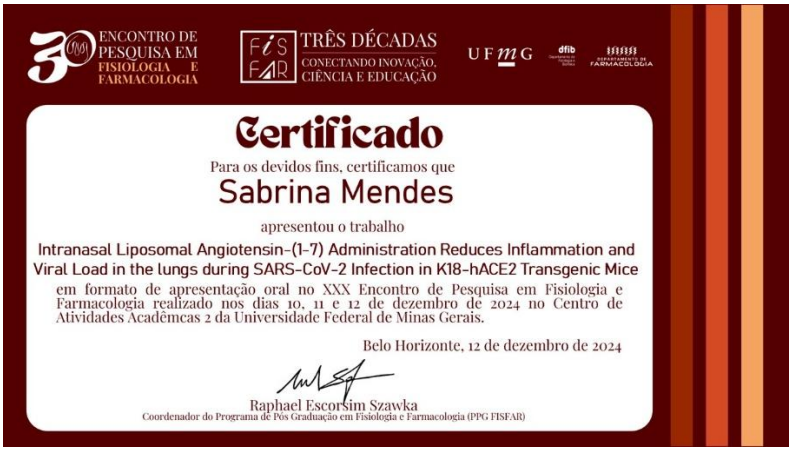

XXIX ENCONTRO DE PESQUISA EM FISIOLOGIA E FARMACOLOGIA

Certificado de menção honrosa

Sabrina Mendes Silva Araujo

Certificamos que o participante recebeu menção honrosa na categoria **Apresentação Oral**, por seu trabalho intitulado **"LIPOSOMAL REMDESIVIR FORMULATION BY INTRANASAL ROUTE PROTECTS AGAINST FATAL SARS-CoV-2 PULMONARY- AND NEURO-INVASION IN K18-HACE2 MICE"**, de autoria de "Sabrina Mendes Silva Araujo; Lays Cordeiro Guimarães; Leonardo Camilo de Oliveira; Pedro Augusto Carvalho Costa; Maria Marta Figueiredo; Pedro Pires Goulart Guimarães; Frederic Jean Georges Frezard", durante o **XXIX Encontro de Pesquisa em Fisiologia e Farmacologia**, ocorrido nos dias 13 e 14 de dezembro de 2023, promovido pelo Programa de Pós Graduação em Ciências Biológicas Fisiologia e Farmacologia, realizado na UFMG, Belo Horizonte.

Prof. Raphael Escorsim Szawka
Presidente Comissão Organizadora
XXIX Encontro de Pesquisa em Fisiologia e Farmacologia

UFMG

50 ANOS PPG FISFAR

XXVIII ENCONTRO DE PESQUISA EM FISIOLOGIA E FARMACOLOGIA

CERTIFICAMOS QUE

Sabrina Mendes Silva Araujo

MENÇÃO HONROSA

Apresentou o trabalho intitulado "**Nanoformulações do Remdesivir com lipossomas: inibição do SARS-COV-2 in vitro e citotoxicidade em comparação ao fármaco livre**" de autoria de "Sabrina Mendes Silva Araujo, Leonardo Camilo de Oliveira, Pedro Pires Goulart Guimarães e Frederic Jean Georges Frezard" na modalidade **PÔSTER** no evento "**XXVIII Encontro de Pesquisa em Fisiologia e Farmacologia**" nos dias 17 e 18 de novembro de 2022 promovido pelo **Programa de Pós Graduação em Ciências Biológicas: Fisiologia e Farmacologia**, realizado na Universidade Federal de Minas Gerais, Belo Horizonte, MG.

Prof. Raphael Escorsim Szawka
Presidente Comissão Organizadora
XXVIII Encontro de Pesquisa em Fisiologia e Farmacologia

Merck Innovation Award

MERCK

Conferimos esse certificado aos ganhadores do Merck Innovation Award.
Para a área de Nanotecnologia com a Startup LipidSolutions

sabrina Mendes silva Araujo
CEO e Cofundadora

Frédéric Jean Georges Frézard
Cofundador e Coordenador Científico-Tecnológico

cynthia peres DeMicheli
Gestão Científica e Administrativa

Por seu compromisso com a inovação e por seu excelente trabalho, inspirando descobertas e elevando a humanidade

Misael Leonardo da Silva
Head of Innovation Ecosystem

7 ARTIGOS E PATENTES - COLABORAÇÃO

1.CUNHA MATOSINHOS, R., FRÉZARD, F., MENDES SILVA ARAÚJO, S. *et al.* Development and characterization of liposomal formulations containing sesquiterpene lactones for the treatment of chronic gout. *Sci Rep* 14, 6991 (2024). https://doi.org/10.1038/s41598-024-57663-1

2.GUIMARÃES, DÊNIA ANTUNES SAÚDE; MATOSINHOS, RAFAELA CUNHA; FRÉZARD, FRÉDÉRIC JEAN GEORGES; DE SOUZA, JACQUELINE; ARAUJO, SABRINA MENDES SILVA. Formulações nanoestruturadas contendo lactonas sesquiterpênicas e uso na produção de medicamentos para o tratamento de tumores, hiperuricemia, doenças inflamatórias e gota. BR 10 2024 020449 2. Titular: Universidade Federal de Ouro Preto - UFOP. Brasil: Instituto Nacional da Propriedade Industrial, 2024.

scientific reports

Check for updates

OPEN

Development and characterization of liposomal formulations containing sesquiterpene lactones for the treatment of chronic gout

Rafaela Cunha Matosinhos[1], Frédéric Frézard[2], Sabrina Mendes Silva Araújo[2], Andressa Magalhães Barbosa[1], Isabela Fernanda de Souza[1], José Dias de Souza Filho[3], Jacqueline de Souza[4], Ana Paula Corrêa Oliveira Bahia[2], Francesca Ietta[5], Agnese Magnani[6] & Dênia Antunes Saúde-Guimarães[1]✉

Gout and hyperuricemia are characterized by high uric acid levels, and their treatment involves medications that have adverse effects. In this study, we evaluated oral liposomal formulations with eremantholide C and goyazensolide as a novel approach to reduce the toxicity associated with these substances while maintaining their anti-hyperuricemic activity. We characterized the formulations and evaluated them based on encapsulation efficiency and stability over 12 months and under simulated physiological environments. We determined the toxicity of the liposomal formulations in Caco-2 cells and the anti-hyperuricemic activity in rats. The formulations exhibited nanometric size, a narrow size distribution, and a negative zeta potential, indicating their stability and uniformity. The efficient encapsulation of the sesquiterpene lactones within the liposomes emphasizes their potential for sustained release and therapeutic efficacy. Stability evaluation revealed a small decrease in the eremantholide C concentration and a remarkable stability in the goyazensolide concentration. In Caco-2 cells, the liposomes did not exert toxicity, but did exhibit an antiproliferative effect. In vivo assays demonstrated that the liposomes reduced serum uric acid levels. Our study represents an advancement in gout and hyperuricemia treatment. The liposomal formulations effectively reduced the toxicity associated with the sesquiterpene lactones while maintaining their therapeutic effects.

Abbreviations

BSA	Bovine serum albumin
DMEM	Dulbecco's-Modified Eagle's Medium
DMSO	Dimethyl sulfoxide
EE	Encapsulation efficiency
EREC	Eremantholide C
FBS	Fetal bovine serum
GOIA	Goyazensolide
HPLC	High performance liquid chromatography
LIPO	Empty (substance-free) liposome
LIPO + EREC	Liposomal formulation with eremantholide C
LIPO + GOIA	Liposomal formulation with goyazensolide

[1]Laboratório de Plantas Medicinais (LAPLAMED), Programa de Pós-Graduação em Ciências Farmacêuticas (CiPharma), Escola de Farmácia, Universidade Federal de Ouro Preto, Ouro Preto, Minas Gerais 35400-000, Brazil. [2]Laboratório de Biofísica e Sistemas Nanoestruturados (LabNano), Departamento de Fisiologia e Biofísica, Instituto de Ciências Biológicas, Universidade Federal de Minas Gerais (UFMG), Belo Horizonte, Minas Gerais 31270-901, Brazil. [3]Laboratório Multiusuário de Caracterização de Moléculas (LMCM), Escola de Farmácia, Universidade Federal de Ouro Preto, Ouro Preto, Minas Gerais 35400-000, Brazil. [4]Laboratório de Controle de Qualidade de Insumos, Fármacos e Medicamentos (LCQ), Escola de Farmácia, Universidade Federal de Ouro Preto, Ouro Preto, Minas Gerais 35400-000, Brazil. [5]Dipartimento Scienze della Vita, Università degli Studi di Siena, 53100 Siena, Tuscany, Italy. [6]Dipartimento di Biotecnologie, Chimica e Farmacia, Università degli Studi di Siena, 53100 Siena, Tuscany, Italy. ✉email: saude@ufop.edu.br

INSTITUTO NACIONAL DA PROPRIEDADE INDUSTRIAL

870240084167
02/10/2024 13:54
29409162305186246

Pedido nacional de Invenção, Modelo de Utilidade, Certificado de Adição de Invenção e entrada na fase nacional do PCT

Número do Processo: BR 10 2024 020449 2

Dados do Depositante (71)

Depositante 1 de 2

Nome ou Razão Social: UNIVERSIDADE FEDERAL DE OURO PRETO - UFOP
Tipo de Pessoa: Pessoa Jurídica
CPF/CNPJ: 23070659000110
Nacionalidade: Brasileira
Qualificação Jurídica: Instituição de Ensino e Pesquisa
Endereço: RUA DIOGO DE VASCONCELOS, 122 - BAIRRO PILAR
Cidade: Ouro Preto
Estado: MG
CEP: 35400-000
País: Brasil
Telefone: 31 3559 1369
Fax: 31 3559 1370
Email: nite@propp.ufop.br

Depositante 2 de 2

Nome ou Razão Social:	UNIVERSIDADE FEDERAL DE MINAS GERAIS - UFMG
Tipo de Pessoa:	Pessoa Jurídica
CPF/CNPJ:	17217985000104
Nacionalidade:	Brasileira
Qualificação Jurídica:	Instituição de Ensino e Pesquisa
Endereço:	Av. Antônio Carlos, 6627 - Unidade Administrativa II - 2º andar- sala 2011
Cidade:	Belo Horizonte
Estado:	MG
CEP:	31270-901
País:	BRASIL
Telefone:	(31) 340 96430
Fax:	
Email:	patentes@ctit.ufmg.br

Nome: SABRINA MENDES SILVA ARAUJO

CPF: 05897961352

Nacionalidade: Brasileira

Qualificação Física: Doutorando

Endereço: Rua Beira Alta, 123, Jaraguá

Cidade: Belo Horizonte

Estado: MG

CEP: 31255-240

País: BRASIL

Telefone: (79) 999 919299

Fax:

Email: sabrinamsa@outlook.com

Inventor 6 de 8

Nome: ANDRESSA MAGALHÃES BARBOSA

CPF: 09868573602

Nacionalidade: Brasileira

Qualificação Física: Mestrando

Endereço: Córrego Boa Esperança, zona rural,

Cidade: São João do Manhuaçu

Estado: MG

CEP: 36918-000

País: BRASIL

Telefone: (33) 984 431842

Fax:

Email: andressa.magalhaes@aluno.ufop.edu.br

Inventor 7 de 8